Effect of internal and external dynamics on galaxy properties and their evolution

A Thesis

submitted in partial fulfillment of the requirements for the award of the degree of

Doctor of Philosophy

IN

Department of Mathematics

by

Meenu

Reg no: 951811001

Under the Supervision of

Dr. Mamta Gulati

Assistant Professor

Department of Mathematics

THAPAR INSTITUTE OF ENGINEERING AND TECHNOLOGY

PATIALA-147004, PUNJAB, INDIA.

January 27, 2025

DEDICATED

TO

THE ALMIGHTY

AND

MY PARENTS

Declaration

I hereby certify that the work, which is being presented in the thesis, entitled **Effect Of Internal and External Dynamics on Galaxy Properties and their Evolution**, in partial fulfillment of the requirements for the award of the degree of **Doctor of Philosophy** and submitted to the institution is an authentic record of my own work carried out during the period **July 2018** to **January 27, 2025** under the supervision of **Dr. Mamta Gulati**, Assistant Professor, Department of Mathematics, Thapar Institute of Engineering and Technology, Patiala. The matter presented in this thesis has not been submitted elsewhere for the award of any other degree or diploma from any institution.

Date: 27/01/2025

Meenu
Candidate

It is certified that the above statement made by the candidate is correct to the best of our knowledge.

Date: 27/01/2025

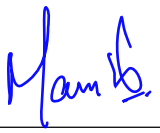

Dr. Mamta Gulati
Supervisor
Assistant Professor
Department of Mathematics
TIET, Patiala-147004, India

Acknowledgements

Firstly, thanks to the Lord for giving me the strength to complete my work.
I would like to express my deep sense of gratitude and indebtedness to my respected teacher and supervisor, Dr. Mamta Gulati. I would like to express my heartfelt gratitude to her for being a great advisor with brilliant ideas and never-failing support. Working with my supervisor, Dr. Mamta Gulati, has been the experience of a lifetime. I joined my Ph.D. without having much idea of what research means, and all the credit for my understanding of how to pursue a research problem goes to her. From the bottom of my heart, I would like to thank Dr. Mamta Gulati for teaching me the depth of subjects like analysis.
I am thankful to Prof. M.K. Sharma, Head of the Department of Mathematics, and Prof. Satish Kumar Sharma, Former Head of the Department of Mathematics, for providing me with the best facilities for research work.
I thank Prof. A. K. Lal, Prof. Ankush Pathania, and Prof. Debabrata Deb as members of my Ph.D. doctoral committee for their support and encouragement. Also, thank you for giving me your precious time to discuss my research problems and give me ideas on how to tackle the problem.
I am thankful to the Ph.D. coordinators (Dr. Harish Garg and Dr. Parimita Roy), all respected faculty members, and the staff of the Department of Mathematics for their kind cooperation. I thank the Director, Registrar, and Dean (Research and Sponsored Projects) of Thapar Institute of Engineering and Technology, Patiala, for providing the necessary facilities and financial support through Teaching Associateship (TA ship) to carry out the present research work.
I wish to thank all my teachers for believing in me and helping me throughout my student life.

I have no words to thank Aunty ji (Mrs. Deepshikha) for their love, care, and tasty food in Patiala like a mother. I thank Karuna Kadiyan for her care and support as an elder sister during my hostel life and Isha Sharma as a younger sister.

I thank Dr. Aswani Kumar and Dr. Parag Choure for helping me. They have always been available for discussion and offered all assistance required. I am grateful to him for believing in me and giving me enough confidence to pursue the research problems that I have worked on. Not only Mathematics, but they have also taught me a lot about having the right attitude in life, for which I can never thank them enough.

Now comes the friends' turn. It is difficult to imagine my life at TIET without friends like Mohit Dhuriya, Watanjeet Singh, Shivani Saini, Nishtha, Herman, Anjali Sharma, Subha Sharma, Ravinder Kumar Sharma and Twinkle Sharma. Apart from this, these are the friends whom I have always relied on since I came to Patiala.

I would like to thank Vinod Thapa as a younger brother at Patiala, for helping me to learn Python.

I thank my best friend Kehksha, who witnessed my journey and the hard times of my life. I also thank to her husband, Jishan, who cares as an elder brother.

I would like to thank Dr. Ankit singh and Dr. Ashish Rayal for his support and encouragement while I finished my work.

Finally, my family has been my biggest support all my life. My parents, my brothers (Mr. Krishna & Mr. Arjun) & my sister in Law (Mrs. Versha) who bestowed unconditional love and support upon me over the years, somebody who never questioned my capabilities and accepted me the way I am. They stood beside me rock-solid in many tough phases of my life when it was much required. I will remain highly indebted to them forever. Without their sacrifices, I could have not come this far. Lastly, thanks to my niece Misty Prajapati, who remove my stress during this time after spending time with her.

List of Publications

Considered Work For Thesis Objectives

1. **Meenu Prajapati**, Mamta Gulati."Enhanced $m = 1$WKB instabilities in nearly Keplerian stellar discs due to the presence of gas ". Astrophysics and Space Science, 367 (6), 56, (2022).
   https:// DOI:10.1007/s10509-022-04077-y. (**SCIE, Impact factor: 1.9**).

2. **Meenu Prajapati**, Mamta Gulati. "Three-Dimensional stellar orbits due to off-centered dark matter halo at the center of the disk galaxies". New Astronomy, 102246, (2024).
   https: // DOI:10.1016/j.newast.2024.102246.(**SCIE, Impact factor: 1.9**).

3. **Meenu Prajapati**, Mamta Gulati. "Galactic magnetic field and spiral arms against gas quenching due to Ram pressure". New Astronomy, 102356, (2025).
   https://doi.org/10.1016/j.newast.2025.102356. (**SCIE, Impact factor: 1.9**)

Additional Publication During This Period

1. Ankit Singh, Shreya Davessar, Mamta Gulati, Jasjeet Singh Bagla, and **Meenu Prajapati**. "Study of dependence of ram pressure stripping on the orbital parameters of the galaxies". MNRAS, 530, 699-709, (2024).
   https://doi.org/10.1093/mnras/stae730. (**SCIE, Impact factor: 4.8**).

Abstract

The current work is an account of few aspects of galaxy evolution, where the galaxies dynamic plays a crucial role. The thesis has been split into five chapters, the first of which includes an introduction to the subject matter and a review of the literature, followed by a summary of the thesis's contents. In the second chapter, we study simple analytic model of nearly Keplerian modes for co-rotating gravitationally coupled gaseous and stellar discs. We present a simple analysis for large-scale, long-wavelength slow modes for $m = 1$ for co-rotating gravitationally coupled gaseous and stellar discs. We derived the dispersion relation using the Wentzel-Kramers-Brillouin (WKB) approximation and explored the stability of modes. Such modes are useful to address the problem of asymmetric light distribution observed in galaxies like M31. In the third chapter, we analyze stellar orbits at the galaxy's central region that are disturbed by an asymmetric dark matter halo potential which are observed in observations as well as numerical simulations recently. We used first-order epicyclic theory to solve the orbits and obtained a central region's azimuthal variation in the effective stellar orbits. We discuss the kinematical lopsidedness of the stellar orbits within a 3 kpc radius of the galaxies. The fourth & fifth chapter discusses the gas-removing mechanism (Ram pressure stripping) when the galaxy passes through the cluster medium. In the fourth chapter, we analyze the effect of spiral arms on the ram pressure in the galaxy; for this, we have considered different types of mass galaxies with different numbers of arms and widths. We analyze how the gravitationally bound force affects the ram pressure on removing gas from the disc, these parameters help us to study this phenomena In the fifth chapter, we analyze the impact of the magnetic field on the ram pressure. The magnetic field is an intrinsic part of the galaxy, and it acts as a restoring force against ram pressure stripping in the galaxies. The resulting in gas retention when a galaxy passes through the cluster medium.

Keywords: Waves - methods, Celestial mechanics, Galaxies - nuclei, Instabilities, Analytical-method, Galaxies-kinematics and dynamics, kinematics and dynamics—galaxies, dark matter—galaxies, internal motions - Galactic center - haloes, galaxies, clusters, intracluster medium-galaxies, evolution-galaxies: general-galaxies, magnetic fields - galaxies, Galaxy environments - Galactic and extragalactic astronomy.

Abbreviations

SMBH = Supermassive Black Hole
BH = Black Hole
DM = Dark Matter
SFR = Star Foramation Rate
AGN = Active Galactic Nuclei
RPS = Ram Pressure Stripping
ISM = Inter Stellar Medium
HST = Hubble Space Telescope
WKB = Wentzel-Kramers-Brillouin
ICM = Intra Cluster Medium
RHS = Right Hand Side
LHS = Left Hand Side

Contents

List of Tables

List of Figures

Chapter 1

Introduction

Galaxies are defined as a massive system bounded by the gravitation. They consist of stars, stellar remnants, dark matter, and an interstellar medium composed of gas and dust. Galaxies are broadly classified into four main types: elliptical, spiral, lenticular, and irregular, as depicted in the Hubble tuning fork diagram. Elliptical galaxies are spheroidal or elongated structures composed mainly of older stars, while spiral galaxies exhibit a rotating disk morphology with spiral arms rich in young stars, gas, and dust. Lenticular galaxies serve as a transitional type between elliptical and spiral galaxies; they feature a disk-like structure but lack prominent spiral arms and are dominated by older stars. Irregular galaxies do not fit neatly into these categories and often display chaotic structures. The primary components of galaxies include stars, the interstellar medium (ISM) comprising gas and dust, and dark matter, which significantly influences their gravitational potential. This study focuses specifically on disk galaxies, a subset of spiral galaxies, examining their structural and dynamical properties. While dark matter and dwarf galaxies play a role in the broader context of galaxy evolution, their contributions are secondary to the primary focus of this work.

The impact of internal and external dynamics of spiral galaxies on their evolution is of paramount importance in the field of galaxy evolution. These galaxies, have a disc morphology, which includes various non-axisymmetric features, including bars and spiral arms. A typical disc galaxy has a Super Massive Black Hole (SMBH) (Gebhardt et al., 2000) at its center, which is responsible for phenomena like launching relativistic jets, formation of accretion disc at the center etc. It also has an elliptical shaped central mass concentration known as a bulge, and it is observed that the entire system is encased in

a sizable and extended Dark Matter (DM) halo (Bailin et al., 2007; Fiřt et al., 2009). The composition of visible mass of galaxies can be broadly classified into stars and gas. A sufficient amount of gas at the right temperatures and densities is necessary for star formation, and this gas is bound to get influenced by various internal and external processes, such as the galactic wind, accretion, supernova explosion, etc. The stars, after their death, add to the gas content of the galaxies. Not only the life cycles of stars and gas depend on each other, but there is also an interplay of forces affecting their dynamics, inturn affecting their evolution.

The present thesis is dedicated to understand few aspects of interplay between galaxies dynamics and their evolution. For this, our work is divided into two parts:

- In the first part, we have addressed two aspects of internal dynamics pertaining to asymmetric features of the galaxy. The first one is the asymmetric features arising due to global characteristics associated with galaxies. For instance, a relationship has been discovered between Black Hole (BH) growth, lopsidedness, and the existence of young stellar populations at the galaxy's centers (Reichard et al., 2009). The second one being local asymmetric feature such as off-centered dark matter halo at the galaxy's center, which is related to the strong lopsidedness. This type of lopsidedness has a significant dynamical impact on the galaxy. For example, it contributes to outward angular momentum, fueling the central Active Galactic Nuclei (AGN). The outward angular momentum transport could be caused by the central region's extremely disturbed, lopsided orbits, enabling gas infall. For lopsidedness in the outer disc, this has been demonstrated by Saha & Jog (2014). This may also help with a long-standing issue of how to fuel a core AGN, even within an isolated galaxy, the growth of the galaxy's BH and increased star formation in its dense regions (Jog, 1999; Jog & Combes, 2009).

- In the second part, the impact of ram pressure stripping on spiral galaxies' gas content has been discussed. Here we attempt to move to an entirely different length and time scale in the universe. A group of galaxies bounded together by each others gravitational pull are called cluster of galaxies. In this part we attempt on studying the effect on the gas content of galaxies as they move in the ambient medium in the cluster of galaxies.

In the next section we introduce the problem which are studied in the thesis in detail.

1.1 Structural properties due to internal dynamics

From the observations and simulations the distribution of mass and light in spiral galaxies is not strictly axisymmetric. Observations show that the stellar disk in a typical spiral galaxy is significantly lopsided (Rix & Zaritsky, 1995; Jog & Combes, 2009), particularly in the outer regions of galaxies, indicating asymmetry in the disk mass distribution.

Firstly, asymmetry in the atomic hydrogen gas's spatial distribution in some galaxies' outer regions was discovered by Baldwin et al. (1980), they appropriately named them "lopsided" galaxies. The distribution of atomic hydrogen gas in the outer region allows for a particularly clear trace of this asymmetry. In addition to spatial mapping (Haynes et al., 1998) for a few samples of galaxies, the asymmetric distribution of the HI gas has also been mapped kinematically (Schoenmakers et al., 1997; Swaters et al., 1999) and for a much larger sample, using global velocity profiles (Richter & Sancisi, 1994). Swaters et al. (2002) found this asymmetry in dwarf galaxies and star-forming regions within irregular galaxies (Heller et al., 2000).

Non-axisymmetric features in the galaxies can impact and be affected by processes at all scales. These lopsidedness significantly impact the galaxy's dynamics, their evolution, star formation, growth of the central black hole, nuclear fueling, double black hole merging and nuclear fueling of the central Active Galactic Nucleus (AGN) in the galaxy. Some internal structure like asymmetry in central region of galaxies like M31 and NGC4486B can be explained by closely examinig the dynamics of stars near the centers. A disturbance in a disc causes its center mass to shift, exerting an indirect force on its original center. A '$m = 1$' modes are supported by such disturbances inherently, which is a unique property seen exclusively in lopsided modes. Here 'm' is the azimuthal wavenumber. This characteristic adds interest and complexity to the dynamical study of these modes. Since the halo potential dominates in the outer regions of galaxies, it is plausible that the lopsided HI gas distribution may be associated with asymmetry in the halo dark matter distribution. This connection has been explored in studies like Jog (2002) and Khoperskov et al. (2012), which suggest that the interaction between baryonic matter and dark matter can play a key role in sustaining the lopsided morphology. Below, we give the details of observed asymmetries of interest for the present work.

1.1.1 Asymmetric features in nearly Keplerian disc

In the astrophysical system, various kinds of discs exist that orbit around massive objects. These could be composed of debris (solid objects) in planetary rings and planetesimal discs, gas around compact objects in binary star systems, gas or stars in galactic nuclei, etc.

The structural and kinematic characteristics of these discs in different astrophysical systems are related to their global properties. These relationships become particularly significant in various scenarios, including the formation of a galaxy and the evolution of the central BH. Understanding the dynamics of these discs is crucial, as it helps to explain their structural characteristics. The gravitational potential in these systems is typically nearly Keplerian because the disc mass ($M_{\rm d}$, say) is much smaller than the central mass (M, say).

Eccentric orbits do not precess in a purely Keplerian potential because the orbital frequency equals the epicyclic frequency. In a nearly Keplerian disc, the difference between the orbital and epicyclic frequencies is small but non-zero. The differences are due to self-gravitating system, the thermal pressure in a gas disc, or random motion in a collisionless disc. This frequency difference manifests as a precession of eccentric orbits at rates significantly smaller than the orbital and epicyclic frequencies. Hence the disc may support slow, large-scale, and lopsided modes (Kato, 1983; Lee & Goodman, 1999; Sridhar & Touma, 1999; Saini et al., 2009). These modes are the only ones with a huge size or a long wavelength. They also experience substantially less damping from collisions, Landau damping, viscosity, and other procedures that dissipate. Consequently, these modes may influence the disc's overall appearance. The slow modes in near-Keplerian discs may be the source of the non-axisymmetric features observed in many systems.

Our focus is to discuss the disc dynamics for the galaxy like M31 (figure–1.1), which, in their stellar distribution, show a $'m = 1'$ perturbed nuclear disc (Lauer et al., 1993; Bacon et al., 1994). Since the spatial extent of the perturbation is only a few parsecs, this suggests that nuclear lopsidedness may occur frequently in galaxies. With the help of the Hubble Space Telescope (HST), the asymmetrical nucleus can be seen splitted into two parts, similar to a double nucleus (Lauer et al., 1993). The bright peak (P1) is offset by 0.5" from the secondary fainter peak (P2), which almost exactly coincides with the bulge center and the location of the black hole (Kormendy & Bender, 1999). Other examples of such lopsidedness have been discovered in galaxy NGC4486B (figure—1.2)

an elliptical galaxy in the Virgo cluster (Lauer et al., 1996).

Both M31 and NGC4486B have distinct morphologies. NGC4486B is an elliptical galaxy, while M31 is a spiral galaxy. Compared to M31, NGC4486B has a physical distance between its peaks that is 5-7 times larger. Both peaks of NGC4486B are placed at identical distances from the photocenter, in contrast to M31, where the fainter peak is located within 0.5" of the photocenter. While the bulge and nucleus are separate components in M31, NGC4486B's surface brightness profile shows no indications of a single nucleus. The detection of double-peak nuclei in two physically different galaxies emphasises the necessity of a reliable theoretical model for the nucleus in which these features naturally spontaneously (Gulati, 2014).

To explain asymmetry features at the galaxy's center, Tremaine (1995) developed an eccentric disc model. According to Tremaine (2001), slow '$m = 1$' stable modes are supported by discs orbiting a central mass. The frequency of these modes are strongly associated with the strength of the collective effects, which can be velocity dispersion or either self-gravity. Afterward, many authors have worked on this problem (Sambhus & Sridhar, 2002; Peiris & Tremaine, 2003; Sridhar & Saini, 2010; Gulati et al., 2012; Gulati & Saini, 2016a,b; Bournaud, 2016; Fensch & Bournaud, 2021). Previous authors considered perturbation in stellar orbits arising due to the self-gravity of the stellar component. However, spiral galaxies also contain interstellar gas, the amount of which varies depending on the Hubble type (Young & Scoville, 1991; Binney et al., 1998). The coexistence of gas and stellar components in the central region of galaxies makes it essential to consider the perturbation in stellar orbit in presence of gas, which we aim to do in the first part of present work. In the next subsection, we describe another observation at the center of disc galaxies which is crucial while studying its dynamics.

1.1.2 Off-centerd dark matter halo in the spiral galaxies

Since the last couple of decades, research on dark matter has been quite active in scenarios like structure formation at small scales to galactic scale. This component does not emit light; hence, direct observational detection is not possible. However, this invisible element is felt because it affects the system's dynamics through gravitational interaction. According to recent studies conducted by the Planck satellite, the baryonic component is approximately 4% of the universe's total matter, whereas the dark matter component is currently estimated to be 23% (Ade et al., 2016).

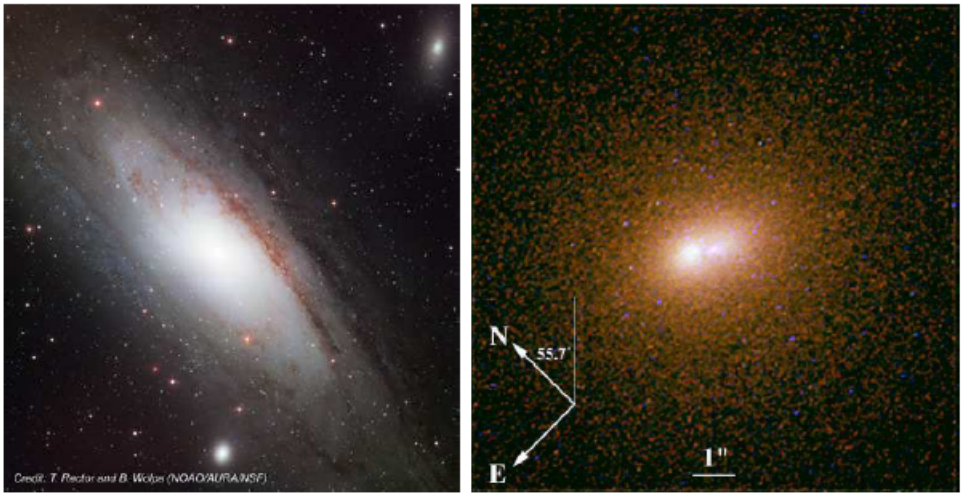

Figure 1.1: Two images of M31; The left panel is the full image of the spiral galaxy M31 (credit: T.Rector and B. Wolpa (NOAO/AURO/NSF) and the image on the right shows the central few arcsec with scale and directions indicated (Lauer et al., 1998). In the second image double peak structure is clearly apparent.

The work done by Rubin & Ford Jr (1970) gave first concrete evidence of dark matter's existence in individual galaxies. Theoretically, a stellar disc's rotation curve is expected to increase in the inner region and then decline in a Keplerian pattern. The authors observed that in stark contrast to the theoretical predictions the measured rotation curves were not seen to fall off in such a Keplerian pattern and instead stayed almost flat in the outer regions of galaxies. This increase in the velocity was attributed to the presence of dark matter.

In dwarf galaxies, which are the most common type of galaxies in the local universe, dark matter halo is relatively more massive and dominates most of the galaxy's disc (Ghosh & Jog, 2018). In the velocity fields, rotation curves, and morphology, as well as in their kinematics, it is common to see the '$cos\phi$' asymmetry in dwarf irregular galaxy (Khademi et al., 2021) or kinematic lopsidedness (a global $m = 1$ perturbation) where ϕ is the azimuthal angle in the plane of the disc (Levine & Sparke, 1998; Schoenmakers et al., 1997). A lopsided halo potential model can explain the asymmetry in the kinematic data reasonably well. A detailed study of the position of the central dark matter density peak showed the difference from the dynamical center of the galaxy (Kuhlen et al., 2013). The offset between the dynamical center and the maximum dark matter density was found

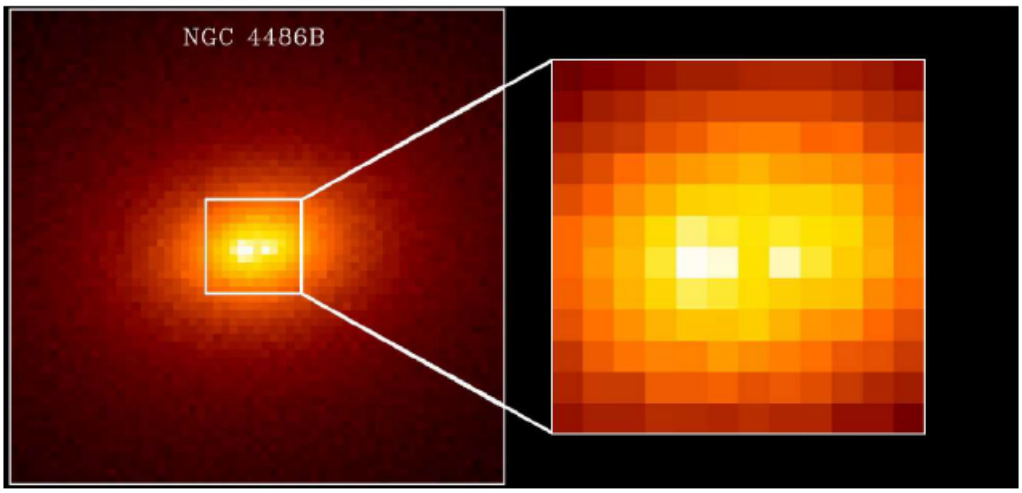

Figure 1.2: Galaxy NGC4486B image (Credit: NASA, Tod Lauer, NOAO, and Karl Gebhardt, University of Michigan). The left panel's dimensions are 2.7 arcsec in the sky, while the right panel enlarges the central 0.5 arcsec. In the right image, the light intensity can be seen separated in two different peaks.

to be around $300 - 400$ pc.

The evolution and assembly of galaxies and their environment (EAGLE) is used to measure the offset between the galaxy's core and cold dark matter (Schaller et al., 2015). The observed lopsidedness has a significant impact on the galaxy's dynamics and future evolution through a variety of processes, including angular momentum transport, nuclear fusion within the galaxy's active galactic nucleus, the expansion of the black hole at its center, and increased star formation in the over dense regions of galaxies (Jog, 1999; Jog & Combes, 2009).

Consequently, it is interesting to investigate different dynamical implications for a galactic disc with a lopsided halo potential placed on the underlying asymmetric potential. Using first-order epicyclic approximation, Prasad & Jog (2017) have studied how such an offset halo affects the orbits and kinematics in the disc's center few kpc. In their work, the stellar orbits in the core of the galaxies are restricted to be planar. A non-planar configuration is, however, intrinsic to the core of galaxies. In the next part of our work, we will generalize their model to investigate the deviation in stellar orbits due to offset in halo potential for a more realistic non-planar configuration at the center of galaxies. In the next section, we discuss a few processes pertaining to external dynamics

Figure 1.3: Ram-pressure stripping impact in removing gas from the spiral galaxy NGC 4921 and its satellite galaxies. Image credit: ICRAR / NASA / ESA / Hubble Heritage Team / STScI / AURA.

which affect the evolution of galaxies.

1.2 External dynamics Effect on the galaxies evolution

In high-density regions, various mechanisms have been proposed by authors (Boselli & Gavazzi, 2006) to explain the diverse evolution of galaxies. The cold interstellar medium (ISM) may evaporate due to the hydrodynamic interaction of galaxies with the hot surrounding intracluster medium (ICM) (thermal evaporation, e.g., Cowie & Mckee (1977)). It may be completely removed due to the external pressure of the surrounding medium exerted on the galaxy's inter-stellar medium. Various physical instabilities in the gas, such as Rayleigh-Taylor and Kelvin-Helmholtz instabilities (Roediger & Hensler, 2008), can be produced by the hydrodynamic friction at the interface between the cold ISM and the hot ICM in galaxies moving at high velocities, and helping in the removal of gas from the galaxy disc. One of the known mechanisms for gas stripping in galaxies is ram pressure (figure-1.3), which we will discuss in the next section.

1.2.1 Ram Pressure Stripping

Galaxies in rich environments are subjected to various disturbances that can significantly impact their evolution. In high-density regions, galaxies evolve differently from their counterparts in the field, is now well known (Dressler, 1980). Early-type galaxies do indeed dominate in rich environments (Postman & Geller, 1984; Dressler, 1980; Whitmore, 1992; Dressler et al., 1997) and quiescent systems (Lewis et al., 2002; Gomez et al., 2003; Peng et al., 2010). Furthermore, the late-type population exhibits systematic differences across cluster and field galaxies. In fact, spiral galaxies have a lower average atomic (Cayatte et al., 1990; Haynes & Giovanelli, 1984; Solanes et al., 2001; Gavazzi et al., 2005) and molecular gas concentration in high-density situations as compared to other objects in the field. The star formation phenomenon is consequently decreased, particularly when the molecular gas reservoir required to feed star formation is affected (Kennicutt Jr, 1983; Boselli et al., 2014; Gavazzi et al., 1998).

It was initially suggested by Gunn & Gott III (1972) that a ram pressure mechanism may be used to remove the ISM from galaxies traveling at a speed of about 1000 km/s through the dense ($\sim 10^{-3}$ – 10^{-4} atoms cm^{-3}) and hot ($\sim 10^{7}$–10^{8} K) Intra Cluster Medium (ICM). The head-tail radio galaxies' explanation (Miley et al., 1972) through the ram-pressure mechanism allow for the prediction of dense IGM in the cluster before X-ray observations actually detected it (Gursky et al., 1972). Galaxy may be depleted of all its gas from the disc if ram pressure overcomes the gravitational pressure that binds the gas to the disc (in figure–1.3).

Analytically for the ram pressure can be expressed by the relation given by Gunn & Gott III (1972) as $P = \rho_{\rm ICM} V^2$, where $\rho_{\rm ICM}$ is the ICM density, and V is the velocity of the infalling galaxies through the cluster medium. This force is acting due to the motion of galaxies relative to the diffuse gaseous ICM, as galaxies experience a wind as they orbit through it. Although the ICM is tenuous, the galaxy's rapid motion forms a massive pressure in front of it. Hydrodynamical simulation of ram pressure confirms that this analytical expression is correct for galaxies that are moving face on (Cayatte et al., 1994; Kenney & Koopmann, 1999; Acreman et al., 2003; Roediger & Brüggen, 2006). However for galaxies which are not falling face-on, before achieving a complete ablation of gas, significant compression is produced in the edge of the galaxy by ram pressure, with the possible formation of a bow shock, and a low-density gaseous tail behind, giving a comet-like shape to the galaxy (Balsara et al., 1994; Mori & Burkert, 2000; Cramer,

2020). The hydrodynamic interaction between the cold ISM and the hot IGM causes the exterior pressure to rise, forming turbulent motions, thermal instabilities, and bow shocks inside the galaxy's disc. All of these occurrences lead to more cloud-to-cloud collisions and cloud collapse, which may be the cause of cluster galaxies' increased star formation activity (Evrard, 1991; Bekki & Couch, 2003).

The environment and galaxy morphology are expected to play a substantial role in removing gas from the galaxy, which directly affects the star formation rate and the evolution of the galaxy. Ram Pressure Stripping (RPS) has been observed in various types of environments and different masses of galaxies, many authors worked on this problem (Abadi et al., 1999; Bravo-Alfaro et al., 2000; Roediger & Brüggen, 2006; Kapferer et al., 2009; Fritz et al., 2017; Köppen et al., 2018; Singh et al., 2019; Boselli et al., 2022; Hu et al., 2024; Kapferer et al., 2009). In this context, we would like to explore the amount of gas removed due to RPS if the density concentration in the form of spiral arms and magnetic fields in disc galaxies are taken into account. In the next section, we give a brief of various equations used to model the physical phenomenas discussed.

1.3 Basic equations

The fundamentals of fluid mechanics form an integral part of the study of the dynamics and formation of galaxies. The fluid (gas) and stellar components coexist in the galaxies. As a result, the constituent particles directly interact through collisions, and collisional relaxation allows for achieving thermodynamic equilibrium. So, the continuum model can be applied to the galactic systems. A fluid's state is determined by its pressure $p(\mathbf{x}, t)$, velocity field $\mathbf{v}(\mathbf{x}, t)$, and mass density $\rho(\mathbf{x}, t)$, as well as perhaps other thermodynamic functions like temperature $T(\mathbf{x}, t)$ and a specific entropy. Here, $\mathbf{x}$ is the position vector representing a point in space and t is the time. Moreover, while considering the mathematical model for the dynamical evolution of galaxies, it is sufficient to consider non-viscous fluid (Binney & Tremaine, 2011). Below we are providing the fundamental equations that govern the dynamics of non-viscous fluids. The notation and the equations in this section are being referred from Feynman et al. (1964), Choudhuri (1998), Binney & Tremaine (2011).

Continuity equation: The continuity equation is a mathematical representation of

the conservation of mass, and is stated as

$$\frac{\partial \rho}{\partial t} + \nabla.(\rho \mathbf{v}) = \mathbf{0}, \tag{1.1}$$

where $\mathbf{v}$ is the fluid velocity and ρ is mass density.

Euler equation: In fluid dynamics, Euler's equation explaining fluid's flow for non-viscous fluids is given by:-

$$\frac{\partial \mathbf{v}}{\partial t} + (\mathbf{v}.\nabla)\mathbf{v} = -\frac{\mathbf{1}}{\rho}\nabla \mathbf{p} + \mathbf{F}, \tag{1.2}$$

where $\mathbf{p}$ indicates the fluid pressure and external force per unit mass is denoted by $\mathbf{F}$. Pressure will be assumed isotropic in the present work as we will only deal with ideal fluids.

Equation of State: We require the equation of state $p = p(\rho, s)$ or $p = p(\rho, T)$ to relate the pressure and density. The simple example of a barotropic equation of state, where the density governs the pressure, is typically sufficient for our purposes, i.e.,

$$p = p(\rho). \tag{1.3}$$

For state to be represented by barotropic equation's a best example is when the fluid is adiabatic and has constant specific entropy. A complete collection of equations for ideal fluids is formed using these equations and the relevant boundary conditions.

Poisson equation: In place of the equation of state, the Poisson equation for a self-gravitating system provides a relationship between the system's mass density and its gravitational potential, forming a complete set of equations for modelling galactic systems. When a particle experiences force $\mathbf{F}$ from the rest of the system's gravitational pull, with a mass density of ρ, $\mathbf{F}$ may be written as $-\nabla \mathbf{\Phi}$. Where the gravitational potential is denoted by Φ. The equationof Poisson is derived from the Newtonian theory of gravity, and it connects density and gravitational potential by the expression,

$$\bigtriangledown^2 \Phi = 4\pi G\rho, \tag{1.4}$$

The integral form of the above equation is known as the Poisson integral, as given by,

$$\Phi = -G \int d^3x' \frac{\rho(x')}{\mid x' - x \mid}. \tag{1.5}$$

Tight-winding approximation: The self-gravity of the galactic disc is the biggest obstacle to perform a global modal analysis within the disc. Dealing with gravitational forces is exceedingly difficult due to their long-range nature, which causes all of the disturbances in the different sections of the galaxy disc to be interconnected. The WKB (Wentzel, Kramers, Brillouin) approximation, also known as the tight-winding approximation or the quasi-classical approximation, has proven to be a useful tool for examining the characteristics of the density waves in a differentially rotating disc. The WKB approximation is stated as:-

$$\frac{d\lambda}{dx} \ll 1, \tag{1.6}$$

or

$$\left| \frac{1}{k^2} \frac{dk}{dx} \right| \ll 1. \tag{1.7}$$

Where λ is the wavelength and k is radial wavenumber. This criterion, indicates that the particle's wavelength must vary slightly along large distance.

Equation of motion for stellar orbits: A star's motion in a galaxy is determined by its gravitational potential Φ, typically considered stationary without collisions. If we consider the star's position as (R, ϕ, Z) and velocity as $(\dot{R},\ \dot{\phi},\ \dot{Z})$ in a cylindrical coordinate system, the equation of motion (calculated using Newton's second law of motion) can be expressed as:

$$\frac{d^2R}{dt^2} = R\dot{\phi}^2 - \frac{\partial \Phi}{\partial R}, \tag{1.8}$$

$$\frac{d}{dt}(R^2\dot{\phi}) = -\frac{\partial \Phi}{\partial \phi}, \tag{1.9}$$

$$\frac{d^2Z}{dt^2} = -\frac{\partial \Phi}{\partial Z}. \tag{1.10}$$

Under steady-state and axisymmetric potentials, the terms with $\partial/\partial t$ or $\partial/\partial\phi$ are equal to zero.

Eppicyclic approximation: To find solutions of equations-(1.8) to (1.10) for nearly circular orbits in three dimensions, the motion equations can be integrated under certain minimum number of assumptions, such as axial symmetry and symmetry plane, in a particular case known as the epicycle approximation. This approach states that every orbit projected onto the symmetry plane depicts an ellipse that originates from the guiding center or epicenter and revolves uniformly around the system's center in a circular orbit. The model relates interesting features of the star motion: the axial ratio of the

planar epicycle, which depends only on local potential features, the planar and vertical epicycle frequencies, and the properties of the local stellar velocity distribution and their relationship to eccentricity statistics.

Assumptions for Epicyclic Approximation:

1. **Perturbations Around Circular Orbit:** The system is considered to be in a nearly circular orbit, i.e, the orbits deviate slightly (epicyclic motion) from the circular path.

2. **Axially Symmetric Gravitational Potential:** The gravitational potential is assumed to be axisymmetric, meaning it depends only on the radial distance from the center and not on the angular coordinate.

3. **Linearized Equations of Motion:** The equations of motion are linearized around the equilibrium circular orbit to simplify the analysis of small perturbations.

The radial motion is governed by the epicyclic frequency κ, which describes small oscillations around the circular orbit. Expanding the gravitational potential $\Phi(R, Z)$ around the equilibrium radius of circular orbits R_0 and linearized radial equation of motion gives,

$$\frac{d^2R_1}{dt^2} + \kappa^2 R_1 = 0, \tag{1.11}$$

where the term of the epicyclic frequency κ is:

$$\kappa^2 = \left(4\Omega^2 + R\frac{d\Omega^2}{dR}\right)_{R=R_0, Z=Z_0},$$

with $\Omega = v_c/R$, the angular velocity for circular orbit and v_c being the circular velocity. The azimuthal motion is described by the perturbations in angular velocity as:

$$\frac{d^2\phi_1}{dt^2} + 2\Omega(R_0)\frac{dR_1}{dt} = 0, \tag{1.12}$$

the vertical oscillations around the mid-plane $Z_0 = 0$ are governed by the vertical frequency ν, which describes harmonic motion in the Z-direction. Expanding the vertical equation of motion around $Z_0 = 0$ leads to:

$$\frac{d^2Z_1}{dt^2} + \nu^2(R_0)Z_1 = 0. \tag{1.13}$$

Here the vertical oscillation frequency ν is given by:

$$\nu^2(R_0) = \left(\frac{\partial^2 \Phi}{\partial Z^2}\right)_{R=R_0, Z=Z_0},$$

This describes the vertical oscillations above and below the galactic plane.

Epicyclic Frequency for Keplerian disc:
In a Keplerian disk, the rotation curve follows $v_c \propto R^{-0.5}$, where v_c is the circular velocity and r is the radial distance from the center. The epicyclic frequency (κ) is equal to the angular velocity (Ω) and is given by:

$$\kappa = \Omega = \sqrt{\frac{GM}{R^3}}$$

where:

- G is the gravitational constant,
- M is the central mass,
- R is the radial distance.

This implies that the epicyclic frequency decreases with increasing distance from the center in a Keplerian disk (Binney & Tremaine, 2011).

Epicyclic Frequency for Flat Rotation Curve:
In a flat rotation curve, the circular velocity remains constant ($v_c = v_0$) as the radial distance increases. The epicyclic frequency (κ) is given by:

$$\kappa = \sqrt{2} \cdot \Omega = \sqrt{2} \cdot \frac{v_0}{R}$$

where:

- v_0 is the constant circular velocity,
- R is the radial distance.

The flat rotation curve is often observed in the outer regions of galaxies, dominated by dark matter, where the circular velocity does not decrease (Binney & Tremaine, 2011).

1.4 Objectives of the Thesis

The present thesis will address the following objectives, the rationales of which are discussed in detail in previous sections.

- **Objective 1:** Derive and analyse the WKB-dispersion relation for a gravitationally coupled gas and stellar disc.
- **Objective 2:** Analyse the effect of off-set in the dark matter halo on 3-dimensional stellar orbits.
- **Objective 3:** Effect of clumping in gas discs on the Ram pressure stripping.

1.5 Organization of the Thesis

This thesis' primary contribution is to study the galaxy's evolution and dynamics. A galaxy contains stars, gas, dust, bulge, and a black hole at the center, and all these affect it's evolution. Different aspects of dynamical processes can lead to different phenomena like BH growth, star formation, the lopsidedness of stellar orbits at centers of galaxies, etc. We shall explore a few of these dynamical processes in the current thesis. In the current chapter (i.e., Chapter 1), we have given an introduction to the subject matter, a review of the literature, basic definitions, and equations, thesis objectives, and a brief summary of the contents of the various chapters of the thesis. The rest of the thesis consists of five more chapters and is organized as follows:

Chapter 2: Jalali (2013) combined gas disc and particle disc, perturbed only particle disc under the assumption that the gas mass is much larger than the particle mass. They found such systems to be unstable. Their analysis is applicable only to the planetary system and helps in understanding planet formation but is not applicable to the galactic system. This assumption translates to $M_{\rm g}/M_{\rm s} \gg 1$, where $M_{\rm g}$ and $M_{\rm s}$ are the masses in the gaseous and particle components of the disc, respectively. Later Kaur (2018) worked in the opposite limit, i.e., $M_{\rm g}/M_{\rm s} \ll 1$, which is a relevant limit for galactic systems. They perturbed only stellar discs and derived the WKB dispersion relation. The approximation of perturbing only the particle component, not the gaseous disc, is adopted from Jalali (2013). Kaur (2018) found that the stellar discs are stable to non-axisymmetric perturbations. The gas component contributes only to unperturbed potential, affecting the rotational velocity of the unperturbed disc. This supports the preceding work in for

considering only stellar discs to study the behavior of asymmetric perturbations. In this chapter, we provide a simple analytic model of nearly Keplerian modes, for co-rotating gravitationally coupled gaseous and stellar discs. We restrict our analysis to '*slow modes*'; their eigenfrequencies being much smaller than the Keplerian orbital frequency to the disc. The dispersion relation using the Wentzel-Kramers-Brillouin (WKB) approximation is formulated and the stability of modes is explored. The presence of gas is found to enhance the instability and slow modes exists only for azimuthal wavenumber, $m = 1$ for the continuum disc.

Chapter 3: In this chapter, we study how stellar orbits at the galaxy's central region are disturbed by an asymmetric dark matter halo potential. Evidence from the observations and simulations in the Milky Way type galaxy suggests that the center of the dark matter halo could be off-centered by a few parsecs concerning the center of the core. The influence of offset in the DM potential halo on orbits and kinematics in the disc's central few kpc was investigated by Prasad & Jog (2017). They discovered that the offset halo causes a considerable disturbance in stellar orbits across the central few kpc by deriving equations of motion in the disc plane in terms of the disc and halo potentials. However, the model given by Prasad & Jog (2017) is restricted only to disc at the centers of galaxies. In this chapter, we generalize their model to examine the offset at the central region (bulge+black hole) of the galaxy in non-planar space, which is a more appropriate model for centers of spiral galaxies.

Chapter 4-5: An analytical expression for Ram pressure was introduced by Gunn & Gott III (1972), given by $P = \rho_{\rm ICM} V^2$, where $\rho_{\rm ICM}$ is the ICM density and V is the velocity by which galaxy is falling in the cluster medium. Singh et al. (2019) did a systematic study of the effect of environment and galaxy parameters on the ram pressure stripping in galaxies. Their study used different types of environments and different galaxy mass profiles at different redshifts. Apart from different masses of infalling galaxies, the galactic asymmetries would also play an important role in quantizing the effect of ram pressure. Motivated by this, in Chapter-4 we calculate the extent of gas removed due to ram pressure in the presence of Spiral arms in disc galaxies. This will act as a restoring force. Spiral arms will contribute toward the gravitational binding force in form of asymmetries, and restoring force will depend on the number of arms, arm strength, spiral pitch angle, etc.

Observations and studies of galaxies indicate that the magnetic field is an intrinsic component of spiral galaxies embedded with the spiral arms. The presence of the magnetic

field in the galaxies is also detected from (polarized) radio continuum emission and Faraday rotation measurements (Beck, 2016). Star formation rate also depends on the magnetic and cosmic-ray pressure (Birnboim et al., 2015) for gas dynamics of a molecular cloud; magnetic fields are also found to be essential (Ade et al., 2016). The magnetic field, being intrinsic to galaxy evolution, can not be ignored when quantizing the effect of ram pressure. So, in Chapter-5, we study the effect on ram pressure in the presence of magnetic field in disc galaxies. The magnetic field will act as a binding force and is assumed to be along the spiral arms for the present work (Alfven, 1942a).

Chapter 6: We summarize the results discussed in the earlier chapters and their conclusions and inferences. The major outcomes of the thesis revolve around the analysis of the galaxies' structures and their evolution depending on the different aspects of phenomena. We also discuss the future scope of the current work.

Chapter 2

Enhanced $m = 1$ WKB instabilities in nearly Keplerian stellar discs due to the presence of gas

2.1 Introduction

Galactic dynamics forms the cornerstone of our understanding of how stars and gas interact under the influence of gravity within galaxies. Stellar dynamics introduces fundamental concepts such as epicyclic frequencies, which describe the radial oscillation of stars around their circular orbits, and provide a key framework for analyzing perturbations in galactic discs. The spiral density wave theory explains the persistence of spiral structures as density enhancements, while the Toomre stability criterion evaluates a disc's susceptibility to gravitational instabilities by considering parameters like surface density, velocity dispersion, and epicyclic frequency. These theoretical tools are indispensable for interpreting the structural and dynamical features observed in galaxies. In particular, non-axisymmetric structures, such as spiral arms and lopsidedness, are prevalent in galaxies and significantly affect their evolution. Lopsidedness, characterized by an $m = 1$ azimuthal perturbation, refers to asymmetries in the distribution of mass and light and is observed not only in the outer regions of galaxies but also in their central nuclei. The centers of galaxies, such as M31 and NGC4486B, exhibit intriguing features, including double-peak nuclei, where one peak is brighter than the other. The origin of such nuclear structures has sparked extensive debate and study. The interpretation of

these double peaks as the result of an eccentric nuclear disc is one of several possibilities.

Tremaine (1995) proposed that the off-centered peaks present at the center of the galaxy M31 are formed by eccentric orbits of stars at the center of the disc. They demonstrated that eccentric orbits in the discs could describe main features in the nucleus of M31, and eccentricity in an initially axisymmetric disc arises from lopsided $m = 1$ lopsided perturbations. However, alternative explanations, such as the possibility that one of the peaks represents the remnant of a recent merger of a smaller stellar system, must also be considered. Peiris & Tremaine (2003) conducted a detailed analysis of eccentric nuclear discs, providing a framework to interpret double nuclei. Their work emphasizes the importance of considering various scenarios, from spontaneous instabilities to external triggers such as mergers. The spatial extent of perturbations in nuclear discs is typically a few parsecs, suggesting that such lopsidedness may be more common than previously thought. Tremaine (2001) studied the behavior of slow modes using the softened self-gravity disc, using both the WKB approximation and the numeric solution of the linear eigenvalue equation. The WKB (Wentzel-Kramers-Brillouin) approximation is a semi-analytical method used to analyze wave-like perturbations in systems where the parameters vary slowly. It is particularly useful in this study for simplifying the analysis of density waves and instabilities in nearly Keplerian systems. This method enables us to linearize and solve complex equations governing the dynamics of the disc, providing valuable insights into the coupling between stellar and gaseous components."

After Tremaine many authors worked on this problem (Bacon et al., 2001; Sambhus & Sridhar, 2002; Salow & Statler, 2001). The interesting question is that how these eccntric orbits are formed was answered by Sambhus & Sridhar (2002) & Touma (2002). They concluded that the lopsided modes could arise from the instabilities generated due to the presence of a small percent of stars in retrograde orbits in the disc at center of galaxies. Touma (2002) showed that a nearly Keplerian disc is unstable to $m = 1$ mode when a certain percentage of disc mass is present in a retrograde orbit. Systematic analysis of properties of these counter-rotating discs eccentric modes was further done by Sridhar & Saini (2010). They studied slow modes in Keplerian stellar discs modeled using softened gravity discs of collisionless counter-rotating matter, using WKB techniques, giving the properties of eigen-spectra for equal counter- rotation. Further Gulati et al. (2012) discussed the nature of these modes by formulating the eigenvalue problem for two-component, softened gravity counter-rotating disc and analyzed the behavior of eigenvalues and eigenfunctions. Both these approaches had certain limitations; for

instance, only slow modes for azimuthal wave number $m = 1$ were supported. Collisionless particle discs, however, support the modes with azimuthal wave-number other than unity as shown by Jalali & Tremaine (2012). This was further analyzed by Gulati & Saini (2016b) for counter-rotating discs. Properties of slow modes have been studied extensively to date. All the work that has been done so far:

- Have modelled stellar discs as continuous softened gravity discs, where the softening length serves as a proxy for stellar velocity dispersion, or
- By considering a particle disc in local thermodynamic equilibrium, with stellar orbits are given by epicyclic approximation.

All these have considered perturbation in stellar orbits arising due to the self-gravity of the stellar component only. However, spiral galaxies also contain interstellar gas, the amount of which varies depending on the Hubble type Young & Scoville (1991); Binney et al. (1998). The significance of gas in galactic dynamics has been examined in a variety of scenarios, and it has been demonstrated that this low-velocity dispersion component, has a significant effect on stability against both local axisymmetric and non-axisymmetric perturbations(Jog & Solomon, 1984b,a; Jog, 1992; Rafikov, 2001). For gravitationally connected stars and gas as in case of a galactic disc, Jog (1996) found the condition for local stability against axisymmetric perturbations, in which stars have higher velocity dispersion than the gas.

In this chapter we formulate the WKB dispersion relation for coupled particle and gas disc when the stellar mass dominates and analyze the behavior of such modes, considering the disturbance in both particle and gas disc. The WKB approximation is vital for this study because it allows the examination of coupled instabilities in nearly Keplerian discs by simplifying the dynamics into manageable analytical forms. Assuming sinusoidal variations of perturbations over small regions it enables us to derive the dispersion relation and study the role of gas in enhancing $m = 1$ instabilities. We start with unperturbed gravitationally coupled co-rotating stellar and gas discs in section–2.2, we discuss the equilibrium solution and discuss the variation of precession in the orbits of stars due to the presence of gas in section–2.3. Section–2.4 is an account of the linearly perturbed disc, we derive the WKB dispersion relation, and in section–2.5, we discuss the stability of the coupled disc. We specialize to slow mode next in section–2.6 and the nature of eigenmodes and the properties of discrete spectrum calculated using

Bohr-Sommerfeld quantization condition is discussed in section–2.7 and 2.8. Lastly, we conclude and discuss our result in Sect–2.9.

2.2 Unperturbed discs

We consider linear non-axisymmetric perturbations in gravitationally coupled co-rotating stellar and gas discs. The gas disc is considered to be a continuous non-viscous fluid disc, orbiting the massive central body. The validity of the assumption of ignoring viscosity comes from the fact that evolution timescales for slow modes are much larger than the rotation period over which viscosity helps in spreading the gas radially via accretion mechanisms (Saini et al., 2009). Hence the contribution of viscosity in the evolution of slow modes can be ignored. The stellar disc is assumed to be a softened gravity disc (Miller, 1971). The softened gravity discs are known to mimic the self-gravitating stellar discs (Binney & Tremaine, 2008). In the rest of the section, we explain the unperturbed disc configuration in detail.

We shall work in cylindrical polar co-ordinates (R, ϕ) in $z = 0$ plane. The parameters defined with an additional subscript 'g' and 's' imply that these correspond to gas and stellar disc, respectively. The continuity equation for individual components in disc plane can be expressed as,

$$\frac{\partial}{\partial t}\left(\Sigma_{\rm g/s}\right) + \frac{1}{R}\frac{\partial}{\partial R}(R v_R \Sigma_{\rm g/s}) + \frac{1}{R}\frac{\partial}{\partial \phi}(v_\phi \Sigma_{\rm g/s}) = 0. \tag{2.1}$$

The Euler's equation for the gas disc are given by,

$$\frac{\partial v_R}{\partial t} + v_R\frac{\partial v_R}{\partial R} + \frac{v_\phi}{R}\frac{\partial v_R}{\partial \phi} - \frac{v_\phi^2}{R} = -\frac{\partial \Phi}{\partial R} - \frac{1}{\Sigma_{\rm g}}\frac{\partial P}{\partial R}, \tag{2.2}$$

$$\frac{\partial v_\phi}{\partial t} + v_R\frac{\partial v_\phi}{\partial R} + \frac{v_\phi}{R}\frac{\partial v_\phi}{\partial \phi} + \frac{v_\phi v_R}{R} = -\frac{1}{R}\frac{\partial \Phi}{\partial \phi} - \frac{1}{\Sigma_{\rm g} R}\frac{\partial P}{\partial \phi}, \tag{2.3}$$

The corresponding components of Euler's equation for stellar disc are given by,

$$\frac{\partial v_R}{\partial t} + v_R\frac{\partial v_R}{\partial R} + \frac{v_\phi}{R}\frac{\partial v_R}{\partial \phi} - \frac{v_\phi^2}{R} = -\frac{\partial \Phi}{\partial R}, \tag{2.4}$$

$$\frac{\partial v_\phi}{\partial t} + v_R\frac{\partial v_\phi}{\partial R} + \frac{v_\phi}{R}\frac{\partial v_\phi}{\partial \phi} + \frac{v_\phi v_R}{R} = -\frac{1}{R}\frac{\partial \Phi}{\partial \phi}. \tag{2.5}$$

where Σ_g and Σ_s are the surface density of the gas and stellar disc, respectively. v_R and v_ϕ are the radial and azimuthal components of the disc velocity. The velocity of gas and stellar discs are the same as both the discs are assumed to be co-rotating. Φ is the total gravitational potential, and P is the pressure of the gas.

We are interested in working in the limit $M_g/M_s \ll 1$, this will restrict our analysis to galactic systems and not applicable to accretion discs around compact stellar objects or protoplanetary systems. For gas in thermodynamic equilibrium, this would translate to the condition $P \ll \Phi$, i.e., gas pressure is much smaller than the total gravitational potential. Reason for the same is that the pressure term will be proportional to the sound speed and the potential term will be proportional to the rotational velocity. For galactic systems not undergoing any mergers and at scales comparable to the galactic scales, sound speed can be neglected as compared to the galactic rotation (Binney & Tremaine, 2008), we hence neglect the pressure term in equation (2.2)–(2.3).

The unperturbed disc is assumed to be steady, axisymmetric, and having only differential rotation with no radial velocity. These assumptions reduce eqns. (2.1)– (2.5) to standard equation defining the rotational velocity,

$$v_\phi = \sqrt{R\frac{\partial \Phi}{\partial R}}. \tag{2.6}$$

The potential 'Φ' at any point is the sum of Keplerian potential due to central mass M and the potential due mass distribution in the disc, i.e.

$$\Phi(R, \phi) = \frac{-GM}{R} + \Phi_d(R, \phi), \tag{2.7}$$

where, $\Phi_d = \Phi_{dg} + \Phi_{ds}$, is the sum of potential arising from the self gravity of gas disc and stellar disc. The gravitational potential of each component is calculated from the respective surface density using Poisson's equation. The unperturbed system is assumed to be axisymmetric, and hence the $\partial/\partial\phi$ is zero, i.e., for unperturbed disc Φ_d is only a function of the radial coordinate R. We shall next discuss the rate of precession for the coupled unperturbed disc.

2.3 Precession rate for coupled disc

For nearly Keplerian limit, i.e., for $M_{\rm g} + M_{\rm s} \ll M$, without loss of generality the origin of the coordinate system can be taken as the position of mass M. If $\Omega(R) \geq 0$ is the azimuthal frequency and $\kappa(R) \geq 0$ is the radial frequency, associated with nearly circular orbits, then apsides of the nearly circular orbit of a coupled system precesses at a rate given by

$$\begin{aligned}\dot{\varpi}(R) &= \Omega(R) - \kappa(R) \\ &= -\frac{1}{2\Omega(R)}\left(\frac{\mathrm{d}^2}{\mathrm{d}R^2} + \frac{2}{R}\frac{\mathrm{d}}{\mathrm{d}R}\right)\Phi_d(R) + O(\epsilon^2). \end{aligned} \tag{2.8}$$

Here the term '$O(\epsilon^2)$' indicates higher-order terms in small quantity $\epsilon \sim (M_{\rm g} + M_{\rm s})/M$. The dominant terms in $\dot{\varpi}$ are the linear in ϵ. Neglecting the higher order terms we shall restrict our analysis to slow modes with mode frequency $\omega \sim \dot{\varpi} \sim \epsilon$ (Tremaine, 2001; Saini et al., 2009; Gulati et al., 2012).

To illustrate the effect of gas on the unperturbed system, we consider a centrally concentrated unperturbed disc. We shall take the surface density of gas and stellar discs to be given by Kuzmin disc profiles. The surface density and potential pair for the same is given by

$$\Sigma_{\rm g/s}(R) = \frac{aM_{\rm g/s}}{2\pi(R^2 + a^2)^{3/2}}, \tag{2.9}$$

$$\Phi_{\rm g/s}(R) = \frac{-GM_{\rm g/s}}{(R^2 + a^2)^{1/2}}, \tag{2.10}$$

where a is the disc scale length and for simplicity, we have assumed it to be the same for both the discs. Using eqn. (2.8), the precession rate of the coupled disc is given by,

$$\dot{\varpi} = \frac{-3a^2GM_{\rm s}}{2\Omega(R)(R^2 + a^2)^{5/2}}(\eta + 1), \tag{2.11}$$

Here we are taking $M_{\rm g}/M_{\rm s} = \eta$, as the fraction of gas mass present as compared to the stellar mass. The precession rate scales with η as $(1+\eta)$. The orbital frequency and surface density are normalized in the units of $\Omega^* = \sqrt{GM/a^3}$, and $\Sigma^* = M_{\rm s}/a^2$ in eqn (2.11) to make it dimensionless. In doing the same, the radial co-ordinate gets

transformed to R/a and is replaced by R in eqn. (2.11) for simplicity. The precession rate is plotted as a function of radial coordinate in figure (2.1) for different values of η. Linear scaling with increasing gas mass can clearly be seen. The maximum value of the magnitude of $\dot{\varpi}$ increases with η-value indicating the possibility of the higher value of mode frequency due to the presence of gas. In the next section, we shall now formulate the dispersion relationship for the linearly perturbed coupled system of gas and stars.

2.4 Formulation of the linear dispersion relation

Though we do our analysis in the context of galaxies (and hence the terminology), however, the dispersion relation derived here is valid for a more general case of a two-component coupled disc in equilibrium where one component behaves like a fluid, and the other is more like a particle disc and the gas pressure can be neglected in comparison to the discs self-gravity. We now formulate the linear dispersion relation for the system described in the previous section. Infinitesimal perturbations are taken in the velocity field and surface densities. We linearly perturb the Euler and continuity equation for stellar and gas discs. Any physical quantity (X) which is perturbed is assumed to be sum of unperturbed (X_0) and the perturbed component (X_1), i.e. $\mathrm{X} = X_0 + \epsilon X_1$. Here, ϵ is the parameter which is much smaller than unity. We shall ignore the higher order terms in ϵ, keep only linear terms in equation (2.1)– (2.5) and use eqn. (2.6) to simplify. The perturbations are then assumed to be of the form $X_1 = X_a(R)\exp[i(m\phi - \omega t)]$, where m is the azimuthal wave number and ω is the temporal frequency of the modes. Following the algebra, equation (2.1)–(2.5) gives,

$$i(m\Omega - \omega)\Sigma_{\mathrm{ag/s}} + \frac{1}{R}\frac{d}{dR}(R\Sigma_{0g/s}v_{Ra}) + \frac{im\Sigma_{0g/s}}{R}v_{\phi a} = 0, \tag{2.12}$$

$$v_{Ra}(R) = -\frac{i}{D}\left[(m\Omega - \omega)\frac{d\Phi_a}{dR} + \frac{2m\Omega}{R}\Phi_a\right], \tag{2.13}$$

$$v_{\phi a}(R) = \frac{1}{D}\left[\frac{\kappa^2}{2\Omega}\frac{d\Phi_a}{dR} + m\frac{(m\Omega - \omega)}{R}\Phi_a\right], \tag{2.14}$$

where

$$D = \kappa^2 - (m\Omega - \omega)^2. \tag{2.15}$$

The radial variation of the perturbed quantities is than assumed to be of the form

$$X_a(R) = X'_a(R) \exp\left[i \int^R k dR\right],$$

where $X'_a(R)$ is a slowly varying function of R, whose variation can be neglected for all practical purposes. Along with this, we employ the Wentzel-Kramers-Brillouin (WKB) approximation (or tight winding approximation) for local stability analysis. The underlying condition for WKB approximation (also discussed in Chapter-1) is $|kR| \gg m$ (Binney & Tremaine, 2008). In comparison to terms proportional to k, this approximation allows us to ignore terms proportional to 1/R. Equations (2.12)–(2.14) are further simplified using this approximation to obtain

$$\Sigma_{\mathrm{ag/s}} = -k^2 \frac{\Sigma_{0g/s}}{D} \Phi_a, \tag{2.16}$$

$$v_{Ra} = \frac{(m\Omega - \omega)}{D} k \Phi_a, \tag{2.17}$$

$$v_{\phi a} = \frac{\kappa^2}{2\Omega D} k \Phi_a. \tag{2.18}$$

The WKB density perturbation may be thought of locally as a plane wave with wavenumber $\mathbf{k} = k\mathbf{e_R}$, where $\mathbf{e_R}$ is the radial unit vector. The gravitational potential from the density distribution of a tightly wrapped spiral perturbation, in the neighborhood of an arbitrary point, for the local stability analysis can be calculated using the Poisson equation. Thus determining the gravitational potential due to stellar and gaseous components for a WKB disturbance is similar to determining the gravitational potential of a planar density wave given in Binney & Tremaine (2008) and are given by

$$\Phi_{as} = \frac{-2\pi G \exp(|k|b)}{|k|} \Sigma_{as}, \tag{2.19}$$

Here the parameter b is the softening length.

$$\Phi_{ag} = -\frac{2\pi G \Sigma_{ag}}{|k|}, \tag{2.20}$$

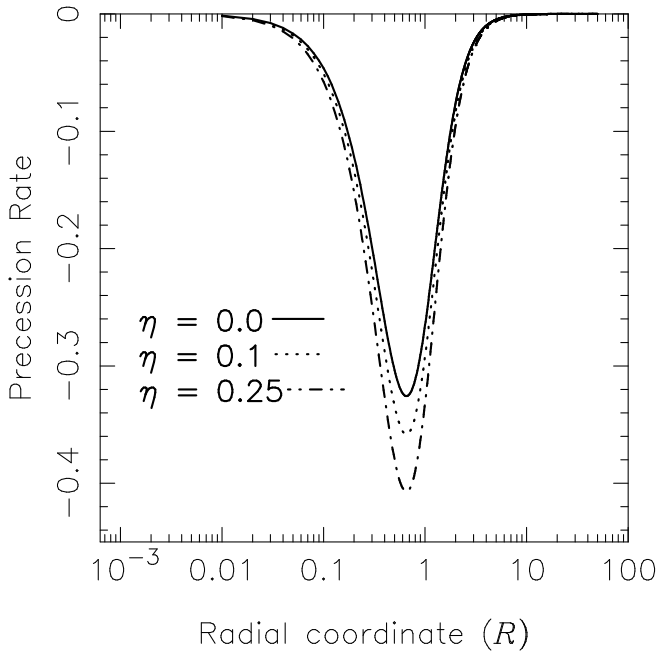

Figure 2.1: Plot of Precession rate as a function of dimensionless radial coordinate for the Kuzmin disc for different values of η.

Σ_{as} and Σ_{ag} are the radial parts of the perturbed surface density of stellar and gas disc, respectively. Since the potential is a scalar quantity, the net perturbed potential at any point is the sum of perturbed potential due to stellar and gas disc,

$$\Phi_a = \frac{-2\pi G}{|k|}\left[\Sigma_{ag} + \exp(-|k|b)\Sigma_{as}\right]. \tag{2.21}$$

Substituting the value of Σ_{ag} and Σ_{as}, from eqn.(2.16) we get the WKB dispersion relation for gravitationally coupled stellar and gas disc as,

$$D = 2\pi G|k|\left[\Sigma_{0g} + \exp(-|k|b)\Sigma_{0s}\right]. \tag{2.22}$$

This is clearly a quadratic equation in ω, allowing the system to be unstable. In the next section, we shall discuss stability for the system from the dispersion relation derived.

2.5 Stability analysis

Analyzing the dispersion relation for stability against the perturbation is one of the strongest tools giving the evolution of the system. The form of dispersion relation derived

suggests that the disc is stable to non-axisymmetric perturbations if it is stable for $m = 0$ perturbations. For $m = 0$ equation (2.22) gives

$$\omega^2 = \kappa^2 - 2\pi G|k| \left[\Sigma_{0g} + exp(-|k|b)\Sigma_{0s}\right]. \tag{2.23}$$

Since all the terms on the right-hand side are real, then the disc is stable against local disturbance if $\omega^2 \geq 0$ and unstable otherwise.
The neutral stability curves, i.e., the line for $\omega = 0$, for axisymmetric tightly wrapped spiral density waves divides the parameter space of the unstable region from the stable one. The value of ω^2 is unchanged under the transformation $k \to -k$, hence it is sufficient to analyze the stability for $k \geq 0$.

- for $k = 0$, $\quad \omega^2 = \kappa^2 \geq 0$ this implies that modes are stable.
- for $k > 0$, we need to find the condition of stability so that $\omega^2 \geq 0$.

Solving $d\omega^2/dk = 0$ provides the solutions for the critical value of wavenumber, k, This divides the range of k for stable and unstable modes. Applying this condition for our model in equation–(2.23), we get the expression $\exp(-kb) = -\eta/(1 - kb)$, this can not be solved analytically for value of k. Numerical methods must be used to find solutions for k. So we will analyze the stability using the neutral stability lines for $\omega = 0$, by using the same Toomre Q parameter for a single softened gravity disc which is given Erickson (1974). The Toomre Q-parameter is introduced as an alternative measure of it provides a dimensionless criterion for the gravitational stability of rotating discs. While the dispersion relation assesses the growth or dissipation of perturbations through wave dynamics, the Q-parameter offers a simplified yet powerful diagnostic to evaluate the overall stability of the disc against axisymmetric perturbations. A $Q < 1$ indicates instability, where self-gravity dominates over stabilizing forces, while $Q > 1$ denotes stability. We shall write the critical wavelength by using $k_c = \kappa^2/2\pi G\Sigma_{0s}$ and $\lambda_c = 2\pi/k_c$. This is the maximum unstable wavelength for a fluid disc with zero sound speed in Newtonian gravity (Dobbs & Baba, 2014). We have chosen the same value of k_c as no analytical solution of $d\omega^2/dk = 0$ exists. Note that using this value of λ_c, the allowed values of λ/λ_c for our analysis to go beyond unity. The solution of $\omega = 0$ line

from eqn-(2.23) can be then written in dimensionless form to get,

$$\frac{Q}{e} = -\left|\frac{\lambda}{\lambda_c}\right| \left[log\left(\left|\frac{\lambda}{\lambda_c}\right| - \eta\right)\right], \tag{2.24}$$

where η is the ratio, Σ_{0g}/Σ_{0s}. Note that this definition of η is same as used in section-2.3, for the disc profile considered there. In figure-2.2 solid line depicts the neutral curves for various values of η taken as constant. $\eta = 0$ means no gas is present in the disc of the galaxy, which is similar to the one studied by Tremaine (2001). The region below the curve in each figure gives the instability parameter space. It is clearly evident that the presence of gas has a considerable effect on the stabilization of the entire coupled star-gas disc. The presence of gas enhances the instabilities and makes the discs more susceptible to the formation of unstable lopsided distributions. This conclusion is similar to the result found by Jog & Solomon (1984b); Jog (1996). The range λ/λ_c can be calculated from eqn- (2.24). For $\lambda > 0$, Q is not defined if $\lambda/\lambda_c - \eta < 0$, giving a lower bound on λ value to be '$\eta\lambda_c$'. These are shown in figure (2.2) with dotted lines for $\eta \neq 0$. Also for $\lambda/\lambda_c - \eta > 1$ the Q value will become negative giving the upper bound on λ to be $\lambda_c(1 + \eta)$. The net effect is a shift in the critical wavelength of WKB-modes by a factor of '$\eta\lambda_c$', which is a function of gas mass in the disc. An immediate consequence of this is that a higher gas mass fraction would allow the formation of stronger asymmetries in the disc, arising due to the perturbation with larger wavelengths. In the next section, we shall study the properties of discrete modes calculated by solving the dispersion relation numerically coupled with the Bohr-Sommerfeld quantization condition.

2.6 Eigen-spectra for slow $m = 1$ modes

A unique characteristic of eccentric orbits is that they do not precess in the Keplerian potential due to 1:1 resonance between the radial and azimuthal frequencies. This implies that the evolution of the eccentricity distribution in an isolated nearly Keplerian disc is dictated by the disc's non-keplerian contributions, no matter how small it is (Tremaine, 2001; Jalali & Tremaine, 2012). For continuous disc (as in our case), the discrete slow modes exists for only $m = 1$ as shown by Jalali & Tremaine (2012). We shall apply the slow modes condition i.e. $\omega/\Omega \sim (M_g+M_s)/M \sim \epsilon \ll 1$ i.e. perturbation frequency is

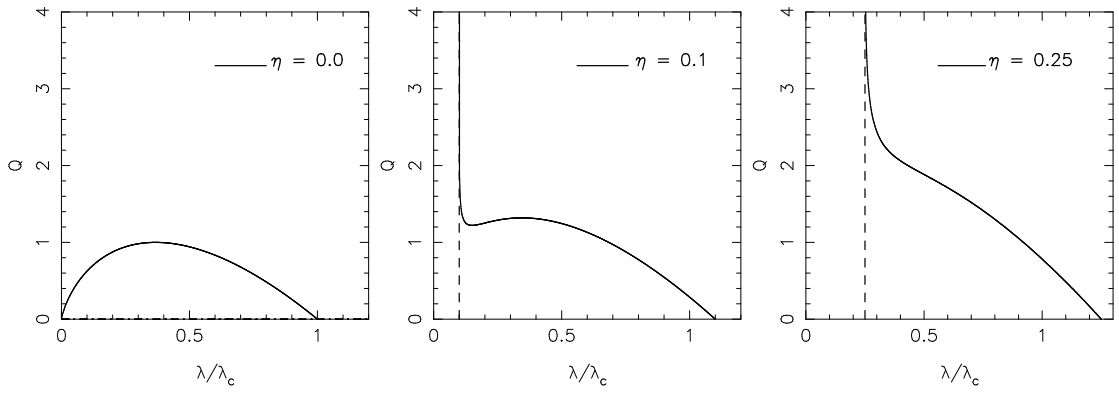

Figure 2.2: Plot of Q versus λ/λ_c for various value of η. Dashed line for $\eta \neq 0$ gives the minimum allowed wavelength. The solid line divides the parameter space for unstable modes (below line) from the stable one's (above the line).

much smaller than rotational velocity. Using this we get,

$$D = 2\Omega(\omega - \dot{\varpi}) + O(\epsilon^2), \tag{2.25}$$

$O(\epsilon^2)$ are the higher-order terms in the small parameter ϵ, which are neglected because we are working in the linear regimme. Using equation (2.25) in equation (2.22) the expression for the dispersion relation for slow modes for coupled disc with azimuthal wavenumber $m = 1$ is,

$$\omega = \dot{\varpi} + \frac{\pi G|k|}{\Omega}\Sigma_{0s}\left[\eta + exp(-|k|b)\right]. \tag{2.26}$$

For our analysis $\eta < 1$ always, and in general, η is a function of the (R,ϕ). Under slow mode approximation, the dispersion relation simplifies, and it becomes linear in 'ω'. Hence the coupled gas and stellar discs are always stable to such nearly Keplerian perturbations. To study the nature of eigenmodes numerically, we shall from here on assume that the surface density of stars in the disc, Σ_{0s} to be Kuzmin disc discussed in section-2.3 (termed as Σ_s) and η value to be constant. Though this is limiting to a special case, it gives the overall nature of eigenmodes quiet well as observed by Gulati & Saini (2016a). We next calculate the mode frequencies from the dispersion relation derived in equation (2.26) for slow modes and discuss the nature of the discrete spectra formed.

2.7 Nature of eigen modes

Contour plots for constant ω-value gives the behavior of eigenmodes. In figure (2.3) we plot the contours of constant ω in $k - R$ plane for the dispersion relation given in equation (2.26). A WKB wave packet at a radial speed moves along a contour of constant ω (Touma, 2002). Long trailing and short leading waves propagate outward, while long leading and short trailing waves propagate inwards. In figure (2.3), we make contour plots for different value of η, like 0, 0.05, 0.1 and 0.25. Dark blue shaded contours in the plots, present for all η values, contains only long waves. An outward-traveling long trailing wave is reflected into an inward-traveling long leading wave, which then reflects back to a long trailing wave as it contains both negative and positive values of k. These modes have $\omega < 0$, i.e., these are retrograde in nature. In light blue shaded region, the closed contour for which could be seen only for $\eta = 0$, 0.05 and 0.1, are for positive values of ω. Such closed contours denote a long trailing wave flowing outward which refracts into a short trailing wave traveling inward, which then refracts back into a long wave. No closed contour for $\omega > 0$ were found for $\eta > 0.1$. This would imply that no discrete spectra for prograde mode is present if the gas exceed 10% of stellar mass component in galaxies. The positive value of ω is of our interest, as they will be the ones giving prograde modes. The retrograde modes with $\omega < 0$ will be short-lived due to processes like viscous dissipation as these will be traveling in the opposite direction relative to the overall rotation of the disc, however, these retrograde modes will put a fraction mass component in retrograde motion w.r.t. the disc and it may give rise instabilities (Gulati et al., 2012). This will require further investigation in the future.

We shall calculate the discrete spectra next. A a closed contour in figure (2.3) represent a standing mode, the phase accumulated over a complete cycle must be an integer multiple of 2π. The turning points contribute a total phase of π (Landau & Lifshitz, 2013) . The closed contours can be quantized using the Bohr- Sommerfeld quantization condition to get the discrete spectra of eigenvalues. The quantization condition is given by

$$\oint k dR = (2n + 1)\pi, \tag{2.27}$$

with a clockwise integration to keep the integral position, here n = number of nodes for the wave form (Landau & Lifshitz, 2013). In other words, standing modes are given by the closed contours in the figure that enclose the area $(2n + 1)\pi$ in the k-R plane.

2.8 Numerical results for discrete spectrum

This subsection contains the numerically calculated values of dimensionless eigenvalue, using the dispersion relation and quantization condition for the centrally concentrated Kuzmin disc. The dispersion relation in equation (2.26) is made to dimensionless using the disc scale radius 'a' in the Kuzmin disc. The surface density and frequency term are rescaled using M_d/a^2 and $\sqrt{GM/a^3}$, respectively. The rescaled dispersion relation for the Kuzmin disc is,

$$\omega = \frac{-3R^2}{2(R^2+1)^{5/2}} + \frac{|k|R^{3/2}}{2(R^2+1)^{3/2}}\left[\eta + exp(-|k|b)\right]. \tag{2.28}$$

The notation of the rescaled terms is kept the same to avoid introduction to a new set of parameters. To analyze the behavior of eigen spectra, we take some specific cases like $\eta = 0$, 0.05, and 0.1. The disc has a diverse range of discrete slow modes that may be ordered according to the number of nodes. In figure (2.4) we give the plot of ω verses n, for different value of η. For $\eta = 0$, the spectrum is consistent with the one given by Gulati et al. (2012) and Tremaine (2001). Following properties of eigen-spectra can be observed from the plot:

1. ω-value decreases with increasing value of the number of nodes.
2. Discrete value of 'ω', does not exists for higher value number of nodes n, for increasing values of η.
3. For the same value of 'ω,' higher is the value of η, the number of nodes is higher.
4. No discrete spectra was found for $\eta = 0.1$ and higher value of η, though closed contours for $\eta = 0.1$ values were observed in figure–(2.3).

The increased parameter space for the disc to be unstable due to the presence of gas in our analysis increases the probability of generation of self-sustained perturbations. The absence of discrete spectra for $\eta \geq 0.1$ is an interesting observation, however the result should be taken with cautions. It could plausibly be due to the reason that for a higher gas fraction, the gas and the stellar disc might not be co-rotating and gas pressure can no longer be neglected. On the other hand, observation suggest that the gas content of galaxies (excluding the irregular galaxies) does not exceed 10 % of stellar content (Alig,

2013) and hence the analysis holds for the systems under consideration in the present work.

2.9 Conclusion and Discussion

We have presented a simple analysis for large scale, long-wavelength slow modes for $m = 1$ in a thin disc composed of both stars and gas orbiting a massive body. The gaseous content is an intrinsic part of discs at the center of galaxies (Genzel et al., 2010; Takekawa et al., 2020). However, the work pertaining to the current study of slow modes have only considered a single component stellar disc. A notable exception is a work by Jog (1996). Their approach, however, is different from the one presented here. They provided a modified Toomre's stability criterion and showed that the presence of gas-induced instability in the disc. We get the same conclusion albeit using a simplified approach as.

- Analyzed large-scale, long-wavelength slow modes for $m = 1$ in a thin disc of stars and gas orbiting a massive body and confirmed that the presence of gas increases instability in the disc.
- Developed an analytical expression for local WKB waves, quadratic in temporal frequency (ω), and analyzed stability using the neutral stability line ($\omega = 0$).
- Higher gas fractions make discs more susceptible to instabilities, consistent with previous studies.
- The non-zero η value also allows the modes to exists for higher values of λ implying that the modes will give rise to perturbations on large scale in presence of gas.
- $m = 1$ modes dominate in nearly Keplerian discs and are stable for one-component discs ($\eta = 0$), which is same as the work by Tremaine (2001).

We next discussed the properties of contour plots for constant ω, which describe the nature of discrete spectra of eigenvalues in the presence of gas as:

- The retrograde modes exist for long leading and trailing waves. However, prograde modes exist for long and short trailing waves.

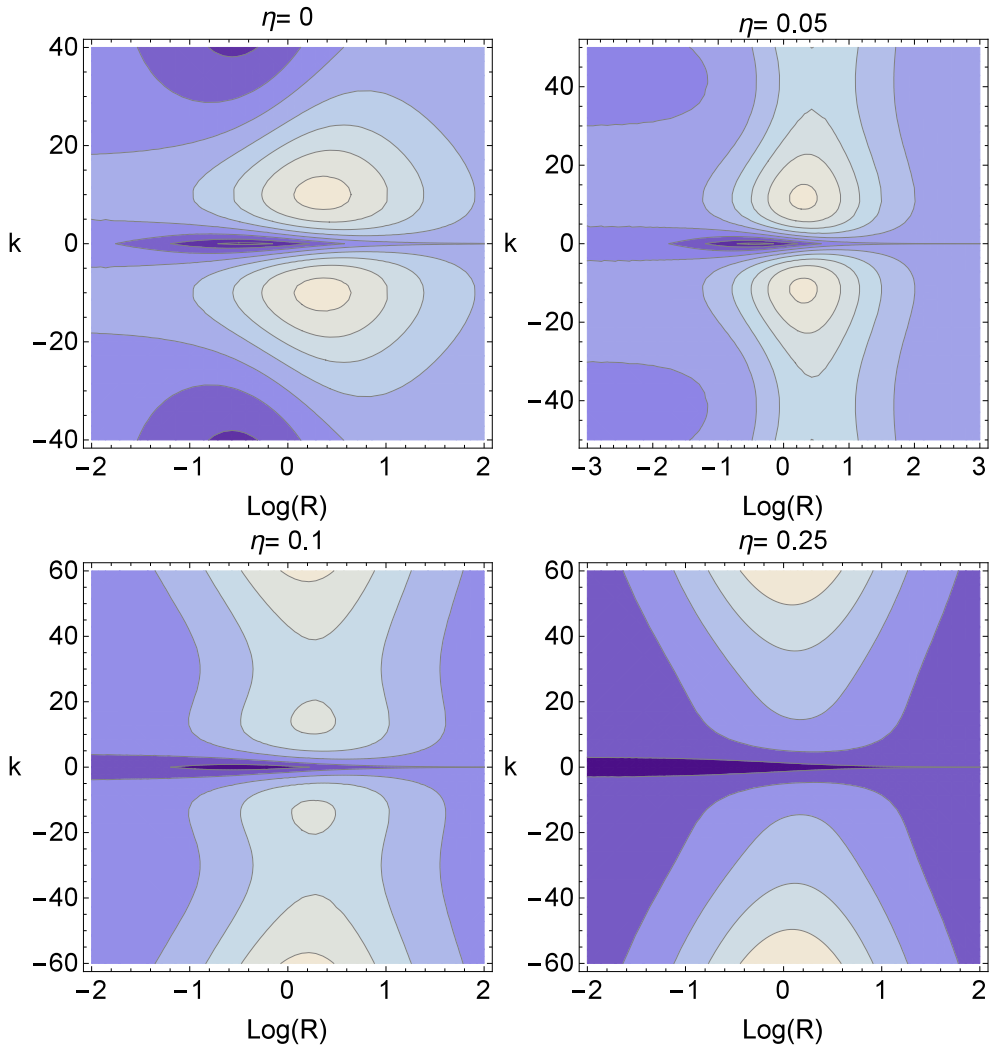

Figure 2.3: Contour plots of constant values ω for WKB slow modes for $m = 1$ for a Kuzmin disc in $k - R$ plane for different value of η. Each panel is labelled for its η value respectively.

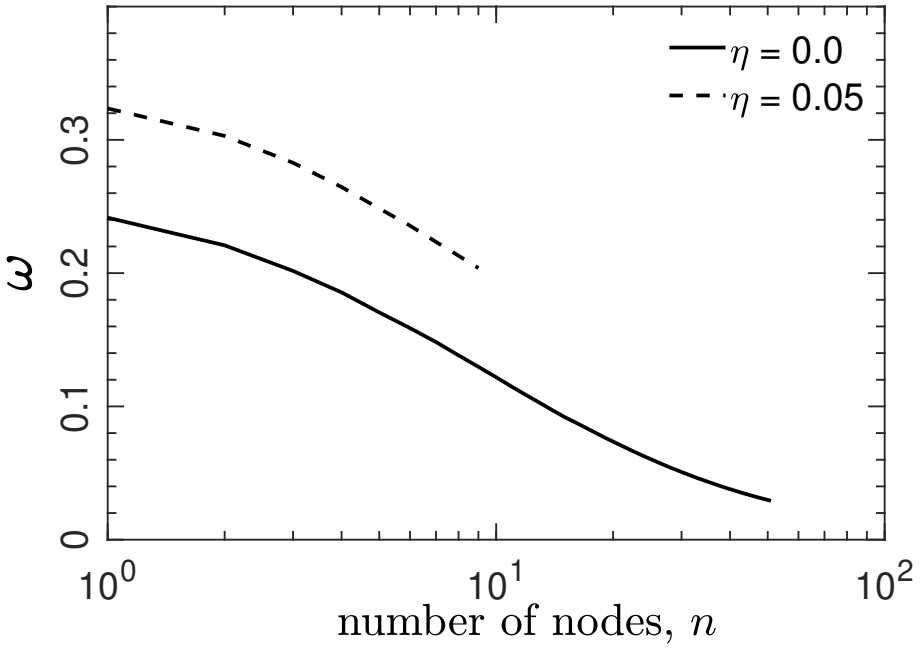

Figure 2.4: Plot of eigenfrequency ω versus number of nodes n for different value of $\eta = 0$ and $\eta = 0.05$.

- Calculation of quantized eigen spectra using the Bohr-Sommerfeld quantization condition. The higher gas fraction in the disc allows the existence of modes with a larger ω value.
- The higher gas fraction in the disc allows the existence of modes with a larger ω value. These will be faster moving perturbation for a similar radial extend compared to the case with no gas.

Such modes could plausibly dominate observations of non-axisymmetric features in the disc. The coexistence of gas and particles in the astrophysical discs paves the way to instabilities in a nearly Keplerian disc. This addresses the presence of asymmetries in an inactive galactic nucleus like that of M31 & NGC4486B. These could be not only the reason for asymmetries observed in the discs but also the enhanced densities could give rise to other phenomena, such as star formation at the centers of galaxies and planet formation in proto-planetary discs. A detailed study of these perturbations by formulating a complete eigenvalue problem for coupled, in which gas and stars are not co-rotating with significant gas pressure, will be helpful in mapping them to the physical phenomena which are possibly triggered by these. We have assumed the gas fraction to

be constant throughout the disc in the present work. A more realistic variation of η from observations will give a much better understanding of slow modes, their formation, and appearance.

Chapter 3

Three-Dimensional stellar orbits due to off-centered dark matter halo at the center of the disc galaxies.

3.1 Introduction

Observations suggest that the light distribution of spiral galaxies's discs is not strictly axisymmetric, as seen in M101 (NGC 5457) (Arp, 1966) and NGC1637 (Sandage, 1961). Many galaxies show lopsided structures at both large and small scales (Levine & Sparke, 1998; Varela-Lavin et al., 2023; Dolfi et al., 2023). This issue was first noticed during the study of galaxies with significant asymmetric spatial extents of atomic hydrogen gas distribution in the galaxy's outer regions (Baldwin et al., 1980). The global HI profile is also demonstrated to be well connected with asymmetric distribution of gas density in outer parts of galaxies for a considerably larger sample of galaxies (Richter & Sancisi, 1994), implying that lopsidedness is a widespread and long-lasting phenomenon.

It is well acknowledged that galaxies are surrounded by enormous dark matter halos (Fiřt et al., 2009; Morley & Buettner, 2016, 2017), which are significantly more massive than their visible component and affect a significant portion of their dynamic, specifically in the outer regions of the galaxies (Bailin et al., 2007). The existence of dark matter halo is established from the study of rotation curve (Rubin, 1983). In dwarf galaxies, which are the most common type of galaxies in the local universe, dark matter halo is relatively more massive and dominates most of the galaxy's disc (Ghosh & Jog, 2018).

In the velocity fields, rotation curves, and morphology, as well as in their kinematics, it is common to see the '$cos\phi$' asymmetry in dwarf irregular galaxy (Khademi et al., 2021) or kinematic lopsidedness (a global $m = 1$ perturbation) where ϕ is the azimuthal angle in the plane of the disc (Levine & Sparke, 1998; Schoenmakers et al., 1997) .

A lopsided halo potential model can explain the asymmetry in the kinematic data reasonably well. Recent observations provide evidence that the location of the dark matter halo in the Milky Way galaxy is off-centered w.r.t. the center of visible matter. A detailed study of the position of the central dark matter density peak showed the difference from the dynamical center of the galaxy (Kuhlen et al., 2013). The offset between the dynamical center and the maximum dark matter density was found to be around $300 - 400$ pc. Later, a detailed investigation of central galaxies in different galaxy clusters facilitated the discovery of spatially separated dark matter halo from their stellar distribution (Massey et al., 2015). Authors have also indicated that 1.62 kpc is the maximum constrained offset, and galaxies far from galactic cluster centers do not have this type of offset. However, M94, a field galaxy in cluster Abell 3827, shows observable evidence for the halo being off-centered w.r.t. the disc (Massey et al., 2015; Chemin et al., 2016).

Numerical simulations also show an offset in only dissipational hydrodynamics simulations and not in collisionless pure dark matter simulations, implying that the evolution of visible matter and the relative shift in the center could be intertwined. The evolution and assembly of galaxies and their environment (EAGLE) is used to measure the offset between the galaxy's core and cold dark matter (Schaller et al., 2015). They discovered that most simulated galaxies have offset lower than the gravitational softening length of 700 pc for field and satellite galaxies in clusters. The observed $m = 1$ type perturbation (lopsidedness) has a significant impact on the galaxy's dynamics and future evolution through a variety of processes, including angular momentum transport, nuclear fusion within the galaxy's active galactic nucleus, the expansion of the black hole at its center, and increased star formation in the over dense regions of galaxies (Jog, 1999; Jog & Combes, 2009).

Consequently, it is interesting to investigate different dynamical implications for a galactic disc with a lopsided halo potential placed on the underlying axisymmetric potential. The influence of such an offset halo on the orbits and kinematics in the disc's central few kpc was also investigated by Prasad & Jog (2017). However, in their work, the stellar orbits in the core of the galaxies are restricted to be planar. A non-planar

configuration is, however, intrinsic to the core of galaxies. We generalized their model to investigate the deviation in stellar orbits due to offset in halo potential for a more realistic non-planar configuration at the center of galaxies. The generalization involves the evaluation of potential due to off-centered halo and further solving the three-dimensional equation of motion under the epicyclic approximation for the off-centered potential to quantize the effect of displaced dark matter halo center.

The remaining part of the present chapter is structured as section–3.2, which contains a detailed account of the gravitational potential profile due to the galaxy's center and the dark matter halo. In section–3.3, we derive 3-dimensional stellar orbits in the core of galaxies using epicyclic approximation. The numerical solution of the perturbed orbits is presented in section–3.4. Our analysis's conclusion and implication are discussed in section–3.5.

3.2 Gravitational potential at the center of galaxy

We shall first calculate the total potential acting on a particle at position (R, ϕ, Z) in a galaxy's central region, including the effects of an off-centered dark matter halo. The dynamics of the gas and stars in many galaxies suggest the existence of a central mass in the form of a massive black hole (Maoz & McKee, 1998). For instance, the best available measurements of line-of-sight velocities and proper motion for Milky Way provide strong qualitative support for the existence of a central point mass (Sellgren et al., 1990; Krabbe et al., 1995; Haller et al., 1996; Eckart & Genzel, 1996). The potential due to this can be represented as:

$$\Phi_{\rm BH} = \frac{-GM_{\rm BH}}{R}, \tag{3.1}$$

here, $M_{\rm BH}$ is the mass of central black hole (Binney & Tremaine, 2011). For the spheroidal component of the galaxy's mass distribution, which is composed of the central bulge and stellar halo as a smooth extension of the bulge, we use Plummer-Kuzmin bulge model (Binney & Tremaine, 2011), whose potential in cylindrical coordinates can be written as

$$\Phi_{\rm B}(R,Z) = \frac{-GM_{\rm B}}{R_{\rm B}}\left(1+\frac{R^2+Z^2}{R_{\rm B}^2}\right)^{-1/2}, \tag{3.2}$$

here, $M_{\rm B}$ is the total bulge mass and $R_{\rm B}$ is the scale radius of the bulge (Blum, 1995; Binney & Tremaine, 2011).

By modeling the halo parameters using the HI disc scale height data and observed rotation curve as simultaneous constraints, a spherical, pseudo-isothermal halo is found to yield the best fit (Mera et al., 1998; Banerjee et al., 2010) for the dark matter halo profile. We use the same, whose potential can be represented as,

$$\Phi_{\rm H}(R,Z) = 4\pi G\rho_0 R_{\rm c}^2 \Bigg[\frac{1}{2}\log(R_{\rm c}^2+R^2+Z^2) + \left(\frac{R_{\rm c}}{(R^2+Z^2)^{1/2}}\right)\arctan\left(\frac{(R^2+Z^2)^{1/2}}{R_{\rm c}}\right) - 1\Bigg], \tag{3.3}$$

here ρ_0 is the core density and R_c is the core radius.

Observations and numerical simulation strongly suggest that the center of the dark-matter halo and the central bulge do not coincide. If d is offset between the centers, in that case, the geometry of the relative locations of centers can be visualized as in figure–3.1. C_B is the center of the bulge and C_H is the center of the dark matter halo in the disc plane, and P is the location at which the potential is calculated. Taking Z to be the height above the plane containing the triangle $C_H C_{H'} P$, such that C_H is the projection of point $C_{H'}$ in the plane, we can write $x_1^2 = Z^2 + x^2 = Z^2 + R^2 + d^2 - 2Rd\cos\phi$ as the distance between P and point $C_{H'}$. The potential including the disturbance in the dark matter halo at point P is then given by,

$$\Phi_{\rm H}(x_1,Z) = 4\pi G\rho_0 R_{\rm c}^2 \Bigg[\frac{1}{2}\log(R_{\rm c}^2+x_1^2+Z^2) + \left(\frac{R_{\rm c}}{(x_1^2+Z^2)^{1/2}}\right)\arctan\left(\frac{(x_1^2+Z^2)^{1/2}}{R_{\rm c}}\right) - 1\Bigg]. \tag{3.4}$$

Note that equation-3.4 reduces to the potential with zero disturbance when $d = 0$. We next assume that $d \ll R$, simplifying and keeping only linear term in the terms contained in RHS of equation-3.4 we get,

$$\frac{1}{2}\log(R_{\rm c}^2+x_1^2+Z^2) \approx \frac{1}{2}\log(R_{\rm c}^2+R^2+2Z^2) - \frac{Rd\cos\phi}{(R_{\rm c}^2+R^2+2Z^2)}, \tag{3.5}$$

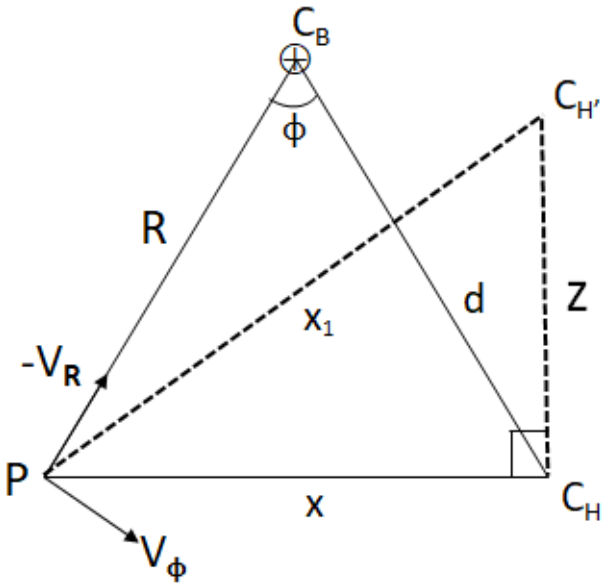

Figure 3.1: The geometry of relative location of centers for different mass components at the center of a galaxy. d represents the distance between center of the bulge and the dark matter halo. C_B is the center of bulge, C_H is the displaced dark matter halo in the disc plane, which is the projection of $C_{H'}$ the displayed center in the 3-dimensional configuration. Dashed lines represent the geometry perpendicular to the disc plane. The radial and azimuthal velocities are also shown at point P.

$$and,\ \frac{R_{\rm c}}{(x_1^2+Z^2)^{1/2}}\arctan\left(\frac{(x_1^2+Z^2)^{1/2}}{R_{\rm c}}\right)=\frac{R_{\rm c}}{R+\sqrt{2}Z}\arctan\left(\frac{(R^2+Z^2)^{1/2}}{R_{\rm c}}\right)+\frac{R_{\rm c}}{R+\sqrt{2}Z}\arctan\left(\frac{(R^2+Z^2)^{1/2}}{R_{\rm c}}\right)\left(\frac{Rd\cos\phi}{(R^2+2Z^2)}\right). \quad (3.6)$$

The net value of $\Phi_{\rm H}$ including a small off-set in the center of halo, is given by,

$$\Phi_{\rm H} = \Phi_{\rm H}(R,Z,d=0)+4\pi G\rho R_{\rm c}^2 d\cos\phi\times\left[\frac{R_{\rm c}}{R(R+\sqrt{2}Z)(1+\frac{2Z^2}{R^2})}\arctan\left(\frac{(R^2+Z^2)^{1/2}}{R_{\rm c}}\right)-\frac{R}{(R_{\rm c}^2+R^2+2Z^2)}\right],$$

where, $\Phi_H(d=0)$ is the contribution of the unperturbed dark matter halo and the second

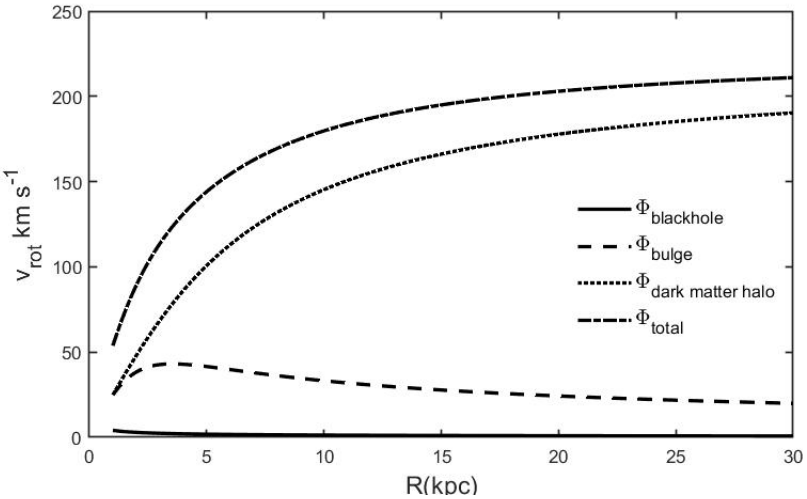

Figure 3.2: The rotation curve plotted due to potential generated for galaxies central black hole (solid-line), central bulge (dashed-line), galaxies dark matter halo (dotted-line), and total potential (dash-dotted line). The rotation curve for pseudo-isothermal halo is consistent with the one given is Sofue (2009).

term in equation-3.7 is the disturbance term caused by the halo's offset, which can be expressed as:

$$\Phi_{\rm pert}(R,\phi,Z) = \psi(R,Z)\cos\phi, \tag{3.7}$$

where,

$$\psi(R,Z) = 4\pi G\rho R_{\rm c}^2 d\left[\frac{R_{\rm c}}{R(R+\sqrt{2}Z)(1+\frac{2Z^2}{R^2})}\arctan\left(\frac{(R^2+Z^2)^{1/2}}{R_{\rm c}}\right) - \frac{R}{(R_{\rm c}^2+R^2+2Z^2)}\right]. \tag{3.8}$$

Consequently, $\Phi(R,\phi,Z)$, the total potential is given by, $\Phi = \Phi_{\rm BH} + \Phi_{\rm B} + \Phi_{\rm H}(d = 0) + \Phi_{\rm pert}$. The second and third terms are the potential w.r.t. the bulge and halo with the same center. The perturbation potential has a lopsided form corresponding to a $m = 1$ azimuthal perturbation since it varies linearly with $\cos\phi$ (Jog & Combes, 2009). This is consistent with the expected mass distribution's geometry. The perturbation

decreases to zero as the offset $d \to 0$, and the net potential is then equal to the sum of the potential related to the central region and a concentric halo. For comparison we give the plot of rotation curve due to potential generated for galaxies central black hole (solid-line), central bulge (dashed-line), galaxies dark matter halo (dotted-line), and total potential (dash-dotted line) in figure (3.2). The rotation curve for pseudo-isothermal halo is consistent with the one given is Sofue (2009).

3.3 Non-planar Epicyclic orbits

The perturbed potential will disturb an initial circular orbit. We shall now calculate the resultant stellar orbit for the perturbed potential calculated in the previous section. We use epicyclic approximation and integrate the equation of motion under the restrictions $d \ll R$ to get a solution for approximately 3-dimensional elliptical orbits for stars at the center of galaxies. We use the method described in Rohlfs (1977), which is a first-order epicyclic theory with a small, non-zero pattern speed for a rotating frame, and get the coupled equations of motion. The equation of motion for stars can be written as $\ddot{\mathbf{R}} = -\nabla\Phi$, whose components in cylindrical coordinates are given by,

$$\hat{R} : \ddot{R} - R\dot{\phi}^2 = -\frac{\partial\Phi}{\partial R}, \tag{3.9}$$

$$\hat{\phi} : \frac{1}{R}\frac{d}{dt}(R^2\dot{\phi}) = -\frac{1}{R}\frac{\partial\Phi}{\partial\phi}, \tag{3.10}$$

$$\hat{Z} : \ddot{Z} = -\frac{\partial\Phi}{\partial Z}. \tag{3.11}$$

Assuming that the orbit deviates slightly from the circular orbit i.e., $R(t) = R_0 + R_1(t)$, $\phi(t) = \phi_0(t) + \phi_1(t)$, $Z(t) = Z_0 + Z_1(t)$ and using $\Phi(R, \phi, Z) = \Phi_0(R, Z) + \Phi_1(R, \phi, Z)$, the equation of motion can be simplified to get the equilibrium solution as,

$$R_0\dot{\phi_0}^2 = \frac{d\Phi_0}{dR}, \quad \dot{\phi_0} = \text{constant} = \Omega_0 \quad \text{and} \quad \frac{\partial\Phi_0}{\partial Z} = 0, \tag{3.12}$$

and hence the azimuthal frequency can be defined as,

$$\Omega_0(R) \equiv \pm\sqrt{\frac{1}{R}\frac{d\Phi_0}{dR}}\Bigg|_{R=R_0}, \tag{3.13}$$

and $\phi_0(t) = \Omega_0 t$. Using Taylor expansion for the unperturbed potential about the unperturbed orbit $R = R_0$ and $Z = Z_0$ and retaining terms up to first-order in the small quantities, the RHS of equations–(3.9) and (3.11) gives.

$$\frac{\partial \Phi}{\partial R} \simeq R_0\Omega_0^2 + R_1 \frac{\partial^2 \Phi_0}{\partial R}\bigg|_{R_0,Z_0} + Z_1 \frac{\partial^2 \Phi_0}{\partial R \partial Z}\bigg|_{R_0,Z_0} + \frac{\partial \Phi_1}{\partial R}\bigg|_{R_0,Z_0}, \tag{3.14}$$

$$\frac{\partial \Phi}{\partial Z} \simeq \frac{\partial \Phi_0}{\partial Z}\bigg|_{R_0,Z_0} + Z_1 \frac{\partial^2 \Phi_0}{\partial Z^2}\bigg|_{R_0,Z_0} + R_1 \frac{\partial^2 \Phi_0}{\partial R \partial Z}\bigg|_{R_0,Z_0} + \frac{\partial \Phi_1}{\partial Z}\bigg|_{R_0,Z_0}. \tag{3.15}$$

Further writing

$$\nu_0^2 \equiv \frac{\partial^2 \Phi_0}{\partial Z^2}\bigg|_{R_0,Z_0} = \text{constant}, \tag{3.16}$$

which is the vertical frequency, and dropping the higher order terms in small quantities like (R_1, ϕ_1, Z_1 etc.), the equations of motion reduce to,

$$\ddot{R_1} + \Big(\frac{\partial^2 \Phi_0}{\partial R^2} - \Omega_0^2\Big) R_1 - 2R_0\Omega_0\dot{\phi_1} + Z_1 \frac{\partial^2 \Phi_0}{\partial R \partial Z}\bigg|_{R_0,Z_0} = -\Big(\frac{\partial \Phi_1}{\partial R}\Big)_{R_0,Z_0}, \tag{3.17}$$

$$\ddot{\phi_1} + 2\Omega_0 \frac{\dot{R_1}}{R_0} = -\frac{1}{R_0^2}\Big(\frac{\partial \Phi_1}{\partial \phi}\Big)_{R_0,Z_0}, \tag{3.18}$$

$$\ddot{Z_1} + \nu_0^2 Z_1 + R_1 \frac{\partial^2 \Phi_0}{\partial R \partial Z}\bigg|_{R_0,Z_0} = -\Big(\frac{\partial \Phi_1}{\partial Z}\Big)_{R_0,Z_0}. \tag{3.19}$$

Note that we have used the condition that the unperturbed potential is axisymmetric and in equilibrium to write the above equations. After solving equation- (3.17)- (3.19) we get the coupled linear differential equations of second-order by using the elimination method. Using the expression for $\Phi_1(R, \phi, Z) = \psi(R, Z)\cos\phi$ as the perturbation potential, the perturbation in R and Z are obtained as follows,

$$R_1 = \frac{1}{\Delta}\left[\left(\frac{\partial^2 \phi_0}{\partial R \partial Z}\right)\left(\frac{\partial \psi}{\partial Z}\right) - \left(\frac{2\psi}{R} + \frac{\partial \psi}{\partial R}\right)(\nu^2 - \Omega^2)\ \cos\phi\right]_{R_0,Z_0}, \tag{3.20}$$

$$Z_1 = \frac{1}{\Delta}\left[-\left(\frac{\partial^2 \phi_0}{\partial R \partial Z}\right)\left(\frac{2\psi}{R} + \frac{\partial \psi}{\partial R}\right) + \Big(\frac{\partial \psi}{\partial Z}\Big)(\Omega^2 - \kappa^2)\cos\phi\right]_{R_0,Z_0}, \tag{3.21}$$

$$\Delta = \left[\frac{\partial^2 \phi_0}{\partial R \partial Z} + (\kappa^2 - \Omega^2)(\Omega^2 - \nu^2)\right]_{R_0,Z_0} \tag{3.22}$$

here, κ & Ω_0 are the epicyclic frequency and angular speed respectively at R_0 and Z_0. The perturbed azimuthal velocity v_ϕ is governed by (using eq-(3.18)):

$$R_0\frac{d^2\phi_1}{dt^2} + 2\Omega_0\frac{dR_1}{dt} = \frac{\psi(R,Z)\sin\phi_0}{R_0}, \tag{3.23}$$

and the net azimuthal velocity is given

$$v_\phi = v_\mathrm{c} + R_0\frac{d\phi_1}{dt} + \Omega_0 R_1, \tag{3.24}$$

v_c is the unperturbed circular velocity and the integration of equation–(3.23) gives the perturbed component δv_ϕ as

$$\delta v_\phi = -\left(\frac{\psi(R,Z)\cos\phi_0}{\Omega_0 R_0} + \Omega_0 R_1\right), \tag{3.25}$$

further radial velocity is given by:

$$v_\mathrm{R} = \frac{dR}{dt} = \frac{d(R_0+R_1)}{dt}, \tag{3.26}$$

and the velocity along the Z direction is

$$v_Z = \frac{dZ_1}{dt}, \tag{3.27}$$

3.4 Numerical Result: Perturbed Orbits

We shall now consider the galaxy's input characteristics and calculate the extend of how much the off-center halo affects the stellar orbits in the central region. The off-center distance is assumed to be fixed at 300 pc (Kuhlen et al., 2013). The perturbed parameters like radial disturbance, height above the disc plane, and the corresponding velocities are investigated for stellar orbits. Using projected mass estimators, stellar velocity data modeling, and Jeans equation, the mass of the central black hole, M_BH is estimated to be $(3.9 \pm 3) \times 10^6 M_\odot$ (Binney & Tremaine, 2011; Genzel et al., 2000). We take the total mass of the bulge $M_\mathrm{B} = 2.8 \times 10^9 M_\odot$ and its scale radius $R_\mathrm{B} = 2.5\ kpc$ (Blum, 1995; Binney & Tremaine, 2011). The halo central density is taken as $\rho_{_0} = 0.035 M_\odot pc^{-3}$, and the core radius $R_\mathrm{c} = 5\ kpc$ (Mera et al., 1998; Prasad & Jog, 2017). As the present work closely resembles the work done by Prasad & Jog (2017), to get a comparison with

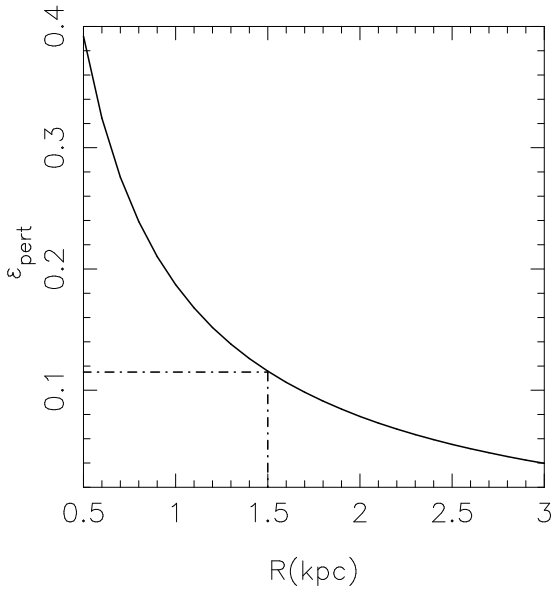

Figure 3.3: Perturbed potential $\epsilon_{\rm pert}$ given by the halo potential which is off-centered by 300 pc w.r.t. the central potential in the galaxies plane (i.e. Z=0)

their work, we begin plotting in figure-3.3 the ratio of the dimensionless perturbation potential ($\varepsilon_{\rm pert}$) given by,

$$\varepsilon_{\rm pert} = \frac{\psi(R,Z)}{\Phi_{\rm B} + \Phi_{\rm H}(d=0) + \Phi_{\rm BH}}. \tag{3.28}$$

We observe that the value of $\varepsilon_{\rm pert}$ increases as R decreases, indicating a stronger perturbative influence of the halo at lower radii, like the perturbation potential's fractional value at $R = 1.5$ kpc is approximately 0.115. The initial circular closed orbits in the central region must exhibit substantial spatial and kinematical lopsidedness as a result of this, as we shall demonstrate next. The variation of $\varepsilon_{\rm pert}$ vs R is similar to the variation obtained by Prasad & Jog (2017). However, the current study shows values that are more than an order of magnitude larger compared to Figure-2 from Prasad & Jog (2017)

With initial radius, $R_0 = 1.5\ kpc$ & $Z_0 = 0$, we first give the plot of net orbital radius R vs. the azimuthal angle ϕ in figure–3.4(a). The plot of the vertical height of the resultant orbit with the same initial conditions is given in figure–3.4(b). A substantial deviation from an initial planar circular orbit can be seen. The perturbed orbits are also seen to have a 180° mirror symmetry in the orbits, making them closed elliptical orbits. The perturbation is maximum along the offset and minimum along its perpendicular.

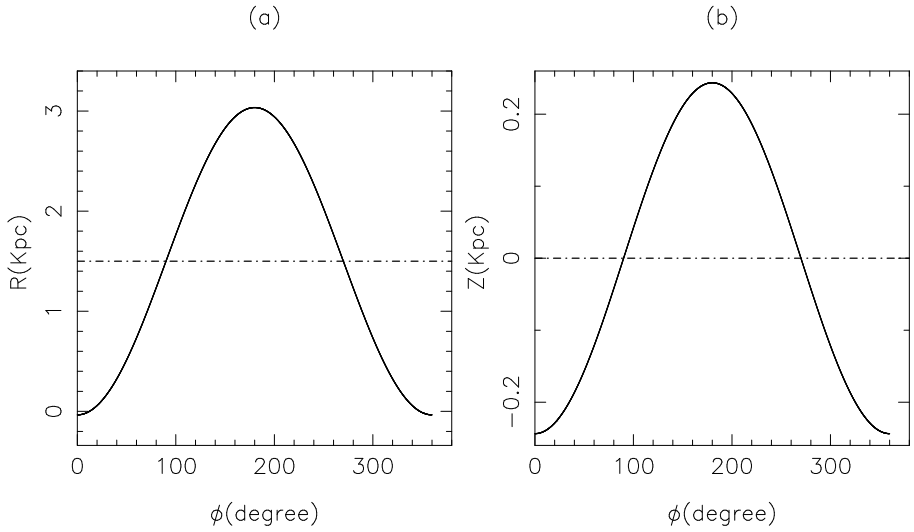

Figure 3.4: The net radius and vertical height of an initial planar circular orbit with $R_0 = 1.5$ kpc and $Z_0 = 0$.

Net radial, azimuthal, and vertical velocities are shown in figure–3.5. At $\phi = 90°$, the resultant radial velocity is highest at 50.6 km/s. The magnitude of the azimuthal velocity at $\phi = 90°$ is 49.5 km/s, and the highest magnitude of the azimuthal velocity, which occurs at $\phi = 180°$ is 168.67 km/s. The highest resultant vertical velocity is 6.146 km/s, which occurs at $\sim 90°$ and the maximum value of negative V_Z is 6.14 km/s at 270°.

Figure– 3.6(a) shows the projection of net lopsided perturbed orbit (i.e. $((R^2 + Z^2)^{1/2})$) against an unperturbed circular orbit at $R_0 = 1.5$ *kpc* & $Z_0 = 0$. The off-center halo's perturbation potential causes the radius and velocity components of the perturbed orbit to be significantly lopsided. By comparing the result of the disc plane orbits with Prasad & Jog (2017), we observe that the lopsidedness increases for the case of non-planar configuration. Moreover, an initial planar orbit becomes a non-planar, implying that a non-spherical potential is crucial to studying the offset effect in the central region. In Figure–3.6(b), we display a polar plot of orbits with different initial radii as $R_0 =$ 1.5 *kpc*, 2 *kpc*, and 2.5 *kpc*, . This shows a reasonable amount of lopsidedness in orbital radius, even when $R_0 > 1.5$ *kpc*. Figure-3.7 displays the perturbed orbits due to off-centered dark matter halo in 3-dimension, i.e., (X, Y, Z)-plane, for different initial radial orbits and Z_0 values, with $R_0 = 1.5$ kpc & $Z_0 = 0$ & 0.02 kpc panel-(a) and $R_0 = 2$ kpc & $Z_0 = 0$ & 0.02 kpc (panel-(b)). Variation in Z_0 value does not change the overall

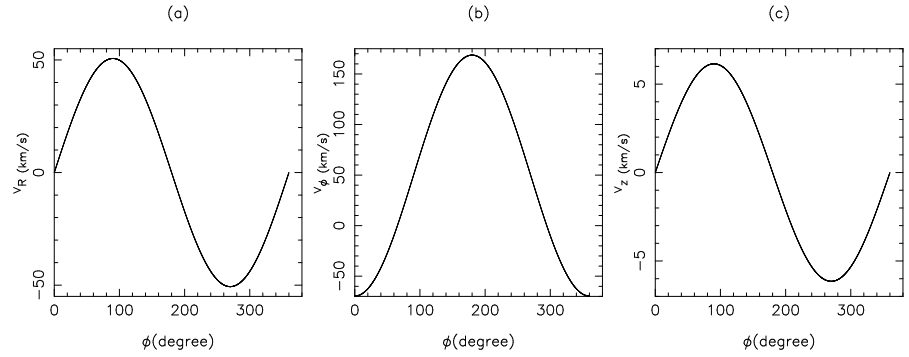

Figure 3.5: The perturbed radial, azimuthal, and vertical velocity components for an initial planar circular orbit.

shape of the orbit, apart from the orbits being displaced in the positive Z-direction for a non-zero Z_0 value.

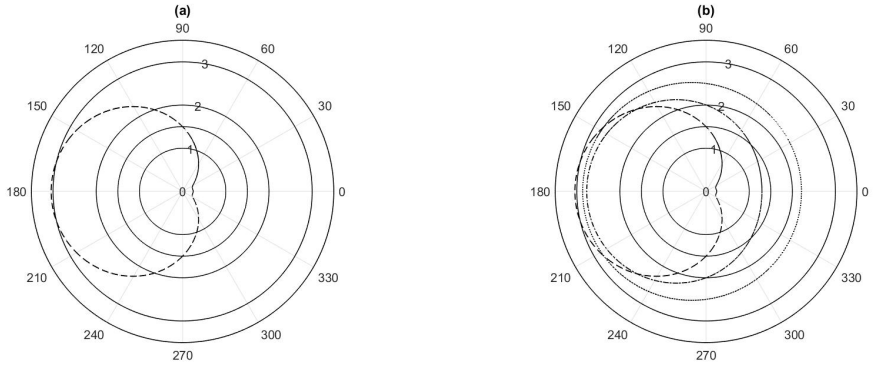

Figure 3.6: Panel-(a) is the polar plot of the perturbed orbit (dashed line) at $R_0 = 1.5$ kpc and $Z_0 = 0$ against the unperturbed orbit (solid line), panel-(b) shows the polar plot for perturbed orbits with initial circular orbits at R_0 of 1.5 kpc (dashed line), 2 kpc (dash-dotted line) and 2.5 kpc(dotted line) respectively. The orbits inside $R_0 = 3$ kpc are incredibly lopsided, especially at small R_0.

In Figure– 3.8(a) & 3.8(b), the fractional change in the orbital radius and azimuthal velocity for the perturbed orbits relative to the undisturbed values are displayed for $\phi = 0°$, i.e., along the direction of offset in the potential. The unperturbed circular velocity is $v_c = R_0\Omega_0$. The spatial and kinematical lopsidedness indicate that the perturbations subside as R approaches a value of 3 *kpc* and beyond. It is also observed that beyond 3.3 *kpc* the change in orbital radius is positive, although the magnitude of the perturbed radius is very small. The possible reason for this might be that we have ignored the

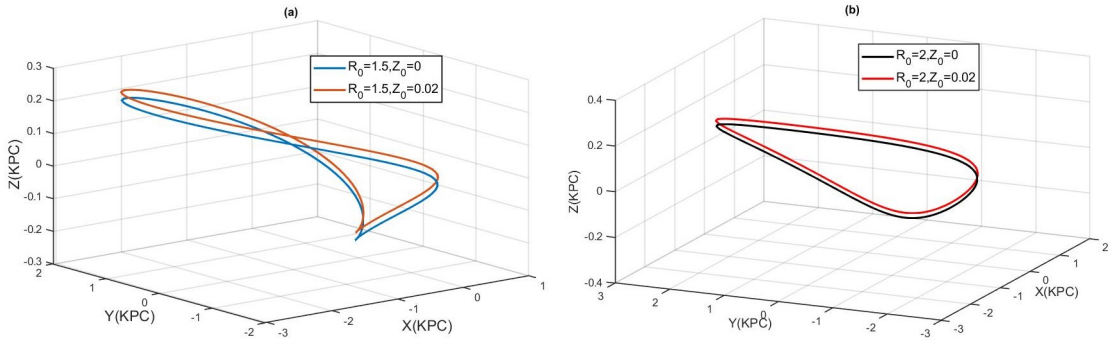

Figure 3.7: Perturbed orbits (X, Y, Z)-plane with initial conditions $R_0 = 1.5$ kpc, $Z_0 = 0$ & 0.02 kpc (panel-(a)), and $R_0 = 2$ kpc, $Z_0 = 0$ & 0.02 kpc (panel-(b)).

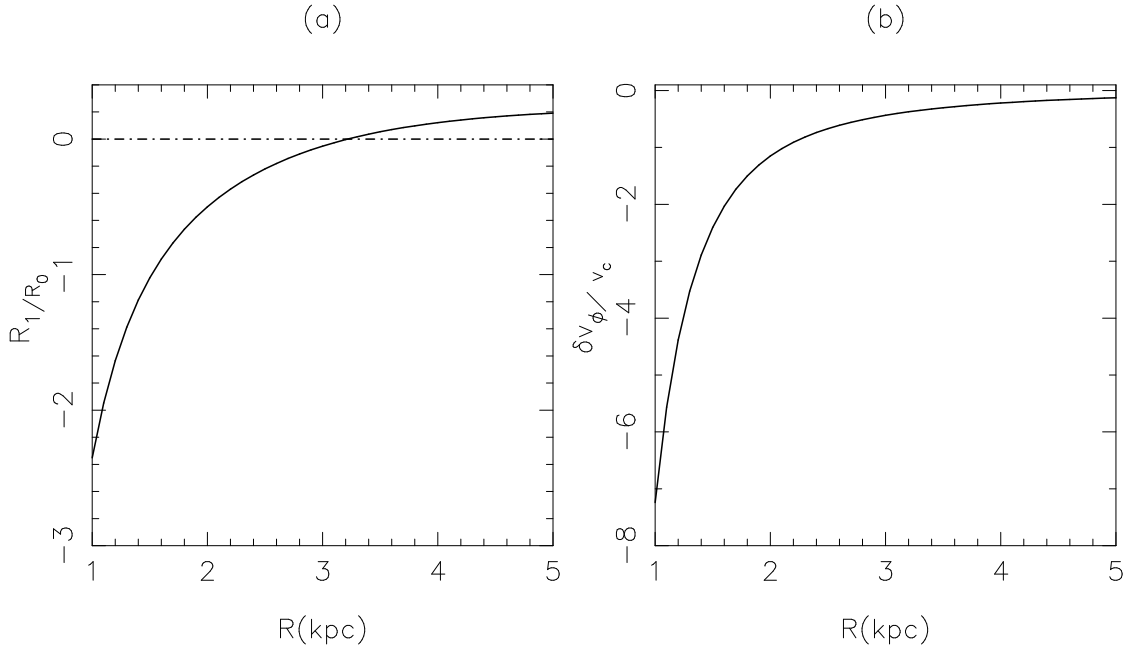

Figure 3.8: The fractional change in orbital radius (panel-(a)) and azimuthal velocity component (panel-(b)) obtained at $\phi = 0°$ for different radii.

non-linear terms, which might balance this increase in radius. Relative perturbation in circular velocity also decreases with increased radius; however, the value always remains negative. Our analysis indicates that small halo asymmetries lead to larger observable stellar asymmetries, and the earlier works indicate that such asymmetries of a few percent in the halo are unavoidable and should be ubiquitous. In the next section, we shall discuss our results and relevant conclusions.

3.5 Conclusion

Galaxies dynamics and evolution are very closely intertwined. In this chapter, we have analyzed how the central region dynamics of the galaxies are affected by an asymmetric dark matter halo. A similar work has been done previously (Prasad & Jog, 2017) however, there are subtle differences in the analysis and results for example, the authors earlier had restricted the geometry of the problem to 2-dimensional orbits, however, we present a complete 3-dimensional analysis of the perturbed orbits which is a much closer treatment for the stellar orbits for the center of galaxies and the results of the following calculations are following as:

- Evaluated the net perturbed potential in the central region due to an off-centered dark matter halo, which exhibits $m = 1$ asymmetry and results in spatial and kinematic lopsidedness.

- Figure-3.3 shows magnitude of the perturbed potential is higher at smaller radii R and depends on the offset distance d, this results compared with the finding of Prasad & Jog (2017). While current result is more than an order of magnitude larger than the result of Prasad & Jog (2017). These differences come from the inclusion of extra-planar geometry and differences in the model parameters. The analysis should clarify that while trivial differences in parameters, such as the choice of potential (Plummer–Kuzmin versus exponential) and the offset distance (300 pc versus 350 pc), do contribute to variations, the primary driver of the observed discrepancies is the extra-planar geometry.

- The conclusion is that this type of lopsidedness strongly depends on the radius, and hence is expected to have a substantial impact on the orbits and kinematics of the central region within a 3 kpc radius (Kuhlen et al., 2013).

Next, in section-3.3, the equation of motion in cylindrical coordinates is formulated, including the terms in which halo potential is concentric w.r.t. the central region along with contribution from the perturbed halo. The net orbital radius and the vertical height for an initially circular planar orbit are shown in figure-3.4. The resultant velocity components are displayed in figure-3.5. Lopsided orbits for a given unperturbed orbital radius R_0 are shown in figure-3.6(a), and the corresponding plot for different R_0 values are given in figure-3.6(b). Perturbed orbits in 3-dimension are displayed in figure-3.7 with different initial radius R_0 and non zero value of Z_0. Lastly, in figure-3.8, we display the variation of fractional change in radius and azimuthal velocity along the direction of maximum perturbation. Major takeaways from these plots are:

1. The resultant circular planar orbit exhibits a high degree of lopsidedness along with non-planarity.

2. The lopsidedness in the orbit decreases at larger radii.

3. The shape of perturbed orbits does not show significant variation with change in initial Z_0 value.

4. Radial and perpendicular velocities are maximum in the direction perpendicular to the direction of off-set.

5. The maximum perturbation in azimuthal velocity occurs along the direction of the offset.

From highly disturbed lopsided orbit at the center of the galaxy, it's possible that these types of orbits cause an outward angular momentum transmission at the center and thus help gas infall inward to the center, as what was indicated for the lopsidedness in the outer area by Saha & Jog (2014), and the infall proposed for the central region (Combes, 2016). This can have significant dynamical effects, such as fueling the central AGN by an outward angular momentum transfer and may help with solving a long-standing issue of how to fuel a core AGN even within an isolated galaxy. Suppose there are enough stars in the region of the lopsidedness so that self-gravity can become dynamically significant; then, the self-gravity will significantly impact how the stars react to such an asymmetry, regardless of how centrally concentrated they are with respect to the dark matter. Furthermore, asymmetric gas accretion is one possible explanation

for the lopsidedness in other components, specifically the neutral gas (Zaritsky et al., 2013). These are some of the implications of the current study that the authors would like to investigate further by comparison with relevant observations.

Chapter 4

Ram pressure stripping in spiral galaxies

4.1 Introduction

The inter-galactic environment plays a significant role in the evolution of a galaxy. Several mechanisms have been investigated to explain the variation in galaxy structure and star formation in galaxies. Gravitational mechanisms such as tidal stripping, galaxy harassment, strangulation (or starvation), and dynamical friction act on the stars and gas within galaxies in unique ways. Tidal stripping involves the removal of stars or gas due to the gravitational pull of nearby massive galaxies or the cluster potential, reshaping the stellar structure of the galaxy (Sharma et al., 2014). Harassment, which consists of repeated high-speed encounters between galaxies, can lead to morphological changes and star formation suppression, as seen in (Moore et al., 1996, 1999, 1998; Aguerri & González-García, 2009; Smith et al., 2010). Strangulation, on the other hand, occurs when a galaxy's supply of cold gas is cut off by interactions with other cluster members or the cluster's gravitational potential, leading to a gradual quenching of star formation. Dynamical friction slows down galaxies or subhalos as they move through dense environments, potentially triggering mergers or tidal disruptions (Balogh et al., 2000; Larson et al., 1980; Peng et al., 2015). Together, these gravitational processes contribute significantly to galaxy evolution in cluster environments. Evidence of galaxy-galaxy interactions (Sulentic, 1976; Solomon & Sage, 1988; Bushouse, 1987; Boselli & Gavazzi, 2006; Yadav et al., 2021) further supports the role of tidal forces in shaping galaxy

properties.

In contrast, Ram-Pressure Stripping (RPS) (Gunn & Gott III, 1972; Poggianti et al., 2017; Gullieuszik et al., 2017; Bellhouse et al., 2019; Campitiello et al., 2021), a purely hydrodynamic interaction, occurs when a galaxy moves through the Intra Cluster Medium (ICM), causing its gas to be stripped away by the pressure of the hot, dense ICM. This process affects any galaxy falling through the ICM. Although these processes are bound to occur at the same time, however, it is important to distinguish their individual contributions toward galaxy evolution. One possible way of distinguishing these is by looking at the evolution of the star formation rate in relation to the environment (Poggianti et al., 2006). Star Formation Rate (SFR) is affected by both internal (mass quenching) and environmental processes. Cluster galaxies have lower SFRs compared to field galaxies (Balogh et al., 1997; Hashimoto et al., 1998). However, the transition from star-forming to passive systems depends on the galaxy's stellar mass. The consensus is that for stellar masses $> 10^{10}\mathrm{M}_{\odot}$, mass quenching dominates. In contrast, at lower stellar masses ($< 10^{8}\mathrm{M}_{\odot}$) passive fraction steadily increases with decreasing stellar mass, which gives a clear indication of RPS. Davies et al. (2015) found close interactions between galaxies significantly enhance star formation activity, particularly in low-mass galaxies, highlighting the importance of environment in galaxy evolution. Darvish et al. (2016) concluded that galaxy quenching is primarily driven by stellar mass at all redshifts, with environmental effects becoming increasingly significant in dense environments, particularly at lower redshifts. This suggests that environmental factors play a secondary but increasingly important role in dense environments, particularly at lower redshifts i.e., is in the recent past of galaxies' evolution history.

While observational studies have revealed much about the prevalence of RPS, theoretical work and simulations are essential to fully understand its mechanisms and consequences. Analytical models, such as the prescription by Gunn & Gott III (1972), laid the foundation for quantifying gas removal due to ram pressure. Over the years, numerical simulations have expanded on this analytical model, providing deeper insights into the mechanisms and efficiency of RPS under various conditions. For instance, Abadi et al. (1999) and Quilis et al. (2000) performed early 3D hydrodynamic simulations to study the dependence of RPS on the structure of galaxies and the properties of the ICM. These simulations demonstrated that the efficiency of RPS increases with the density of the ICM and the galaxy's velocity, but also depends significantly on the internal distribution of gas and the galaxy's orientation relative to the direction of motion.

Roediger & Brüggen (2006) further refined these simulations by incorporating realistic cluster environments, including gradients in ICM density and temperature. Their work highlighted the complex interplay between the external ICM and the internal gravitational forces within galaxies, showing that the stripping process often occurs in multiple stages, starting with the outer regions and progressing inward.

In recent decades, the effects of RPS on morphology and star formation have been a topic of interest to various researchers (Gavazzi et al., 2001; Yoshida et al., 2004; Scott et al., 2010). Numerical simulations indicate that ram-pressure can successfully remove cold gas from galaxies and, in some situations, can momentarily accelerate star formation activity before quenching it completely (Steinhauser et al., 2016; Choi et al., 2022). There are several observation sets that show the stripping to spirals happens in clusters. Giovanelli & Haynes (1983) define a deficit parameter as the difference between the measured HI mass of a galaxy and the expected HI mass in a field galaxy of the same shape and optical size. Galaxies are found to be HI deficient in the Coma cluster (Bravo-Alfaro et al., 2000), the Virgo cluster (Chung et al., 2009; Giovanelli & Haynes, 1983; Kenney et al., 2004; Boselli et al., 2010; Watts et al., 2023; Roberts et al., 2023), and other adjacent cluster (Solanes et al., 2001). Solanes et al. (2001) report that the average deficiencies increase with decreasing distance to the cluster centers and that deficient galaxies often have more eccentric orbits.

Cayatte et al. (1994) analyzed the neutral hydrogen surface density distribution of 17 bright spiral galaxies in the Virgo cluster with pieces of evidence of gas stripping. They make a quantitative estimate of different gas removal mechanisms for selected individual galaxies and compare this estimate with observed HI morphology. They observed that the HI disc is stripped by RPS in some galaxies. Kenney & Koopmann (1999) & Crowl & Kenney (2006) studied the Virgo cluster galaxy, NGC4522, and concluded that this spiral galaxy is one of the best spiral candidates to study the effect of undergoing RPS. They found evidence of RPS indicated by the absence of HII regions in the outer disc and the existence of HII regions in the extraplanar gaseous filaments. In this particular case, even molecular gas has been removed from the outer disc due to stripping (Kenney & Koopmann, 1999). Jaffé et al. (2018) presented the results of the first comprehensive investigation of the orbital histories of jellyfish galaxies in clusters, using a large spectroscopic sample of cluster galaxies from the Omega WINGS and Wide-field Nearby Galaxy-cluster Survey (WINGS). Based on their findings, the population of jellyfish galaxies are a recently accreted cluster galaxies on radial orbits that are stripped

by ram pressure as they travel at extremely high speeds through the dense cluster center. Furthermore, in cluster and group environments, late-type spiral galaxies have a gas deficiency comparable to the field environment (Cortese et al., 2021).

The ram pressure prescription used extensively in the literature is one provided by Gunn & Gott III (1972) given by $P = \rho_{\rm ICM} V^2$, where $\rho_{\rm ICM}$ is the ambient ICM density and V is the velocity by which galaxy falls in the cluster medium. Because of the galaxy's motion relative to the diffuse gaseous ICM, galaxies experience wind as they orbit through it. Depending on the binding energy of the interstellar medium within the galaxy, the ICM will either be forced to flow around it or blow across it, eliminating part or all of its interstellar gas.

Hydrodynamical simulation of RPS suggests that analytical expression of Gunn & Gott III (1972) ($\rho_{\rm ICM} V^2 > 2\pi G \Sigma_{\rm s} \Sigma_{\rm g}$) is appropriate, at least for galaxies, which are moving face on (Abadi et al., 1999; Quilis et al., 2000; Schulz & Struck, 2001; Marcolini et al., 2003; Acreman et al., 2003; Roediger & Brüggen, 2006). An analytical treatment for RPS based on the system's pure kinematics was provided by Köppen et al. (2018). However, their study is limited to the cluster environment, and there is a lack of information regarding how the galaxies configuration affect stripping. Singh et al. (2019) did a systematic study of the effect of environment and galaxy parameters on the RPS in galaxies. Their study used different environments (Cluster & Group) and galaxy mass profiles at different redshifts. Singh et al. (2019) only modeled asymmetries in the disc due to gas clouds or clumping however did not consider asymmetrical features in the disc galaxies due to the spiral arms of the galaxy. Apart from different masses of infalling galaxies, the galactic asymmetries would also play an important role in quantizing the effect of ram pressure. In this chapter, we calculate the extent of gas removed due to ram pressure in the presence of spiral arms in disc galaxies. Spiral arms will contribute toward the gravitational binding force in the form of asymmetries. This will depend on the different parameters of the galaxies, such as the strength of the arms, the number of the arms, and the width of the arms.

In this chapter, we analyze the effect of the asymmetric features of spiral galaxies on RPS when they fall into the cluster medium. we discuss the ram pressure model and the galaxy's restoring force in section 4.2. Section 4.3.1 accounts for the Intra-cluster medium's properties. We discuss the properties and structure of infalling galaxies in section 4.3.2. Our results are presented for spiral galaxies in section 4.4. We conclude and discuss the implications of our results in section 4.5.

4.2 Ram Pressure and restoring force of the system.

We consider a galaxy traveling through the ICM, with the ambient density $\rho_{\rm ICM}$, and the galaxy's relative velocity w.r.t. the ambient medium as V. The ram pressure, which is the force per unit area acting on the galaxy, is $\rho_{\rm ICM}V^2$, and this is pushing onto the gas in the direction opposite to the motion of the infalling galaxy. This force is capable of stripping gas from the disc whenever it is stronger than the binding force or restoring force of the galaxy. Gunn & Gott III (1972) represented this condition as

$$\rho_{\rm ICM}V^2 > 2\pi G\Sigma_{\rm s}\Sigma_{\rm g}. \tag{4.1}$$

The RHS of the relation in 4.1 is the gravitational binding force of the infalling galaxy (denoted by $F_{\rm res}$ here on), here $\Sigma_{\rm s}$ and $\Sigma_{\rm g}$ are the surface density of the stellar and gaseous components, respectively. Thus, the resultant force acting on gas cloud depends on the ambient medium density ($\rho_{\rm ICM}$), velocity of the infalling galaxy (V), and the physical properties of the infalling galaxy like $\Sigma_{\rm s}$ & $\Sigma_{\rm g}$. Singh et al. (2019) calculated acceleration experienced by the galactic gaseous disc per unit area using the following relation

$$a(R_{\rm c}, R, \theta) = \frac{F_{\rm ram}(R_{\rm c}) - F_{\rm res}(R, \theta)}{\Sigma_{\rm g}(R)}. \tag{4.2}$$

Here, $R_{\rm c}$ is the cluster-centric radius, and R is the disc radius of the galaxy. The significance of the above expression is the velocity of the galactic disc and acceleration on the disc work in the opposite direction.

The numerical method followed closely resembles (Singh et al., 2019) although with subtle differences. The cluster environment set up in the present work is the same as used by the authors, except that the radially infalling galaxies are assumed to begin at $R_{\rm vir}$ with velocity $V_{\rm vir}$. The galaxies fall face-on in a spherically symmetric medium, i.e. the disc plane is perpendicular to the direction of velocity. The value of $F_{\rm ram}$ is calculated at each cluster centric radius $R_{\rm c}$. The galactic disc is divided into concentric annuli of thickness $'dR = 0.5Kpc'$. Further, each annulus is divided in azimuthal angles from 0 to 360 degrees, with an angular difference, $d\theta = 1$ degree.

At each value of $R_{\rm c}$, we evaluate $'F_{\rm res}$ on a 2-dimensional grid over (R, θ). The value of $a(R_{\rm c}, R, \theta)$ is further evaluated using equation (4.2). If ram pressure dominates, then the acceleration is positive, and the gas component of the annulus is pushed out of the

galactic plane. A gas is deemed detached from the disc annulus if it has traveled more than one vertical scale height ($z_{\rm d} = 300pc$) above the disc plane. We consider gas once removed from the disc is removed from the system. Our model can also calculate the gas accretion to the galaxy, this arises when acceleration becomes negative. We do not compute it here because once the gas travels from the disc more than $z_{\rm d}$, it is enough outside the gravitational pull of the galaxy to be accreted by the galaxy. To incorporate the effect of spiral structure, we modify the restoring force by using an appropriate form for $\Sigma_{\rm g}$ and $\Sigma_{\rm s}$ are used, representing the spiral structure in disc plane as discussed in detail in section 4.3.2. The Python script for the algorithm discussed can be accessed at: `https://github.com/meenu228/Ram_pressure_1`. In the next section, we shall discuss the properties of the ambient medium, i.e., the ICM and the spiral disc galaxy profile considered in our analysis.

4.3 Model for ICM and spiral galaxies properties

ICM and the galaxy properties constitute integral components for any quantitative description of ram pressure and hence, considering an appropriate form for these is important.

4.3.1 ICM Model

Hubble & Humason (1931) used measurements of galaxy velocities in cluster regions and the virial equilibrium of galaxy motions to show that the total gravitating cluster masses for the Coma (Zwicky, 1937; Kravtsov & Borgani, 2012) and Virgo cluster (Smith, 1936) were enormous. We shall assume the ICM to be a spherically symmetric cloud of gas. Although the exact profile of surface density of ICM is still debatable, beta profile is one of the most commonly used function to give the radial variation (King, 1962), which is given by

$$\rho_{\beta}(R_{\rm c}) = \frac{\rho_{\rm g0}}{[1 + (R_{\rm c}/R_{\rm core})^2]^{3\beta/2}}, \tag{4.3}$$

where $R_{\rm core}$ is the core radius, which we take to be one-tenth of the $R_{\rm vir}$, central density ($\rho_{\rm g0}$) value is taken as 5.21×10^{-5} $\rm M_{\odot}/pc^3$ is taken from the NFW profile (Navarro J. F., 1996) and value of β is a constant. The virial radius $R_{\rm vir}$ for a virialized halo of

Parameter	Value	Definition
Ω_m	0.3089	Dark matter density[1]
Ω_A	0.6911	Dark energy density[1]
Ω_k	0.0	Cosmological constant[1]
H_0	67.8	Hubble constant[1]
β	0.6	Constant[2]
δ	1	Cluster environment constant[3]
f_{uni}	0.158	Universal baryon mass fraction[1]

Table 4.1: Parameter values for cluster medium. References: [1]Planck Collaboration et al. (2016), [2] Ota et al. (2003), [3] Sharma et al. (2012).

mass M is calculated as (Duffy et al., 2008)

$$R_{\rm vir} = 0.784 \left(\frac{M}{10^8 h^{-1} M_\odot}\right)^{1/3} \left(\frac{\Omega_m^z 18\pi^2}{\Omega_m \Delta_c}\right)^{1/3} \times \left(\frac{1+z}{10h^{-1}}\right)^{-1} kpc, \tag{4.4}$$

where

$$\Omega_m^z = \frac{\Omega_m (1+z)^3}{\Omega_m (1+z)^3 + \Omega_k (1+z)^2 + \Omega_\Lambda}. \tag{4.5}$$

Here, $M = 10^{15} M_\odot$ is the cluster mass, $\Delta_c = 18\pi^2 + 82d - 39d^2$, $d = \Omega_m^z - 1.0$ and z is the redshift of the collapse, which is assumed to be same for both the ambient medium and the infalling galaxy (Barkana & Loeb, 2001) and is taken as the present epoch ($z = 0$) for simplicity. Not considering $z \neq 0$ is justified for the present work as Singh et al. (2019) in their work have used different values of redshift and showed that the RPS is independent of redshift variation. All other parameter values are described in Table- 4.1 along with its values.

For dark matter halo in the cluster, we have used NFW profile from Navarro J. F. (1996). We calculate the ratio of total gas mass $M_{\rm g}$ and the dark matter mass $M_{\rm bg}$ in cluster medium,

$$\Delta = M_{\rm g}/M_{\rm bg}, \tag{4.6}$$

where value of Δ is equal to $f_{\rm uni}\delta$, the constant δ depends on the environment, and f_{uni} is the universal baryon mass fraction. The values of these constants are given in Table-4.1.

4.3.2 Infalling galaxies properties

We are interested in studying the extent up to which the gas is retained in the spiral galaxies in the presence of density concentration in the spiral pattern in the disc. The spiral galaxy mass density profile used for the infalling galaxy is discussed below.

Galaxy's mass profile

We represent thin galactic disc as a zero thickness disc, which is the sum of unperturbed surface density Σ_0, and the perturbed density $\Sigma_1(R, \phi)$ representing the spiral pattern in the frame that rotates at an angular speed Ω_p relative to the galactic rotation. The azimuthal coordinate in the rotating frame of reference is given by $\phi = \theta - \Omega_\mathrm{p} t$, where θ is the angle in the inertial frame (Binney & Tremaine, 2011).

The unperturbed surface density for both gas and stars is assumed to be exponentially decaying density profiles and spiral arms are assumed to be co-rotating (though with different pitch angles) for both components. The Junqueira et al. (2013) model provides a self-consistent representation of spiral density profiles in galaxies, addressing limitations in traditional sine-function-based models. It assumes spiral arms are regions of enhanced stellar density caused by orbital crowding, with the density profile following a logarithmic spiral and a Gaussian-shaped groove. This approach allows precise control of the spiral density contrast and arm width. The model successfully reproduces observed features like symmetric arms within resonance regions. The distribution functions for both are given as (Junqueira et al., 2013);

$$\Sigma_{0_{\mathrm{g/s}}}(R) = \Sigma_{\mathrm{d_{g/s}}} \exp(-R/R_{\mathrm{d_{g/s}}}), \tag{4.7a}$$

$$\Sigma_{1_{\mathrm{g/s}}}(R, \theta - \Omega_\mathrm{p} t) = \Sigma_{\mathrm{x_{g/s}}} \exp(i[m(\theta - \Omega_\mathrm{p} t) + f_{m_{\mathrm{g/s}}}(R)]), . \tag{4.7b}$$

Here, $\Sigma_{\mathrm{d_{g/s}}}$ are the central surface density and $R_{\mathrm{d_{g/s}}}$ are the exponential disc's scale length, which is taken as 4 kpc for both stellar and gaseous discs, $f_{m_{\mathrm{g/s}}}$ is the shape function for spiral arms. To calculate $\Sigma_{\mathrm{d_{g/s}}}$ for the gas and stellar disc, we integrate their respective surface density profiles from zero to the outer radius R_out. This gives the total mass of the disc within the radius R_out, and putting it equal to their respective masses, we find the value of $\Sigma_{\mathrm{dg/s}}$ for both the gas and stellar disc.

To see the effect of galaxy's parameter on ram pressure, we are taking regular galaxy

Property	Symbol	Value	Unit
Number of arms	m	4	—
Half width	σ	4.7	kpc
Scale length	ϵ_s^{-1}	2.5	kpc
Spiral pattern speed	Ω_p	23	$km\ s^{-1}kpc^{-1}$

Table 4.2: Used spiral arms properties

with fully evolved spiral patterns. For calculating the spiral density profile, $\Sigma_{\mathrm{x_{g/s}}}$ and $f_{m_{\mathrm{g/s}}}$, we have used the model given by Junqueira et al. (2013). The spiral arm components e.g. old stars, star-forming regions, molecular gas, and atomic gas have a spatial offset w.r.t. the stellar arms (Hou & Han, 2015), prediction given by the quasi-stationary density wave theory. In the Milky Way, measurements of the parameters for spiral arms like pitch angle, number, and inter-arm separation were carried out between 1980 and early 2005, using several methodologies that generated slightly or widely divergent results, depending on hidden or unknown biases (Vallée, 2008). for gas arms and stellar arms, we have used the different pitch angle as $i = 13^\circ$ and $i = 18^\circ$ (Vallée, 2008), respectively. Other used parameters are defined in Table-4.2.

M_{gal} is the galaxy's total mass (baryons + dark matter) and M_d is the mass of the disc, which are related as

$$M_d = f_d\ f_{uni}\ M_{gal},$$

where $f_d = 0.1$ (Sharma et al., 2012) is a parameter employed in the current work and represents the visible mass fraction in the galactic disc. Of this mass M_d, 10% is assumed to be in gas, and the remaining is in stars (These numbers are taken from the corresponding Milky Way galaxy model (Binney & Tremaine, 2011)). Infalling galaxies in our calculations are assumed to follow a radial trajectory, falling face-on in the medium where the Viral velocity V_{vir} of the galaxy at the virial radius and is calculated using

$$V_{\mathrm{vir}} = \left(\frac{M}{10^8 h^{-1} M_\odot}\right)^{1/3} \left[\frac{\Omega_m^z 18\pi^2}{\Omega_m \Delta_c}\right]^{1/6} \times \left(\frac{1+z}{10h^{-1}}\right) kms^{-1}. \tag{4.8}$$

The cosmological parameters used here are already described in table- 4.1.

4.4 Results

To see the effect of spiral arms on the ram pressure in the galaxy, we take an RPS model similar to the one used by Singh et al. (2019), briefly discussed in the section 4.2. The gas and stellar surface density representing the spiral disc structures employed in our analysis are discussed in section 4.3.2. We first consider spiral galaxies of the mass range $10^{12}M_{\odot}$ and $10^{11}M_{\odot}$, both galaxies contain four spiral arms with 4 *kpc* arms width, galaxies moving with a velocity $V_{\rm vir}$ is subjected to the ICM's radially varying density (ICM density profile is discussed in section 4.3.1). In Figure–4.1(a), we display the fraction of gas in the galaxy's wake to the overall ISM gas mass as a function of $R_c/R_{\rm vir}$ for both masses. The gaseous disc is totally stripped when galaxies fall in the ICM face-on. For a galaxy with mass $10^{11}M_{\odot}$ (dashed line), gas is removed earlier as compared to the galaxy with a mass of $10^{12}M_{\odot}$ (solid line). In Figure–4.1(b), we compare the ratio of gas mass removed for different arm widths for $10^{11}M_{\odot}$ and 4-armed spiral galaxy. Smaller width would give a high-density spiral arm and is expected to retain more gas as observed in our analysis. Same variation is observed in case of 2-armed spirals. In Figure–4.1(c), the fraction of gas removed is plotted for the same mass galaxy with an arms width of 2 *kpc* with a different number of arms. It is seen that an increase in the number of arms decreases the gravitational binding of gas with disc due to sparse density and hence removing the gas faster.

Uptill now we have analyzed the effect of galaxy parameters like strength and the number of spiral arms on the RPS. This parametric exploration leads us to the conclusion that the asymmetries would act against RPS and gas removal will be difficult due to RPS alone. These are consistent with conclusions by Singh et al. (2019) that the presence of asymmetries does help in the retention of gas.

In Figure–(4.2), we present the snapshots of spiral gas density in $x-y$ plane for a face-on galaxy at different values of $R_c/R_{\rm vir}$. From the Figure, we observed how the gas density in spiral arms reduces as the galaxy moves through ICM. The gas removal begins from the outer edges of the galaxies, decreases arm strength, and eventually removes all the gas as the galaxy approaches the center of the cluster. In the previous works on RPS simulations, it has been demonstrated that during the start of the galaxy's encounter with the ICM, the spiral arms are squeezed in the first $50Myr$ of applying ram pressure, and a considerable increase in ICM density is observed. Furthermore, the stripping of the gaseous disc begins on the galaxy's edges (Steinhauser et al., 2012). These are clearly

evident in our simple semi-analytical approach. The present model demonstrates that spiral arms significantly impact the process of ram pressure stripping (RPS), and a direct comparison with Singh et al. (2019) has now been made explicit. Now by comparing our results (with spiral structure, figure–4.1) with the study of Singh et al. (2019) (with exponential disk (Σ_0), figure-4) gas is left in the arms as the galaxy moves close to the center of the cluster, while the exponential disk is stripped of all gas. From Singh et al. (2019) results, for $10^{12} M_{\odot}$ galaxy retains only 35% gas till it reaches half of the cluster radius, while in our results (from the figure–3), 50% gas is left when the galaxy reaches the same distance of the cluster radius. So spiral structure (Σ_1) are the regions in the spiral arms that contribute higher surface density region as compared to other regions of the disk, and the spiral patterns significantly contribute to retaining the gas as the galaxy moves towards the cluster center. we can conclude that the presence of spiral arms does help in gas retention to some extend and can explain the presence of gas-rich spirals in a rich environment. However, the gas does get stripped much before it reaches the center. This contradicts with the observations of the presence of gas in disc galaxies in dense environments, implying an additional restoring force might be acting against ram pressure, supporting the gas retention in discs. One such force component could be the magnetic pressure which we shall discuss in Chapter-5.

4.5 Conclusion and Discussion

Detailed observations of galaxies reveal gas deficiencies (Giovanelli & Haynes, 1985), lopsided gas distribution (Jog & Combes, 2009) and tail-like features as seen in jellyfish galaxies (Jaffé et al., 2018). Such observed features could arise due to stripping of gas owing to ram pressure (Gunn & Gott III, 1972). Several authors have studied how the gas is removed due to ram pressure as the disc galaxy moves through the intra-cluster medium (Cayatte et al., 1994; Kenney & Koopmann, 1999). Ram pressure does support the observed gas deficiency and distorted gas distribution in the galaxies. Of a particular interest to us is the work by Singh et al. (2019), in which they give the relation between mass of gas removed or the radius up to which the gas is removed from the disc galaxy as the galaxy follows its trajectory in the intra-cluster medium. However, the authors could only comment on the upper limit of the gas mass removed due to the simplified model for disc galaxies' mass distribution, orbital parameters, and intra-cluster medium.

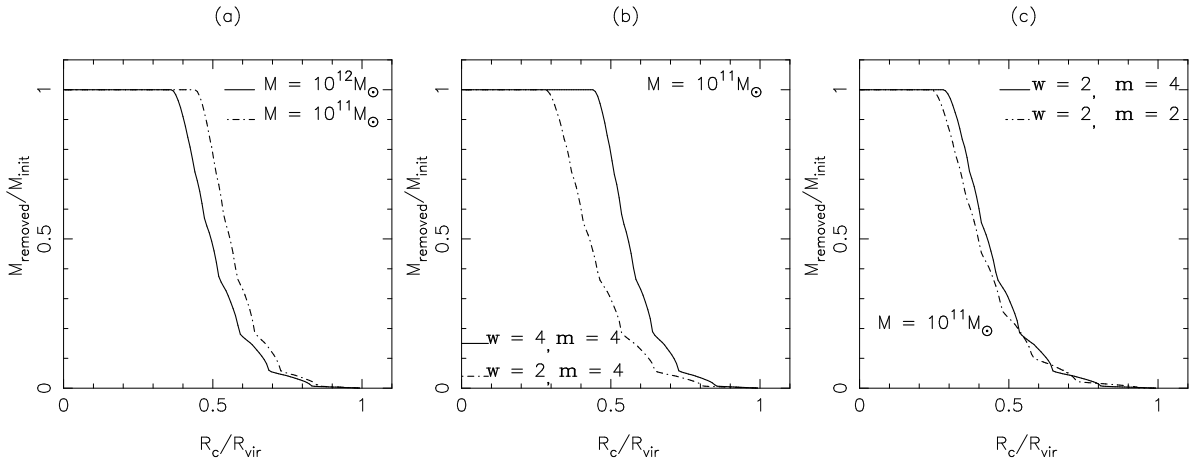

Figure 4.1: Plots for a fraction of gas mass removed vs R_c/R_{vir} due to RPS as the galaxy falls in the cluster. (a) galaxy with different mass profile of $10^{12}M_\odot$ and $10^{11}M_\odot$ with 4 spiral arms and width = 4 kpc (b) $10^{11}M_\odot$ galaxy with 4 spiral arms and different arm width of 4 and 2 kpc (c) galaxy mass of $10^{11}M_\odot$ with different number of arms i.e, 4 and 2 with arms width = 2 kpc.

In this study, we identify a more appropriate mass distribution for the spiral galaxies along the spiral arms in the galaxies. Appropriate modifications are done in the semi-analytical model given by Singh et al. (2019), as discussed in section-4.2. Such features are expected to bound the gas to the disc galaxy. Details of the profiles used for ICM and spiral galaxies used are discussed in section 4.3.1 and 4.3.2. The ambient medium considered is spherically symmetric and the galaxy passes face-on through the medium on a radial orbit. For dark matter halo, we assume an isothermal profile and a beta model for the ambient medium's gas distribution, which are discussed in section 4.3.1. Spiral arms structure and morphology for gas and stellar disc, used for our study have been discussed in detail in section 4.3.2.

Galaxies are represented as a collection of annuli, and for each annulus, we test for RPS of gas. This gives us the ability to calculate the gas mass stripped at a given position (R_c/R_{vir}) in the intra-cluster medium as the galaxy travels in the ambient medium. We perform a detailed analysis of the amount of gas removed due to the discs' spiral structure. The parameters explored are the mass of the infalling galaxy, the number of spiral arms, and arms thickness. The variation of the fraction of mass removed versus the clustercentric radius with these parameters is shown in the Figure-4.1. The main conclusions of this work are listed as:

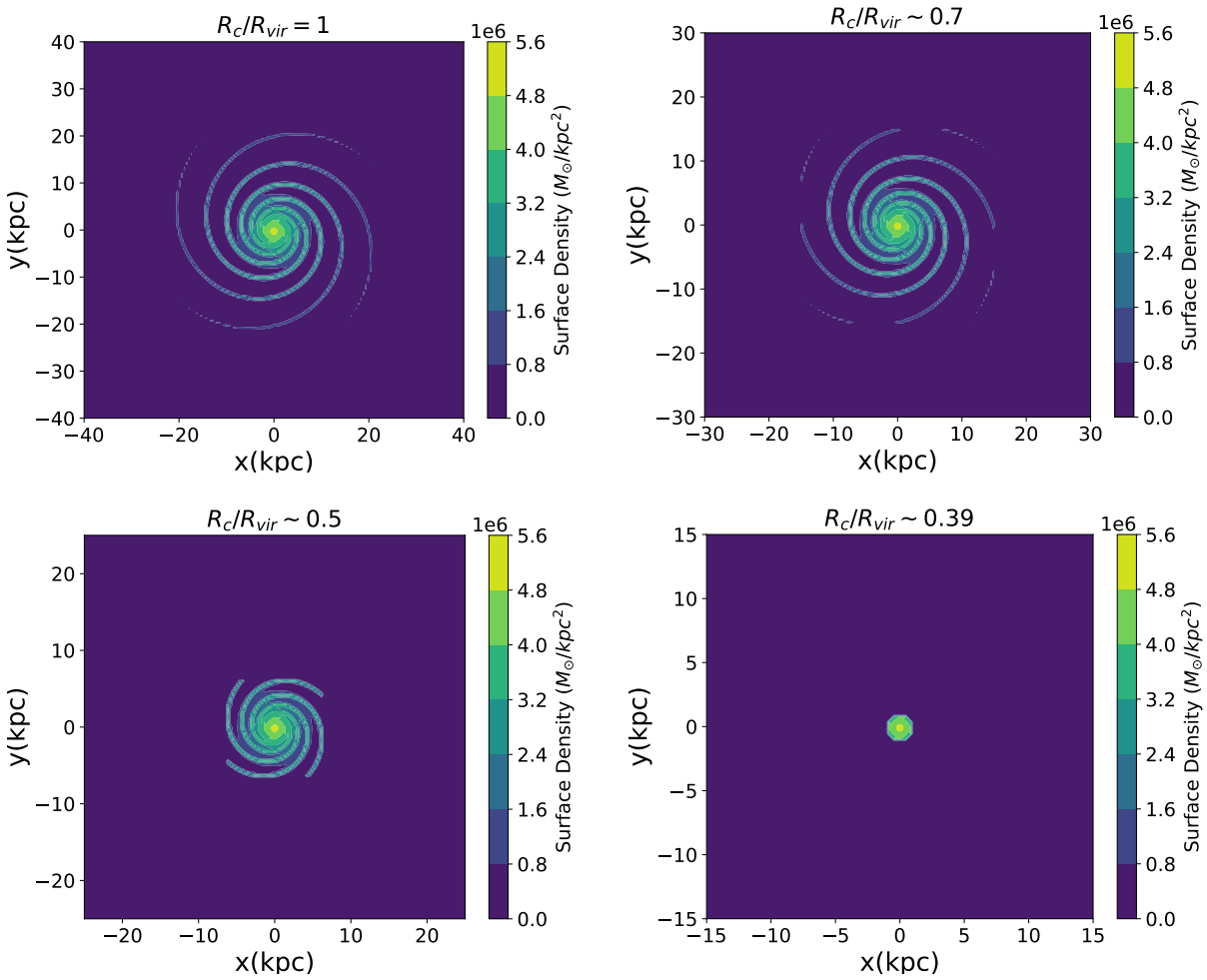

Figure 4.2: The gas projection plotted at various cluster-centric distances, indicated at the top of each panel, for the $10^{12} M_\odot$, 4-armed spiral galaxy.

- Higher mass galaxies retained gas for a long time.
- Two armed spiral galaxies could retain gas longer as compared to the four armed spirals.
- Thinner and more dense spiral arms retained more gas when compared with thicker and sparse spiral arms.

The first one is consistent with the results by Singh et al. (2019). However, when a comparison is made between same-mass galaxies (spiral galaxy), in the present work and the analysis done by the Singh et al. (2019) (exponential galaxy), the spiral structures do help in retaining gas to a larger extent. A possible reason for the second and third points mentioned above could be that as we increase the number of arms or arms width, the density of gas in arms is decreased, making it loosely bound and hence removing it faster due to ram pressure. To further verify how the gas is removed, we plot the projection of gas mass in the galaxy for the various values of $R_{\rm c}/R_{\rm vir}$ in Figure-4.2. We observe that the arm thickness is decreased in the beginning, eventually leading to the complete removal of gas much before the cluster center. This work is an analysis of ram pressure in the presence of spiral structures. Studying ram pressure acting on galaxies in the presence of asymmetries in the ICM-like filaments will also be useful at this stage. Moreover, it is important to study the evolution of removed gas from the disc to get a one-on-one mapping of our semi-analytical model with the observations.

Chapter 5

Effect on the Ram pressure with the presence of the magnetic field in the disc galaxies

5.1 Introduction

One of the intrinsic components of disc galaxies, which is by far the most neglected one in studies pertaining to RPS is the magnetic field embedded along the spiral arms (sometimes also found predominantly in inter-arm regions) in the galaxies. The presence of the magnetic field in spiral galaxies is detected from (polarized) radio continuum emission and Faraday rotation measurements (Beck, 2016). Brown & Hazard (1951) first detected the magnetic field in nearby spiral galaxy M31 using Synchrotron emission. Faraday rotation and measurement of linearly polarized emission require good resolution and sensitive receiving systems. This was first successfully achieved in the Milky Way by Westerhout et al. (1962) & Godwin (1962) and for spiral galaxy M51 by Mathewson et al. (1972). Microgauss order magnetic fields are found in all types of galaxies (Jagannathan et al., 2021) as well as clusters of galaxies in the present-day universe (Kronberg, 1994; Widrow, 2002; Carilli & Taylor, 2002). The regular magnetic field in an evolving spiral galaxy is discussed by Beck et al. (1994). Observation of damped Lymann alpha systems reveals the presence of a magnetic field in the young galactic disc. Observations have also shown that in many Virgo cluster spirals during RPS, ridges of enhanced linear radio polarization along the leading edges with magnetic field associated with the

leading edges (Vollmer et al., 2007, 2008). Ram pressure has an impact on the dust lanes morphology, especially the C-shaped characteristics that are neatly curved and anchored close to young star complexes, the almost linear filaments connecting with the dust front perpendicularly, and the relatively straight and smooth lanes away from young star complexes, strongly suggests that magnetic fields partially bind and are connected to the distant regions of the ISM. So, C-shaped filaments give evidence of magnetic binding in the galaxy, which plays an important dynamic role during RPS (Kenney et al., 2015). Star formation rate depends on the magnetic field (Nixon & Pringle, 2019) and cosmic-rays pressure (Birnboim et al., 2015), so for gas dynamics of a molecular cloud, magnetic fields are also found to be essential (Ade et al., 2016). It has been proposed that magnetic fields only weakly slow down the rate of stripping and smooth the stripped features in the tail between simulations (Ruszkowski et al., 2014; Tonnesen & Stone, 2014; Ramos-Martínez et al., 2018; Ruszkowski et al., 2014). For example, Ruszkowski et al. (2014) demonstrated through MHD simulations that magnetic fields could reduce gas stripping in galaxies by acting as an additional restoring force, particularly in regions of the ISM compressed by the ICM. Tonnesen & Stone (2014) observed that while magnetic fields might not significantly reduce the total amount of stripped gas in unmagnetized galaxies, their effects become pronounced in regions with organized magnetic field structures. Müller et al. (2021) demonstrated the role of magnetic fields during the gas stripping process using radio observations. By mapping the polarized synchrotron emissions, they revealed that magnetic fields align with gas filaments during stripping, providing resistance to gas removal by increasing the structural stability of the ISM. Their results showed enhanced magnetic pressure in regions where the ICM compresses the gas, reducing the efficiency of stripping. Additionally, their comparison with MHD simulations confirmed the stabilizing effects of magnetic fields in mitigating RPS. These findings are particularly relevant to the current study, as they bridge the gap between observational and theoretical approaches.

In this chapter, we analyze the effect of the magnetic fields in galaxies on RPS when they fall into the cluster medium. Intra cluster medium properties and the infalling galaxy's mass profile used in this work are the same as discussed in section 4.3.1 and 4.3.2 in the Chapter-4. Magnetic field profiled of the infalling galaxy disscussed in section 5.2. In section 5.3, we discuss the generalized model for ram pressure and the restoring force in the galaxy. In section 5.4, our results are presented for the magnetic field in the spiral galaxies. We conclude and discuss the implications of our analysis in

section 5.5.

5.2 Galaxy's magnetic field

Magnetic field in spiral galaxies is known to have a regular and random component. Background and embedded radio sources and Rotation Measure (RM) synthesis are used to investigate magnetic field in the literature. The observation of RM of the pulsars in our Galaxy shows that our Galaxy contains a regular magnetic field (Beck & Wielebinski, 2013). The structure of the galactic magnetic field has been mapped with observations of pulsars, allowing for a three-dimensional "tomography" of the galactic magnetic field (Han et al., 2018). The RM of pulsars within our Galaxy has made it possible to map out the presence of regular magnetic fields in the Galactic plane (Sofue et al., 1986; Han, 2008; Han et al., 1999).

However, observations of different spiral galaxies do not give conclusive evidence about the exact configuration of the magnetic field, for instance, some point toward the magnetic field with 2π symmetry configuration (i.e., Bisymmetric spiral(BSS), (Sofue et al., 1986; Fletcher et al., 2011)) whereas some observations suggest π symmetry configuration (i.e., Axisymmetric spiral (ASS), (Stanev, 1997)). The radial and azimuthal variation of magnetic field in galactic plane for BSS configuration is given as (Indrani & Deshpande, 1999),

$$B(R,\theta) = B_0(R)\ \cos\left(\theta - \beta \ln \frac{R}{R_0}\right). \tag{5.1}$$

Corresponding radial and azimuthal components of the magnetic field can be written as,

$$B(R) = B(R,\theta)\sin(p), \quad B(\theta) = B(R,\theta)\cos(p), \tag{5.2}$$

The BSS configuration is suitable for representing the regular magnetic fields observed in many spiral galaxies, where p is the pitch angle of the magnetic field spirals and the value of pitch angle is the same as that of the gaseous spiral arms, $\beta = 1/\tan(p)$, R_0 is a constant, and $B_0(R)$ is the magnitude of the field as a function of galactocentric distance, for Milky Way $B_0(R)$ can be taken as $b_0 R_\odot/R$, b_0 is the average magnetic field strength in units of Gauss and $R_\odot$ is the distance of the sun from the center taken as 8.5 kpc (Sofue & Fujimoto, 1983; Rand & Kulkarni, 1989; Stanev, 1997; Indrani & Deshpande, 1999; Tinyakov & Tkachev, 2002). Our Milky Way galaxy contains a BSS rather than

a concentric structure or ASS, as deduced from the observations of RM (Sofue et al., 1986). In this work, we use BSS configuration. In that case, the acting hydrostatic and hydrodynamic force on the fluid must be supplemented by the forces obtained from the magnetic field stress tenor, which is equal to $B^2/8\pi$ along the line of force and transverse pressure (Shukurov & Subramanian, 2021). In the next section, we shall discuss the net effect of RPS acting on the galaxies in the presence of magnetic field.

5.3 Generalized model for RPS

In this section, we discuss the generalization of the model given by Singh et al. (2019) to incorporate the effect of the magnetic fields on ram pressure, which contributes to the restoring force. The net force per unit mass per unit area is

$$a(R_{\rm c}, R, \theta) = \frac{F_{\rm ram}(R_{\rm c}) - (F_{\rm res}(R,\theta) + F_{\rm mag}(R,\theta))}{\Sigma_{\rm g}(R,\theta)}, \tag{5.3}$$

where restoring force due to magnetic field is denoted by $F_{\rm mag}(R,\theta) = B^2/8\pi$. For astrophysical systems like galaxies, the magnetic field lines can be assumed to be frozen along the material upon in galaxies using the flux freezing theorem (Alfven, 1942a). Hence the magnetic pressure term will add to the restoring force. The details of the magnetic profile used are given in section–5.2.

At each value of $R_{\rm c}$, we evaluate $'F_{\rm res} + F_{\rm mag}\ '$ on a 2-dimensional grid over (R,θ). The value of $a(R_{\rm c}, R, \theta)$ is further evaluated using equation-(5.3). If $a(R_{\rm c}, R, \theta) > 0$, and this acceleration is to move the gas cell, starting from rest to a distance of $300\,pc$ away from the disc the gas is assumed to be removed from the disc as well as the system. Before moving to the next $R_{\rm c}$ value, we also calculate the total gas mass removed from the disc. In the next section, we discuss the results of the present work.

5.4 Results

We analyze the impact of magnetic field on the ram pressure. For this, we take $10^{12} M_{\odot}$ galaxy and in Figure-5.1(a) plot the $M_{\rm removed}/M_{\rm init}$ vs R_c/R_{vir} for galaxy containing magnetic field (dash-dotted line) in the disc and without magnetic field (solid line). The taken magnetic field strength is $10^{-5} G$. The galaxy retains some amount of gas against the ram pressure, even as the galaxy reaches the center of the cluster medium. The

effect of decreasing magnetic field strength on RPS is shown in Figure-5.1(b), which represents $M_{\rm removed}/M_{\rm init}$ vs $R_{\rm c}/R_{\rm vir}$ with magnetic field strength of $10^{-5}G$ and $10^{-6}G$, for a 4-armed spiral galaxy with mass $10^{12}M_{\odot}$. The galaxy is depleted of all its gas when $10^{-6}G$ magnetic field is present, albeit slowly compared to the case of no magnetic field, as can be concluded by comparing solid line plots in both Figures-5.1(a) & 5.1(b). We give the snapshots of the galactic disc at different $R_{\rm c}/R_{\rm vir}$ for $10^{12}M_{\odot}$ spiral galaxy with magnetic field of strength $10^{-5}G$ in Figure -(5.2). Comparing the corresponding snapshots in Figure-(5.2) with the relevant snapshots in figure-(4.2) it can be concluded convincingly that the gas is retained to a larger extent due to the presence of the magnetic field.

The value of magnetic field strength, which will support retaining gas throughout its orbit, can be calculated analytically. For the acceleration defined in equation-(5.3), we put $a(R_{\rm c}, R_{\rm inner}, \theta_0) = 0$, where $R_{\rm inner}$ is taken $R_{\rm d}/2$, $R_{\rm d}$ is the disc scale length, θ_0 is taken such that the peak of spiral pattern is selected. The reason for choosing this value of disc radius and azimuthal angle is that the disc restoring force will be maximum here, and if the gas is stripped close to the center, it will be stripped from the outer as well. For different values of magnetic field, we solve for $R_{\rm c}/R_{\rm vir}$ analytically. The values are displayed in the first and second columns of table-5.1. This $R_{\rm c}/R_{\rm vir}$ corresponds to the cluster radius at which almost all the gas from the disc will be removed. The value of $R_{\rm c}/R_{\rm vir}$ for which $M_{\rm removed}/M_{\rm init} = 1$ from our numerical simulation is displayed in the third column of table-5.1. The close match between the analytical and numerically calculated $R_{\rm c}/R_{\rm vir}$ values testifies to our numerical results. Moreover, it can be clearly seen that for magnetic fields equal to or lower than $10^{-6}G$, the gas will be completely stripped from the disc of the spiral galaxy before reaching the center of the cluster medium. For $B = 10^{-5}G$, $M_{\rm removed}/M_{\rm init}$ is never equal to 1 in our simulation and no solution exists for $a(R_{\rm c}, R_{\rm inner}) = 0$ analytically, implying that the gas in the galaxy disc will be retained by the galaxy throughout its orbit. The ram pressure stripping is less efficient in regions where the disc is strongly magnetized. Also, for lower magnetic fields, the same value of R_c/R_{vir} for complete removal of gas hints that the clustering of mass due to spiral arms dominate the restoring force due to the magnetic field.

In the following section, we conclude our findings and discuss their implications.

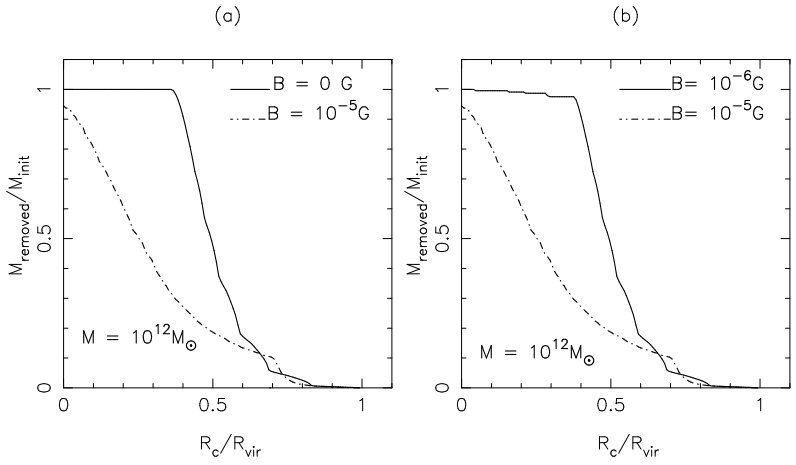

Figure 5.1: The evolution of the mass lost from the disk normalized by the initial disk mass, plotted as a function of the ratio of clustercentric distance (R_c) and the cluster's virial radius ($R_{\rm vir}$). (a) Comparison of mass evolution in absence of magnetic fields (solid line) and in presence of magnetic fields of $10^{-5}G$ (dash-dotted line) for the $10^{12}M_{\odot}$ galaxy. (b) Comparison of the evolution for $10^{12}M_{\odot}$ galaxy containing different magnetic field strengths of $B = 10^{-5}G$ and $B = 10^{-6}G$.

Magnetic field strength, **B**	R_c/R_{vir} calculated Analytically	R_c/R_{vir} obtained from Numerical modeling
$10^{-6}G$	0.0399	0.0391
$10^{-7}G$	0.3599	0.3505
$10^{-8}G$	0.3599	0.3505

Table 5.1: The analytically derived and numerically calculated values for the cluster-centric radius up to which all of the gas in the galactic disc is removed as the galaxy moves through the background medium with the different magnetic field strength.

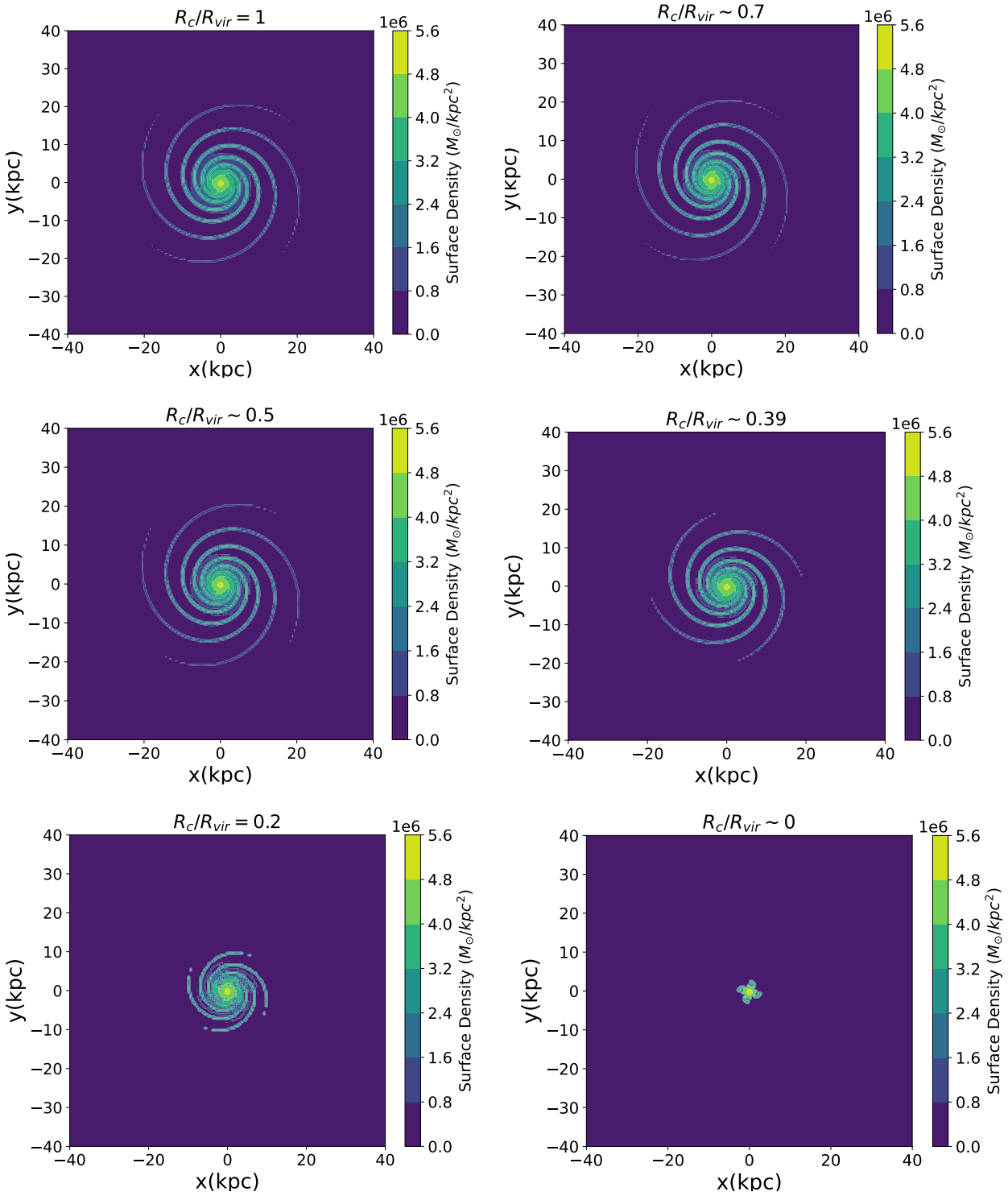

Figure 5.2: This plot shows the evolution of projected gas density/surface density at various cluster-centric distances (indicated at the top of each panel) for a $10^{12} M_\odot$ galaxy with 4 spiral arms containing magnetic field of strength $B = 10^{-5} G$.

5.5 Conclusion and Discussion

We analyze the effect on ram pressure in the presence of magnetic field with the same parameters of ICM, which is discussed in section-4.3.1 and galaxy with 4 spiral arms and width of 4 kpc for $10^{12} M_{\odot}$ galaxy, profile discussed in the section-4.3.2. An appropriate form of magnetic field component as the restoring force along the spiral arm is introduced, which is discussed in details in section-5.2. A strong magnetic field has a considerable contribution against ram pressure. Using a bisymmetric spiral (BSS) configuration, the model incorporated magnetic fields as an additional restoring force through the magnetic pressure term ($F_{mag} = B^2/8\pi$). This magnetic pressure directly opposes RPS, reducing the stripping efficiency and retaining gas in the galactic disc. Results are highlighted in Figures-5.1(a), & 5.1(b) and table-5.1. The major outcomes of this study are listed as follows:

- The strong magnetic field supports the gas retention in the disc all the way up to the center of the cluster.
- The galaxy with magnetic field strength greater than $10^{-6}G$ all gas is not stripped for the complete orbit of the galaxy.
- For fields weaker than $10^{-7}G$, the magnetic fields are inefficient in gas retention and self-gravity is the dominant restoring force.

A comparison of the gas removal mechanism in the spiral arms of the galaxy without the magnetic field and with the magnetic field could be seen in Figures-4.2 & 5.2. From these figures, we can see that at $R_c/R_{vir} = 0.39$, a small part of the gas is left in the disc galaxy in the case without magnetic binding, while a larger part of the gas is retained in the galaxy with the magnetic binding. A galaxy with a magnetic field retains gas at its center when it passes through the center of the cluster. The conclusion references an additional indirect effect, where magnetic fields align with gas structures, leading to a stabilization of the interstellar medium (ISM). This alignment enhances gas density in regions where the magnetic field is strong, effectively increasing the gravitational restoring force. So, a particular amount of magnetic field plays a substantial role in retaining gas in the galaxy. It could also be seen in the MHD simulation given by Ramos-Martínez et al. (2018). These studies show that magnetic fields reduce gas stripping by providing structural support and enhancing gas concentration in the disc.

In this work, the reason behind the retention of gas in the disc is that the magnetic field is aligned with the gas arms, so it will increase the gas density of the galaxy (Kenney et al., 2015), which will work against the ram pressure. According to the HST images, magnetic fields are dynamically important during RPS. Small-scale (< 10 pc) simulations of cloud–wind interactions provide evidence for magnetic binding (Kenney et al., 2015). The only simulations that produce linear headtail features connected to a downstream perpendicular ISM front are ones with magnetic fields (Leao et al., 2009).

Tonnesen & Stone (2014) also investigated the role of magnetic field on the RPS. They run magnetohydrodynamic (MHD) simulations of RPS that included only a galactic magnetic field. Based on their simulations, Tonnesen & Stone (2014) have concluded that magnetic fields in the galaxies do not significantly impact the total amount of stripped gas in galaxies compared to the removed gas in unmagnetized galaxies. This work considers magnetic fields aligned with spiral arms, which amplify the restoring force and highlight conditions where magnetic fields play a significant role. Thus, the novelty of this study lies in analyzing the combined effects of spiral structures and magnetic fields, providing new insights into the dynamic role of magnetic fields in mitigating gas stripping. In contrast, Ruszkowski et al. (2014); Vijayaraghavan & Sarazin (2017) simulated the evolution of a disk galaxy in the presence of a uniformly magnetized wind, representing a magnetized ICM. They found that for a face-on galaxy, the stripping rate of gas is compressed as compared to the pure hydrodynamical simulation. Ruszkowski et al. (2014) found that a magnetized ICM can create magnetic draping layers, which can enhance the stability of the galaxy's gas disk against stripping.

Magnetic draping is a significant process in the context of RPS. Idealized simulations of cloud and wind interactions (Dursi & Pfrommer, 2008) and (Pfrommer & Dursi, 2010), have shown that magnetic draping of the intra-cluster medium (ICM) over a projectile or galaxy can significantly affect the evolution of stripped gas in the tail. In the scenario of magnetic draping, as a galaxy moves through the ICM, the magnetic field lines are stretched and wrapped around the galaxy, creating a draping layer. This layer provides additional magnetic pressure that acts perpendicular to the direction of motion, offering maximum restoring pressure against the RPS. The studies by Pfrommer & Dursi (2010) indicate that for typical ICM conditions with densities of $10^{-4}\mathrm{cm}^{-3}$, a uniform ICM magnetic field strength of the order of 7μG is essential to explain the morphology of some RPS galaxies. This field strength is comparable to the field strength used in our study but is applied in the context of an ordered magnetic field in the ICM rather than

the ISM.

The regular magnetic fields in the disk of the galaxy would also be compressed by the impinging ICM wind, especially if the wind is unmagnetized. The orientation of the magnetic field lines perpendicular to the ICM wind can thus provide significant resistance to gas stripping. While our current model focuses on the magnetic fields within the galaxy, the insights from magnetic draping studies highlight the importance of considering both internal and external magnetic fields in understanding the full dynamics of RPS. Future studies should aim to integrate these effects for a more comprehensive understanding.

Chapter 6

Conclusion & Future Scope

6.1 Conclusion

This thesis deals with a study of the internal and external dynamical effects on the galaxy's evolution and formation. We begin by giving an introduction to the subject matter, a review of the literature, basic definitions and equations, thesis objectives, and a brief summary of the contents of the various chapters of the thesis in Chapter 1. The work carried on in this thesis is divided into two parts and we aim to understand certain aspects of the galaxy structural evolution and kinematics. We discuss these individually below:

- **In the first part of the thesis** we studied the internal dynamics effect on the galaxy's observational features and vice-versa. All galaxies with bulge or spheroids are known to have a massive central black hole at the center (Gebhardt et al., 2000), and the dynamics of the galaxies at the center play an important role in the evolution of galaxies on a larger scale as well. This part is related to the asymmetric features observed by many researchers in the galaxy's central region, known as the lopsidedness feature in the galaxy. The gravitational potential of galaxies' core area, or nuclear disc is near to the Keplerian, and these Keplerian discs are known to support stable non-axisymmetric features (Lopsideness) at the galaxy's center. We shall explore these eccentric modes as possible reasons for observed lopsidedness in the centers of galaxies. A detailed explanation of this section of the thesis is given below:

  Firstly Chapter– 2 of this thesis is related to discs like acceration discs or discs

composed of stars and gas, orbiting the heavy mass at the galaxy's center. The disc dynamics of such galactic systems are affected by the gravitational force of the central massive object, and this type of disc is called the Keplerian disc. The precession in stellar orbits around massive black holes may arise due to disc self-gravity or from pressure gradients in thin accretion discs. These kinds of nearly Keplerian discs enable stable non-axisymmetric slow modes.

We formulated the dispersion relation for the coupled disc system and explored the stability of modes. The presence of gas enhances the instabilities and makes the discs more susceptible to the formation of unstable lopsided distributions. The higher gas fraction in the disc allows the existence of modes with larger values of ω value. We analyze slow modes for azimuthal wavenumber $m = 1$ for the continuum disc because these are the only modes that exist (Binney & Tremaine, 2011). We also study the nature of discrete eigen-spectra by quantizing the modes using the Bohr-Sommerfeld quantization condition. An analysis of discrete spectra for different fractions of gas mass is performed and prograde modes exist only for gas mass less than 10% of total visible mass. However, retrograde modes exist for higher mass fractions as well. These could possibly give rise to instabilities due to gas mass now being in counter-rotation (Gulati et al., 2012). Though simplified, our analysis gives a physically relevant framework for the formation and existence of eccentric discs at the center of galaxies without invoking any external factor.

Another lopsided feature seen from the simulation and observations in the Milky Way-type galaxy, which is of interest to us for present work, is that the center of the dark matter halo could be off-centered by a few parsecs w.r.t. the center of the core in the spiral galaxies. In context to this, we studied how stellar orbits at the galaxy's central region is disturbed by an asymmetric dark matter halo potential (Chapter-3). We derived equations of motion of stars in the core of galaxies in terms of three-dimensional perturbed potential arising from the observed configuration of dark matter halo with an offset. We used first-order epicyclic theory to solve the orbits and analyze the magnitude of this perturbation, which grows at small radii and exhibits $m = 1$ azimuthal fluctuations. We studied central region within 3 kpc radius and observed that even a small halo offset of 300 pc caused surprisingly strong spatial and kinematical lopsidedness. Such a significant impact on the dynamics of central region could help fuel the active galactic nucleus.

- **In the second part of this thesis**, we studied the effect of external dynamics on the galaxies' evolution. The work related to this is discussed in Chapters 4 and 5. We first studied the gas-removing mechanism, namely ram pressure stripping, in the galaxies when they pass through the cluster medium. Gas deficiency in the galaxy directly affects the star formation rate and the evolution of the galaxy. When a galaxy falls into a cluster of galaxies, the infalling galaxy experiences a force which is caused by the interstellar medium of the cluster.

  RPS has been seen in different types of environments and for different masses of galaxies. So, the environment and galaxy morphology are expected to play a substantial role in quantifying the gas removal from the galaxies. We studied this phenomenon with different parameters of the galaxies, such as the masses of the galaxy, the number of arms, and the arm widths. Our analysis gives us that higher mass galaxies retained gas for a long time. Two-armed spiral galaxies could retain gas longer as compared to the four-armed spirals. An increase in the number of arms decreases the gravitational binding of gas with disc due to sparse density and hence removing the gas faster.

  Further,the magnetic field in spiral galaxies is an integral part of galaxies evolution and is known to have a regular and random component, with total field intensities of roughly a few μG (Ruszkowski et al., 2014). In Chapter 5, we studied the impact on the ram pressure stripping in the galaxy when the galaxy's magnetic field is included as a restoring force. Because of Alfven's flux freezing theorem for astrophysical systems, the magnetic field lines must be frozen along the plasma (Alfven, 1942a), and hence magnetic field is expected to act against the ram pressure. We report that magnetic fields of the order of μG have a considerable contribution against the ram pressure mechanism. The strong magnetic field supports the gas retention in the disc all the way up to the center of the cluster. This outcome is bound to get a crucial input for numerical simulations of galaxy formation and evolution.

6.2 Future Scope

The current work has given us some interesting outcomes, which are important for the study of galactic dynamics, its evolution, and their correlation. The results, along with

their pros and cons, were discussed in detail earlier. There are few intensity outcomes that needs further investigation, which are discussed below:-

- We studied the instability of slow modes for a coupled disc system. Several avenues of research remain open for further investigation, such as due to retrograde modes which exist for long leading and trailing waves. The retrograde modes with eigenfrequency $\omega < 0$ will be short-lived due to processes like viscous dissipation. But they may be responsible for trigger instabilities in the coupled system (Gulati et al., 2012). This could be further explored in future work. Also, a detailed study of the eigenvalue problem by using more rigorous mathematical formulation in order to reveal previously undiscovered aspects of the behavior of the coupled system will be of further interest

- In our work, we assumed that η is a constant. For many practical purposes, the value of parameter η is not constant. This would be lead to a more realistic model of the system, allowing for spatial or temporal variations in η, which could reveal the nature of instabilities or stabilize certain modes for the coupled system and can be taken formed in future.

- Studying the off-centered dark matter halo from the center of the galaxy provides insights into many unusual phenomena within the galaxy, as discussed earlier. The comparison with high-resolution images of centers of galaxies to quantify the perturbation derived in this current study is something of interest and can be taken up during future observational studies.

- In the present we studied the gas mass removed due to ram pressure stripping for different galaxy's morphology. Future research could be on examining how ICM filaments influence the RPS process. These large-scale structures may change the interaction intensity with galaxies and the local density of the ICM, which might impact the pattern and efficiency of stripping. Also, a detailed comparative study of RPS on different components of galaxies will provide insight into how spiral arms are deferentially affected by stripping, enhancing our understanding of the process's impact on overall galaxy structure during future studies. In the present study, the effect on RPS is due to the magnetic field in the galaxy. Further investigations of the RPS in the presence of a magnetized ICM and understanding how they

influence the stripping process is something that is unexpected and can lead to interesting consequences.

Bibliography

Abadi M. G., Moore B., Bower R. G., 1999, Monthly Notices of the Royal Astronomical Society, 308, 947

Acreman D. M., Stevens I. R., Ponman T. J., Sakelliou I., 2003, Monthly Notices of the Royal Astronomical Society, 341, 1333

Ade P. et al., 2016, Astronomy & Astrophysics, 594, A27

Aguerri J. A. L., González-García A. C., 2009, Astronomy & Astrophysics, 494, 891

Alfven H., 1942a, Arkiv för Matematik, Astronomi och Fysik, 29, 7

Alig C., 2013, PhD thesis, lmu

Arp H., 1966, The Astrophysical Journal Supplement Series, 14, 1

Bacon R., Emsellem E., Combes F., Copin Y., Monnet G., Martin P., 2001, Astronomy & Astrophysics, 371, 409

Bacon R., Emsellem E., Monnet G., Nieto J., 1994, Astronomy and Astrophysics, 281, 691

Bailin J., Simon J. D., Bolatto A. D., Gibson B. K., Power C., 2007, The Astrophysical Journal, 667, 191

Baldwin J., Lynden-Bell D., Sancisi R., 1980, Monthly Notices of the Royal Astronomical Society, 193, 313

Balogh M. L., Morris S. L., Yee H., Carlberg R., Ellingson E., 1997, The Astrophysical Journal, 488, L75

Balogh M. L., Navarro J. F., Morris S. L., 2000, The Astrophysical Journal, 540, 113

Balsara D., Livio M., O'Dea C. P., 1994, The Astrophysical Journal, 437, 83

Banerjee A., Matthews L. D., Jog C. J., 2010, New Astronomy, 15, 89

Barkana R., Loeb A., 2001, Physics reports, 349, 125

Beck R., 2016, The Astronomy and Astrophysics Review, 24, 1

Beck R., Poezd A., Shukurov A., Sokoloff D., 1994, Astronomy and Astrophysics, 289, 94

Beck R., Wielebinski R., 2013, Planets, stars and stellar systems, 5, 641

Bekki K., Couch W. J., 2003, The Astrophysical Journal, 596, L13

Bellhouse C. et al., 2019, Monthly Notices of the Royal Astronomical Society, 485, 1157

Binney J., Michael M., Merrifield M., 1998, Galactic astronomy. Princeton University Press

Binney J., Tremaine S., 2008, Princeton Series in Astrophysics

Binney J., Tremaine S., 2011, Galactic dynamics. Princeton university press

Birnboim Y., Balberg S., Teyssier R., 2015, Monthly Notices of the Royal Astronomical Society, 447, 3678

Blum R., 1995, Astrophysical Journal, Part 2-Letters (ISSN 0004-637X), 444, L89

Boselli A., Cortese L., Boquien M., 2014, Astronomy & Astrophysics, 564, A65

Boselli A. et al., 2010, Publications of the Astronomical Society of the Pacific, 122, 261

Boselli A., Fossati M., Sun M., 2022, The Astronomy and Astrophysics Review, 30, 3

Boselli A., Gavazzi G., 2006, Publications of the Astronomical Society of the Pacific, 118, 517

Bournaud F., 2016, Galactic Bulges, 355

Bravo-Alfaro H., Cayatte V., Van Gorkom J., Balkowski C., 2000, The Astronomical Journal, 119, 580

Brown R. H., Hazard C., 1951, Monthly Notices of the Royal Astronomical Society, 111, 357

Bushouse H. A., 1987, The Astrophysical Journal, 320, 49

Campitiello M. G. et al., 2021, The Astrophysical Journal, 911, 144

Carilli C., Taylor G., 2002, Annual Review of Astronomy and Astrophysics, 40, 319

Cayatte V., Kotanyi C., Balkowski C., Van Gorkom J., 1994, The Astronomical Journal, 107, 1003

Cayatte V., Van Gorkom J., Balkowski C., Kotanyi C., 1990, The Astronomical Journal, 100, 604

Chemin L., Huré J.-M., Soubiran C., Zibetti S., Charlot S., Kawata D., 2016, Astronomy & Astrophysics, 588, A48

Choi W., Kim C.-G., Chung A., 2022, The Astrophysical Journal, 936, 133

Choudhuri A. R., 1998, The physics of fluids and plasmas: an introduction for astrophysicists. Cambridge University Press

Chung A., Van Gorkom J., Kenney J. D., Crowl H., Vollmer B., 2009, The Astronomical Journal, 138, 1741

Combes F., 2016, Proceedings of the International Astronomical Union, 11, 245

Cortese L., Catinella B., Smith R., 2021, Publications of the Astronomical Society of Australia, 38, e035

Cowie L. L., Mckee C. F., 1977, The Astrophysical Journal, 211, 135

Cramer W. J., 2020, PhD thesis, Yale University

Crowl H. H., Kenney J. D., 2006, The Astrophysical Journal, 649, L75

Darvish B., Mobasher B., Sobral D., Rettura A., Scoville N., Faisst A., Capak P., 2016, arXiv preprint arXiv:1605.03182

Davies L. J. et al., 2015, Monthly Notices of the Royal Astronomical Society, 452, 616

Dobbs C., Baba J., 2014, Publications of the Astronomical Society of Australia, 31

Dolfi A., Gómez F. A., Monachesi A., Varela-Lavin S., Tissera P. B., Sifón C., Galaz G., 2023, Monthly Notices of the Royal Astronomical Society, 526, 567

Dressler A., 1980, The Astrophysical Journal, 236, 351

Dressler A. et al., 1997, The Astrophysical Journal, 490, 577

Duffy A. R., Schaye J., Kay S. T., Dalla Vecchia C., 2008, Monthly Notices of the Royal Astronomical Society: Letters, 390, L64

Dursi L., Pfrommer C., 2008, The Astrophysical Journal, 677, 993

Eckart A., Genzel R., 1996, Nature, 383, 415

Erickson S. A., 1974, PhD thesis, Massachusetts Institute of Technology

Evrard A. E., 1991, Monthly Notices of the Royal Astronomical Society, 248, 8

Fensch J., Bournaud F., 2021, Monthly Notices of the Royal Astronomical Society, 505, 3579

Feynman R., Leiton R., Sands M., 1964, The feynman lectures on physics, london: Addison-westley pub

Fiřt R., Rein G., Seehafer M., 2009, Communications in Mathematical Physics, 291, 225

Fletcher A., Beck R., Shukurov A., Berkhuijsen E., Horellou C., 2011, Monthly Notices of the Royal Astronomical Society, 412, 2396

Fritz J. et al., 2017, The Astrophysical Journal, 848, 132

Gavazzi G., Boselli A., Van Driel W., O'neil K., 2005, Astronomy & Astrophysics, 429, 439

Gavazzi G., Catinella B., Carrasco L., Boselli A., Contursi A., 1998, The Astronomical Journal, 115, 1745

Gavazzi G., Marcelin M., Boselli A., Amram P., Vílchez J., Iglesias-Paramo J., Tarenghi M., 2001, Astronomy & Astrophysics, 377, 745

Gebhardt K. et al., 2000, The Astrophysical Journal, 539, L13

Genzel R., Eisenhauer F., Gillessen S., 2010, Reviews of Modern Physics, 82, 3121

Genzel R., Pichon C., Eckart A., Gerhard O., Ott T., 2000, Monthly Notices of the Royal Astronomical Society, 317, 348

Ghosh S., Jog C. J., 2018, New Astronomy, 63, 38

Giovanelli R., Haynes M., 1983, The Astronomical Journal, 88, 881

Giovanelli R., Haynes M., 1985, The Astrophysical Journal, 292, 404

Godwin H., 1962, Nature, 195, 984

Gomez P. L. et al., 2003, The Astrophysical Journal, 584, 210

Gulati M., 2014, PhD thesis, Raman Research Institute, Bangalore.

Gulati M., Saini T. D., 2016a, Monthly Notices of the Royal Astronomical Society, stw2780

Gulati M., Saini T. D., 2016b, Monthly Notices of the Royal Astronomical Society, 460, 1019

Gulati M., Saini T. D., Sridhar S., 2012, Monthly Notices of the Royal Astronomical Society, 424, 348

Gullieuszik M. et al., 2017, The Astrophysical Journal, 846, 27

Gunn J. E., Gott III J. R., 1972, The Astrophysical Journal, 176, 1

Gursky H., Solinger A., Kellogg E., Murray S., Tananbaum H., Giacconi R., Cavaliere A., 1972, Astrophysical Journal, 173, L99

Haller J. W., Rieke M., Rieke G., Tamblyn P., Close L., Melia F., 1996, The Astrophysical Journal, 456, 194

Han J., Manchester R., Qiao G., 1999, Monthly Notices of the Royal Astronomical Society, 306, 371

Han J., Manchester R., Van Straten W., Demorest P., 2018, The Astrophysical Journal Supplement Series, 234, 11

Han J. L., 2008, in AIP Conference Proceedings, American Institute of Physics

Hashimoto Y., Oemler Jr A., Lin H., Tucker D. L., 1998, The Astrophysical Journal, 499, 589

Haynes M. P., Giovanelli R., 1984, The Astronomical Journal, 89, 758

Haynes M. P., Hogg D. E., Maddalena R. J., Roberts M. S., van Zee L., 1998, The Astronomical Journal, 115, 62

Heller A. B., Brosch N., Almoznino E., Van Zee L., Salzer J. J., 2000, Monthly Notices of the Royal Astronomical Society, 316, 569

Hou L., Han J., 2015, Monthly Notices of the Royal Astronomical Society, 454, 626

Hu D. et al., 2024, Monthly Notices of the Royal Astronomical Society, 527, 1062

Hubble E., Humason M. L., 1931, The Astrophysical Journal, 74, 43

Indrani C., Deshpande A., 1999, New Astronomy, 4, 33

Jaffé Y. L. et al., 2018, Monthly Notices of the Royal Astronomical Society, 476, 4753

Jagannathan S., Malik S., Jain D., Seshadri T., 2021, New Astronomy, 84, 101531

Jalali M. A., 2013, The Astrophysical Journal, 772, 75

Jalali M. A., Tremaine S., 2012, Monthly Notices of the Royal Astronomical Society, 421, 2368

Jog C. J., 1992, Astrophysical Journal, 390, 378

Jog C. J., 1996, Monthly Notices of the Royal Astronomical Society, 278, 209

Jog C. J., 1999, The Astrophysical Journal, 522, 661

Jog C. J., 2002, Astronomy & Astrophysics, 391, 471

Jog C. J., Combes F., 2009, Physics Reports, 471, 75

Jog C. J., Solomon P., 1984a, Astrophysical Journal, 276, 127

Jog C. J., Solomon P., 1984b, Astrophysical Journal, 276, 114

Junqueira T., Lépine J., Braga C., Barros D., 2013, Astronomy & Astrophysics, 550, A91

Kapferer W., Sluka C., Schindler S., Ferrari C., Ziegler B., 2009, Astronomy & Astrophysics, 499, 87

Kato S., 1983, Publications of the Astronomical Society of Japan, 35, 249

Kaur A., 2018, PhD thesis

Kenney J. D., Abramson A., Bravo-Alfaro H., 2015, The Astronomical Journal, 150, 59

Kenney J. D., Crowl H., van Gorkom J., Vollmer B., 2004, in Symposium-International Astronomical Union, Cambridge University Press

Kenney J. D., Koopmann R. A., 1999, The Astronomical Journal, 117, 181

Kennicutt Jr R. C., 1983, The Astronomical Journal, 88, 483

Khademi M., Yang Y., Hammer F., Nasiri S., 2021, Astronomy & Astrophysics, 654, A7

Khoperskov S., Shustov B., Khoperskov A., 2012, Astronomy reports, 56, 664

King I., 1962, The Astronomical Journal, 67, 471

Köppen J., Jáchym P., Taylor R., Palouš J., 2018, Monthly Notices of the Royal Astronomical Society, 479, 4367

Kormendy J., Bender R., 1999, The Astrophysical Journal, 522, 772

Krabbe A. et al., 1995, The Astrophysical Journal, 447, L95

Kravtsov A. V., Borgani S., 2012, Annual Review of Astronomy and Astrophysics, 50, 353

Kronberg P. P., 1994, Reports on Progress in Physics, 57, 325

Kuhlen M., Guedes J., Pillepich A., Madau P., Mayer L., 2013, The Astrophysical Journal, 765, 10

Landau L. D., Lifshitz E. M., 2013, Quantum mechanics: non-relativistic theory. Elsevier

Larson R., Tinsley B., Caldwell C. N., 1980, The Astrophysical Journal, 237, 692

Lauer T. R., Faber S., Ajhar E. A., Grillmair C. J., Scowen P. A., 1998, The Astronomical Journal, 116, 2263

Lauer T. R. et al., 1993, Astronomical Journal, 106, 1436

Lauer T. R. et al., 1996, The Astrophysical Journal, 471, L79

Leao M., De Gouveia Dal Pino E. M., Falceta-Gonçalves D., Melioli C., Geraissate F., 2009, Monthly Notices of the Royal Astronomical Society, 394, 157

Lee E., Goodman J., 1999, Monthly Notices of the Royal Astronomical Society, 308, 984

Levine S. E., Sparke L. S., 1998, The Astrophysical Journal, 496, L13

Lewis I. et al., 2002, Monthly Notices of the Royal Astronomical Society, 334, 673

Maoz E., McKee C. F., 1998, The Astrophysical Journal, 494, 218

Marcolini A., Brighenti F., D'Ercole A., 2003, Monthly Notices of the Royal Astronomical Society, 345, 1329

Massey R. et al., 2015, Monthly Notices of the Royal Astronomical Society, 449, 3393

Mathewson D., Van Der Kruit P., Brouw W., 1972, Astronomy and Astrophysics, 17, 468

Mera D., Chabrier G., Schaeffer R., 1998, Astronomy and Astrophysics, 330, 953

Miley G., Perola G., Kruit P. V. D., Laan H. V. D., 1972, Nature, 237, 269

Miller R., 1971, in International Astronomical Union Colloquium, Cambridge University Press

Moore B., Katz N., Lake G., Dressler A., Oemler A., 1996, Nature, 379, 613

Moore B., Lake G., Katz N., 1998, The Astrophysical Journal, 495, 139

Moore B., Lake G., Quinn T., Stadel J., 1999, Monthly Notices of the Royal Astronomical Society, 304, 465

Mori M., Burkert A., 2000, The Astrophysical Journal, 538, 559

Morley P., Buettner D., 2016, International Journal of Modern Physics D, 25, 1650089

Morley P., Buettner D., 2017, International Journal of Modern Physics D, 26, 1750069

Müller A., Ignesti A., Poggianti B., Moretti A., Ramatsoku M., Dettmar R.-J., 2021, Galaxies, 9, 116

Navarro J. F., Frenk C. S. W. S. D. M., 1996, in Symposium-international astronomical union, Cambridge University Press

Nixon C., Pringle J., 2019, New Astronomy, 67, 89

Ota N., Hattori M., Pointecouteau E., Mitsuda K., 2003, in The Proceedings of the IAU 8th Asian-Pacific Regional Meeting, Volume 1

Peiris H. V., Tremaine S., 2003, The Astrophysical Journal, 599, 237

Peng Y., Maiolino R., Cochrane R., 2015, Nature, 521, 192

Peng Y.-j. et al., 2010, The Astrophysical Journal, 721, 193

Pfrommer C., Dursi J., 2010, Nature Physics, 6, 520

Planck Collaboration P. A. et al., 2016, Astronomy & Astrophysics, 586, A136

Poggianti B. M. et al., 2017, The Astrophysical Journal, 844, 48

Poggianti B. M. et al., 2006, The Astrophysical Journal, 642, 188

Postman M., Geller M., 1984, The Astrophysical Journal, 281, 95

Prasad C., Jog C. J., 2017, Astronomy & Astrophysics, 600, A17

Quilis V., Moore B., Bower R., 2000, Science, 288, 1617

Rafikov R. R., 2001, Monthly Notices of the Royal Astronomical Society, 323, 445

Ramos-Martínez M., Gómez G. C., Pérez-Villegas Á., 2018, Monthly Notices of the Royal Astronomical Society, 476, 3781

Rand R. J., Kulkarni S. R., 1989, The Astrophysical Journal, 343, 760

Reichard T. A., Heckman T. M., Rudnick G., Brinchmann J., Kauffmann G., Wild V., 2009, The Astrophysical Journal, 691, 1005

Richter O.-G., Sancisi R., 1994, Astronomy and Astrophysics, 290

Rix H.-W., Zaritsky D., 1995, arXiv preprint astro-ph/9505111

Roberts I. D. et al., 2023, Astronomy & Astrophysics, 675, A78

Roediger E., Brüggen M., 2006, Monthly Notices of the Royal Astronomical Society, 369, 567

Roediger E., Hensler G., 2008, Astronomy & Astrophysics, 483, 121

Rohlfs K., 1977, Lectures on density wave theory

Rubin V. C., 1983, Science, 220, 1339

Rubin V. C., Ford Jr W. K., 1970, The Astrophysical Journal, 159, 379

Ruszkowski M., Brüggen M., Lee D., Shin M.-S., 2014, The Astrophysical Journal, 784, 75

Saha K., Jog C. J., 2014, Monthly Notices of the Royal Astronomical Society, 444, 352

Saini T. D., Gulati M., Sridhar S., 2009, Monthly Notices of the Royal Astronomical Society, 400, 2090

Salow R. M., Statler T. S., 2001, The Astrophysical Journal Letters, 551, L49

Sambhus N., Sridhar S., 2002, Astronomy & Astrophysics, 388, 766

Sandage A., 1961, The Hubble atlas of galaxies. Carnegie Institution of Washington Washington, DC

Schaller M., Robertson A., Massey R., Bower R. G., Eke V. R., 2015, Monthly Notices of the Royal Astronomical Society: Letters, 453, L58

Schoenmakers R., Franx M., De Zeeuw P., 1997, Monthly Notices of the Royal Astronomical Society, 292, 349

Schulz S., Struck C., 2001, Monthly Notices of the Royal Astronomical Society, 328, 185

Scott T. et al., 2010, Monthly Notices of the Royal Astronomical Society, 403, 1175

Sellgren K., McGinn M., Becklin E., Hall D., 1990, The Astrophysical Journal, 359, 112

Sharma M., Nath B. B., Chattopadhyay I., Shchekinov Y., 2014, Monthly Notices of the Royal Astronomical Society, 441, 431

Sharma P., McCourt M., Parrish I. J., Quataert E., 2012, Monthly Notices of the Royal Astronomical Society, 427, 1219

Shukurov A., Subramanian K., 2021, Astrophysical Magnetic Fields: From Galaxies to the Early Universe, Cambridge Astrophysics. Cambridge University Press

Singh A., Gulati M., Bagla J. S., 2019, Monthly Notices of the Royal Astronomical Society, 489, 5582

Smith R., Davies J. I., Nelson A. H., 2010, Monthly Notices of the Royal Astronomical Society, 405, 1723

Smith S., 1936, The Astrophysical Journal, 83, 23

Sofue Y., 2009, Publications of the Astronomical Society of Japan, 61, 153

Sofue Y., Fujimoto M., 1983, The Astrophysical Journal, 265, 722

Sofue Y., Klein U., Beck R., Wielebinski R., 1986, in Third Asian-Pacific Regional Meeting of the International Astronomical Union, Springer

Solanes J. M., Manrique A., García-Gómez C., González-Casado G., Giovanelli R., Haynes M. P., 2001, The Astrophysical Journal, 548, 97

Solomon P., Sage L., 1988, The Astrophysical Journal, 334, 613

Sridhar S., Saini T. D., 2010, Monthly Notices of the Royal Astronomical Society, 404, 527

Sridhar S., Touma J., 1999, Monthly Notices of the Royal Astronomical Society, 303, 483

Stanev T., 1997, The Astrophysical Journal, 479, 290

Steinhauser D., Haider M., Kapferer W., Schindler S., 2012, Astronomy & Astrophysics, 544, A54

Steinhauser D., Schindler S., Springel V., 2016, Astronomy & Astrophysics, 591, A51

Sulentic J. W., 1976, The Astrophysical Journal Supplement Series, 32, 171

Swaters R., Schoenmakers R., Sancisi R., Albada T. V., 1999, Monthly Notices of the Royal Astronomical Society, 304, 330

Swaters R., Van Albada T., Van Der Hulst J., Sancisi R., 2002, Astronomy & Astrophysics, 390, 829

Takekawa S., Oka T., Iwata Y., Tsujimoto S., Nomura M., 2020, The Astrophysical Journal, 890, 167

Tinyakov P. G., Tkachev I. I., 2002, Astroparticle Physics, 18, 165

Tonnesen S., Stone J., 2014, The Astrophysical Journal, 795, 148

Touma J., 2002, Monthly Notices of the Royal Astronomical Society, 333, 583

Tremaine S., 1995, Astronomical Journal, 110, 628

Tremaine S., 2001, The Astronomical Journal, 121, 1776

Vallée J. P., 2008, The Astronomical Journal, 135, 1301

Varela-Lavin S., Gómez F. A., Tissera P. B., Besla G., Garavito-Camargo N., Marinacci F., Laporte C. F., 2023, Monthly Notices of the Royal Astronomical Society, stad1724

Vijayaraghavan R., Sarazin C., 2017, The Astrophysical Journal, 848, 63

Vollmer B., Soida M., Beck R., Urbanik M., Chyży K., Otmianowska-Mazur K., Kenney J., Van Gorkom J., 2007, Astronomy & Astrophysics, 464, L37

Vollmer B., Soida M., Chung A., Van Gorkom J., Otmianowska-Mazur K., Beck R., Urbanik M., Kenney J., 2008, Astronomy & Astrophysics, 483, 89

Watts A. B. et al., 2023, Publications of the Astronomical Society of Australia, 40, e017

Westerhout G., Seeger C. L., Brouw W., Tinbergen J., 1962, Bulletin of the Astronomical Institutes of the Netherlands, 16, 187

Whitmore B. C., 1992, Physics of Nearby Galaxies, 425

Widrow L. M., 2002, Reviews of Modern Physics, 74, 775

Yadav J., Das M., Barway S., Combes F., 2021, Astronomy & Astrophysics, 651, L9

Yoshida M. et al., 2004, The Astronomical Journal, 127, 90

Young J., Scoville N., 1991, Annual review of astronomy and astrophysics, 29, 581

Zaritsky D. et al., 2013, The Astrophysical Journal, 772, 135

Zwicky F., 1937, The Astrophysical Journal, 86, 217